ABSTRACT

UGALE, PRATEETI MILIND. Evaluation of Components of High Altitude Stratospheric Airship. (Under the direction of Dr. Abdel-Fattah M. Seyam and Dr. Philip Bradford).

Stratospheric airships are Lighter-Than-Air (LTA), powered, and navigable ships that hover at an altitude of 20 km from the sea level. Being placed at this height, airships provide platform for intelligence, surveillance, reconnaissance (ISR) purpose and more. They do provide space-like observatory, but the high altitude unfortunately leads to unavoidable space-like challenges as well. The environment in the stratosphere has low temperatures, low air pressure, high solar irradiance, and intense ultraviolet (UV) radiations. There has always been considerable interest in developing airships resistant to these environmental conditions, but unfortunately the attempts in the past have not been very successful. Airships have many advantages over other High-Altitude Platforms (HAPs), especially satellites in term of development cost. Hence, researchers have been putting significant efforts in developing airship materials that will be stable in the harsh stratospheric conditions over longer durations.

This study focuses on evaluation various airship components. Airship hull base laminate with woven fabric from Zylon® as reinforcement was evaluated to know its strength in warp and weft directions. Seam parametric study was carried out systematically to optimize a seam. Seams can be considered as the most crucial component of an airship hull as they have the highest potential of causing failure since they are still relay on labor skills. An experimental design was developed to evaluate the effect of three different overlap seam lengths, and low and high seaming temperature, pressure, and speed on the tensile property of the seams. Another experimental design was developed to evaluate the effect of low and high seaming temperature, pressure, and speed on

the peeling property of the seams. Seams are exposed to ozone and varying temperatures in stratosphere. Therefore, weathering was conducted on seams to evaluate the effect of weathering on their tensile strength.

Additionally, components to support solar cells, battery, and motor namely, solar cap fabric and two harnesses referred to as, harness A and harness B were subjected to weathering due to UV radiations and ozone concentrations, to evaluate the weight and strength loss.

It was found that the laminate gave higher strength in the weft direction compared to warp. The statistical analysis of the tensile test for the seams showed that the overlap seam length and the seaming temperature significantly affected the seam strength, whereas seaming speed did not show any effect. The seam that gave highest tensile strength was 7.62 cm overlap seam, seamed at 155 °C temperature, 400 kPas pressure, and 6 m/min speed. While determining the peeling property of the seams, it was observed that the vacuum deposited aluminum coating was peeled away from the Kapton film of the multi-layered laminate. The seam that gave highest peel strength was seamed at 155 °C temperature, 400 kPa pressure, and 6 m/min speed. Ozone concentration and then low and high temperature cycle did not significantly affect the seam tensile strength. UV treated solar cap fabric, harness A, and B for 6 days showed 25%, 61.63%, and 16.08% reduction in the strength, respectively. The ozone treatment did not have any effect on the weight or strength of these fabrics.

Evaluation of Components of High Altitude Stratospheric Airship

by
Prateeti Milind Ugale

A thesis submitted to the Graduate Faculty of
North Carolina State University
in partial fulfillment of the
requirements for the degree of
Master of Science

Textile Engineering

Raleigh, North Carolina

2018

APPROVED BY:

Dr. Abdel-Fattah M. Seyam Committee Co-Chair	Dr. Philip Bradford Committee Co-Chair
Dr. Xiangwu Zhang	Dr. Ericka Ford

DEDICATION

To my wonderful family who believes in me and my dreams. I am blessed to have been born in a family which is so supportive and always encouraging. Helping me to achieve my dreams has been their aim in life.

To my aunt and uncle. I wouldn't have made it without their help.

To my dear friends who made a difference. They have been inspiring and have always helped me to be on track. I am happy to have found them.

BIOGRAPHY

Prateeti Ugale was born in Pune, India on the 11th of November 1994. She grew up in Mumbai, where she lived with her family. Since childhood she loves dance and art.

She earned her Bachelor of Technology degree in Fiber and Textile Processing Technology at Institute of Chemical Technology, Mumbai, in 2016. While studying for four years she developed immense interest in the field of textiles and hence wanted to study further. That same year she got admitted to North Carolina State University, College of Textiles, to pursue a Master of Science degree in Textile Engineering. She was fortunate enough to have had Dr. Abdel-Fattah M. Seyam as her graduate advisor.

Prateeti plans to graduate in Summer 2018. She believes that passion is the difference between having a job and a career. She hopes to have a fulfilling career for herself in the future and wants to grow along with the people around her to make a difference to the society.

ACKNOWLEDGMENTS

Primarily, I would like to thank Dr. Abdel-Fattah M. Seyam to have given me this opportunity to work on such an interesting topic. I did not know what it took to be a professional individual, however, under his guidance, I have not just learnt a lot academically, but have also developed professionally. I cannot thank him enough for his valuable inputs to my research and for believing in me. He has been an incredible advisor has always been understanding, considerate, and helpful. I would like to thank Dr. Philip Bradford for putting forth is innovative ideas which helped me in the thesis, and Dr. Xiangwu Zhang, and Dr. Erika Ford for serving on my master's committee.

I appreciate the help from Teresa White, Judy Elson, and Tri Vu. It is because of them that I was able to finish my testing systematically. Secondarily, I would like to thank the two-wonderful people, Ang Li and Hadir Eldeeb, who made this journey so smooth for me. Their support has been immense. I am grateful to have known them and work with them. I would also like to give special thanks to Dr. Rahul Vallabh, for guiding me and sharing with me his knowledge.

Last but not the least, all this wouldn't have been possible without SCEYE S.A. funds. I would like to thank Dr. David Kim for his encouragement and sharing his knowledge on the field of Airship.

TABLE OF CONTENTS

LIST OF TABLES

LIST OF FIGURES

LIST OF ABBREVIATIONS

AFM	Atomic Force Microscopy
CRC	Corrosion Resistant Coating
EVOH	Ethylene Vinyl Alcohol Polymer
FTIR	Fourier Transform Infrared Spectroscopy
HAP	High-Altitude-Airship
HF	High Frequency
HMPE	High Modulus Polyethylene
HSD	Honest Significant Difference
ISR	Intelligence Surveillance Reconnaissance
LEMV	Long Endurance Multi – Intelligence Vehicle
LDPE	Low Density Polyurethane
LTA	Lighter-Than-Air
PBO	Polybenzaxole
PET	Polyethylene Terephthalate
PI	Polyimide
PVC	Polyvinyl Chloride
PVF	Polyvinyl Fluoride
TOR	Triton Oxygen Resistant
TPU	Thermoplastic Polyurethane
VDA	Vacuum Deposited Coating
UHMWPE	Ultra-High Modulus Polyethylene

1. INTRODUCTION

Airship, also called as Aerostat, Dirigible, Blimp, Zeppelin, or a hybrid airship is a Lighter-Than-Air (LTA) aircraft which can navigate through the air using its own power. It is one of the type of High Altitude Platform (HAP) Stations. It gains its lift from lifting gas which is less dense than the surrounding air. In earlier days, the most commonly used gas was hydrogen due to its abundance availability. Since 1960s, helium gas is used because it is non-flammable even though it is rare and relatively expensive than hydrogen gas. It was only United States that started using helium gas earlier. An airship might contain single gas bag or multiple gas-filled cells. It can carry engines, crew and/ or payload accommodation in one or more gondolas suspended below the envelop.

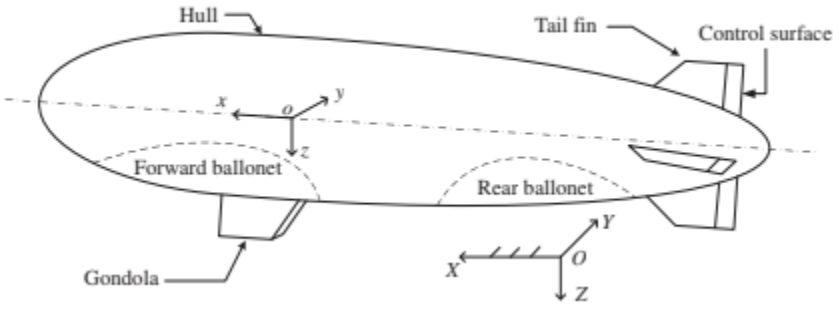

Figure 1.1: A Typical Airship (Li et al. 2011)

Airships can be classified based on construction (rigid, semi-rigid and non-rigid airship), way of producing vertical force (lighter-than-air, heavier-than-air, and hybrid), and payload capability (heavy lift and medium lift) (Liao & Pasternak 2009). Rigid airship has an outer structural framework that maintains the shape of the airship with lifting gas filled in one or more internal gas bags. Rigid airships are also called as ‘zeppelins’ because it was first flown by Count Zeppelin.

Semi-rigid airships retain their shape by maintaining internal pressure with a supporting structure attached to it. Non-rigid airships are commonly called as ‘blimps’ and the pressure difference within the airship and the atmosphere retains their shape. It has small ballonets that contain air. The payload of the traditional vehicles was usually less than 30 tons, whereas heavy lift air vehicles can reach as high as 500 tons (Liao & Pasternak 2009). At sea-level, the ballonets are filled with air and when the altitude increases, the lifting gas expands. This process should be reversed when the airship must be brought to the ground.

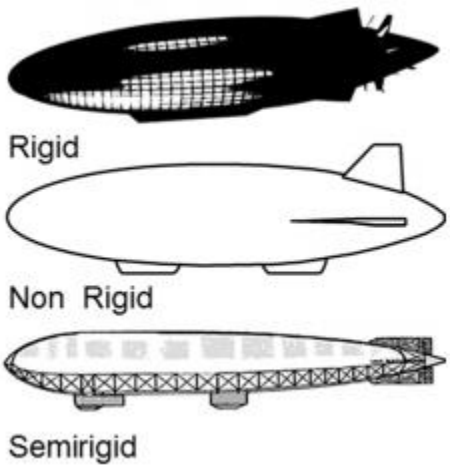

Figure 1.2: Airship Types (Anon n.d.)

A powered airship operates at altitudes near 20 km where the stratospheric winds are the lightest (5 – 15 m/s) and the airship can hover for a long duration like for days, weeks or even months (Zhai & Euler 2005). The winds might vary daily or throughout the year exceeding 25 m/s or even higher and hence one of the most difficult problems in airship design is the propulsion power (Fesen & Brown 2015). To overcome this problem airships can be tethered to the ground station, however, no tethered stratospheric airship has been flown up till now due to obstacles like aviation restriction, tether strength, weight, and tether wind drag etc. Tethered airships do have advantages

like no propulsion motors or propellers, no solar panel arrays, and no batteries for night time propulsion is needed (Fesen & Brown 2015).

Airships in general have wide range of capabilities and combine the advantage of both ships and airplanes. Airships can hover for a very long time without the need for immediate refueling which reduces the cost for energy consumption and operational cost. The speed of the airship is much higher than that of a ship, and the vibrations are lower compared to that of an aircraft. They do not require long runways, cause no air or water pollution, and are unaffected by sea state and corrosive environment (Liao & Pasternak 2009).

Airships were most commonly used before 1940s, but unfortunately their use decreased over time as its capabilities were surpassed by those of airplanes. Their decline was further accelerated by high profile accidents like the burning of British *R101*, crash of the twin airborne aircraft carrier, USS *Akron, USS Macon*, and the famous burning of the *Hindenburg* to name a few. The first non-rigid airship flight was recorded in the 18th century by Jean – Pierrre Blanchard (1784). It consisted of a balloon fitted with a hand powered propeller for propulsion. Henri Giffard in 1852 was the first person to construct an engine powered flight. He flew 27 kilometers in a steam powered airship. Twenty years later, in 1872, Paul Haenlein flew an airship over Vienna which was powered by combustion engine (Sami et al. 2015). A British company called Thermo Skyship prepared a radio controlled lenticular airship in 1975. From then till 1990, Mario Sanchez Roldan and Michael K. Walden constructed rigid airships MLA – 24, MLA – 32 – A, and MLA – 32 – B. The MLA – 32 – B was the first manned airship in operation for more than fifty years (Liao & Pasternak 2009).

20th century marked important developments in airships and their flight. The mass production of Astra – Torres non-rigid airship was successful by the French, success of Zeppelin series, emergence of new production companies in Germany, Italy, France and the Goodrich company in the US, and the first trans-Atlantic crossing attempt (Baird et al. 2014). The launch of Zeppelin was the start of the 'Golden Age of the Airships'. In the first half of the 20th century, the airships became popular for passenger transportation, and military uses such as bombing, reconnaissance, surveillance, and communications (Sami et al. 2015). Airships were capable of bombing and machine gunning but had a few disadvantages like mechanical failure of airship hull, bad weather, and bombardment inaccuracy (Baird et al. 2014). The first American airship, USS Shenandoah, operated by the US Navy in 1923 was the first airship to use helium gas as the lifting gas. In 1937, just before the landing, Germany's Hindenburg, a hydrogen filled rigid airship burst to flame at Lakehurst, New Jersey on May 6th. It was the most famous and widely remembered airship disaster in which 36 people got killed onboard. Due to this incident, people's confidence in airships lowered, and the airships saw a deployment after the second World War. After this, US used airships for patrolling and convoy escorts for ships to detect enemy U – boats. Hence, years since the war, airships saw a decline and since then were only used for advertising, sightseeing, surveillance, and research purpose (Sami et al. 2015). Even after so many problems, interest in airship did not disappear. US kept constructing simple, dependable, helium filled, non-rigid airship for three decades (Liao & Pasternak 2009).

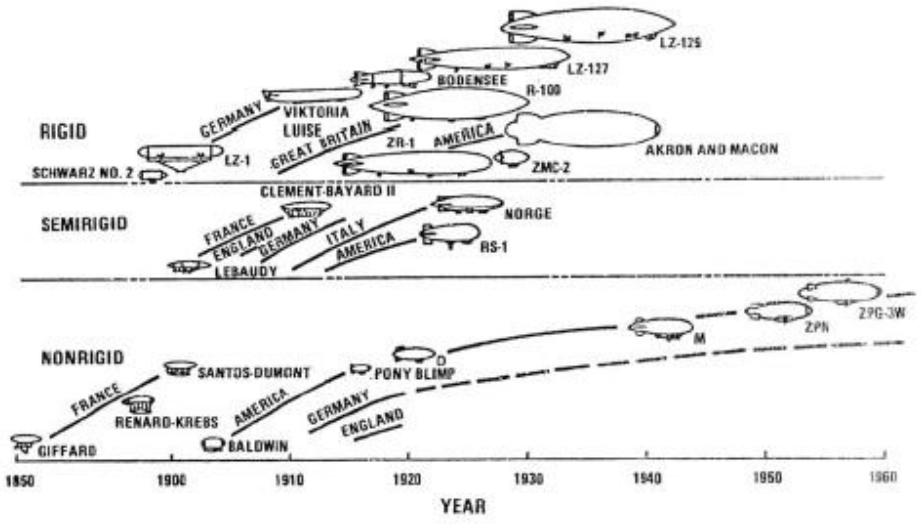

Figure 1.3: History of Airship Developments Before 1960 (Liao & Pasternak 2009)

Many projects were launched from 1990 to 2000 but not all of them continued. In 2014, Google and Facebook, the two major internet companies invested in the new High – Altitude Platforms (HAPs) to provide internet in the region where there is no satellite coverage. All HAPs are usually positioned 20 km away from the earth's surface for telecommunication and remote sensing purposes for the military and civilians. The stratosphere has the temperature of about – 60° C, starting from 7 km at the poles to 18 km at the equator. 20 km altitude is selected because there is less wind speed intensity, therefore, less power to keep the airship at one place. 20 km altitude also provide large coverage area (D'Oliveira et al. 2016).

In recent years, some important developments took place. The purpose of HiSentinel program was to develop low cost, unmanned airship, which could carry payloads from 9 to 90 kg at high altitudes for time duration greater than 30 days and to obtain its performance data. The HiSentinel family consists of 3 major airships, HiSentinel 20, 50 and the most recent 80 that could carry 9, 23 and 36 kg of payloads, respectively (D'Oliveira et al. 2016). The first flight of the most recent

HiSentinel80 was completed on 10th of November 2010. It was launched from Page, Arizona and was tracked northeast towards Utah and Colorado. The objective of this flight was to demonstrate engineering feasibility and potential military utility of high altitude systems for persistent payload operations. HiSentinel80 was at an altitude of 20 km for about 8 hours. This flight collected valuable command and control of payload data before terminating the flight. (Smith et al. 2011).

Figure 1.4: HiSentinel80 inflation and system integration (Smith et al. 2011)

HiSentinel80 was 63.09 m in length and 13.72 m in diameter. After the completion of the mission, the payload released from the hull to return to the ground with the help of a parachute and was recovered for inspection. HiSentinel airships have provided persistent communication and ISR capabilities for warfighter (Smith et al. 2011).

2. LITERATURE REVIEW

The literature review was conducted to learn the reasons why airships were constructed, the materials used for constructing the airship and their selection criteria depending upon the properties required to sustain in the stratosphere. The primary focus of this review is to know the reason the past airships failed, and to learn the alterations done in the material selection over the period to overcome the challenges faced in the past.

2.1. Purpose of Airships

Historically, airships were built for transportation and military purposes, but in recent years, they were used for telecommunication relay, weather forecasting, and surveillance purposes. The military was always interested in airship system for missile defense and homeland defense efforts (Zhai & Euler 2005). There is a great demand for real time communication for military surveillance services. Airship at a height of 20 km covers about 325 km in distance, meaning that it could cover the entire of Afghanistan (Fesen n.d.). It is also less interfered by obstacles like building or ground elevations (D'Oliveira et al. 2016). Hence, an airship can be used as a surrogate satellite, that offers shorter transmission at higher resolution for sensor surveillance of ground targets (Fesen n.d.). Stratospheric airships can also be used for coastal monitoring, climate monitoring, and emergency communication services (Davey et al. 2008).

Airships, unlike aircraft, can generate lift from buoyancy and not aerodynamics. Moreover, airships do not have to remain aloft, they can loiter over a specific location as well as move to a new location. Addition to this, airships can carry large-volume and heavy payloads. All these

characteristics make airships a great candidate for long-endurance surveillance missions (Colozza & Dolce 2005).

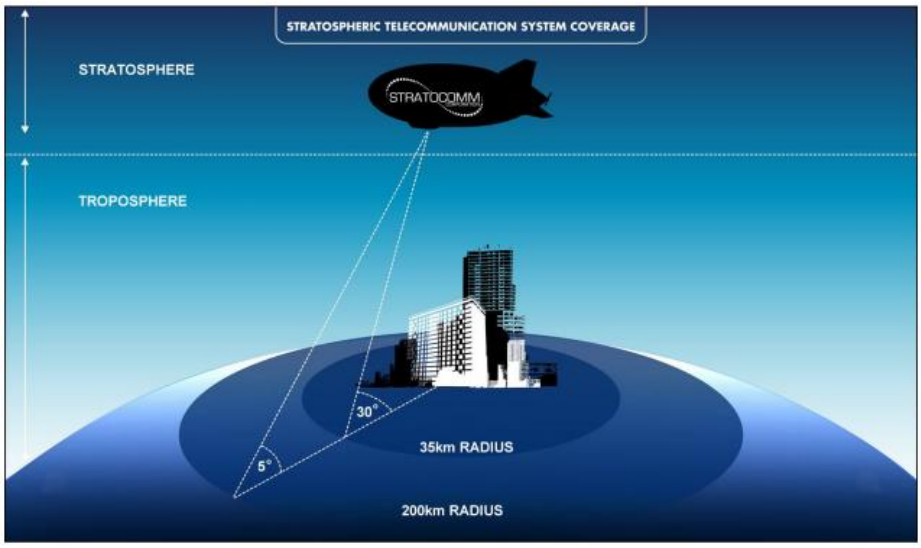

Figure 2.1: Wireless coverage area for stratospheric airship (Davey et al. 2008)

ILC Dover has been designing and developing High – Altitude Airships (HAAs) since early 1980s. ILD Dover has specifically designed airships for Intelligence, Surveillance and Reconnaissance (ISR) applications. It developed airship for Long Endurance Multi – Intelligence Vehicle (LEMV) to provide extended ISR coverage by carrying higher mass payload sensors to high altitude for long time. This is the world's largest hybrid vehicle. Van Wagner Outdoor Advertising and Zeppelin used ILC's airship as a high – profile advertising vehicle. LZN07 220-foot-long airship fabricated for Zeppelin was designed to interface with a semi-rigid passenger airship structure (Reliable & Airships n.d.).

In current era, demand for wireless communication has increased and it is provided by terrestrial and satellite system. The HAAs hover at 17 to 22 km above the earth's surface and hence have

been the proposed mobile services in stratosphere which have advantages of both terrestrial and satellite. They also help in providing 3G, emergency services, broadcasting services, telephony, and WI – MAX. They have applications in broadband fixed wireless access application, 2G, 3G, and 4G applications, emergency and disaster scenarios, military communication and earth monitoring and positioning. HAAs give high facility services at low cost (Sami et al. 2015).The mission of an airship has always been to maintain a position to cover a certain area. The propulsion that is required would always be to stay in one place resisting the winds. Microwave transmissions, solar power, and fuel cells are certain candidates for the source of power. As the technology is advancing, airships can also be used to explore other planets. Low temperature airships would be very applicable in the atmosphere of Mars and upper atmosphere of Venus. The future of the airship is extremely bright as it has been for past twenty years (Seely & Smith 2002).

Airships help in understanding the transport of pollutants and the natural reactive processes occurring in the atmosphere. Similarly, a long time stable airship could enable persistent observations of regions around the Earth that have never been explored. An airship has the potential for week-long endurance, movability at multiple altitudes as well as the capability to hold position. Airship can help explore the parts of the world that have not be explored yet (Baird et al. 2014). Recent successes, new capabilities and research would bring yet another quantum leap in the theory (Seely & Smith 2002).

One of the advantages of HAA is great astronomical image quality due to reduced atmospheric effects as there is no weather at an altitude as high as 20 km. The pilots operating HAAs at this high-altitude report smooth flying conditions throughout the earth. Another advantage of

astronomical HAAs is that they do not require ground-site to be purchased or developed. Great horizon-to-horizon observation is possible due to the absence of atmospheric air, water vapor, and overhead dust particles. Unlike LEO satellites the data transfer from and to the airship would involve simple line-of-sight communication for 24*7. Therefore, for more than a decade, several communication companies are considering HAAs to economically expand high – bandwidth data services to their customers (Fesen n.d.).

2.2. Material Requirements of Airship Envelop

This section will deal with the material requirements for specifically non – rigid airships. In comparison to the rigid and semi – rigid airships, non – rigid airships are easy to design, build, and maintain. Their structure is comparatively simple with low fabrication cost and manufacturing time. These airships have much less issue with the weight unlike the rigid and semi – rigid airships. Figure 2.2 shows a typical configuration of a non – rigid airship. The shape of a non – rigid airship is maintained by a pressure differential between the lifting gas within the airship and the surrounding gas outside the airship. Buoyancy is produced by adjusting the air volume inside the ballonets and gas volume in the airship. Hence, due to all these advantages, more efforts have been put in study and development of a non – rigid airship envelop (Liao & Pasternak 2009).

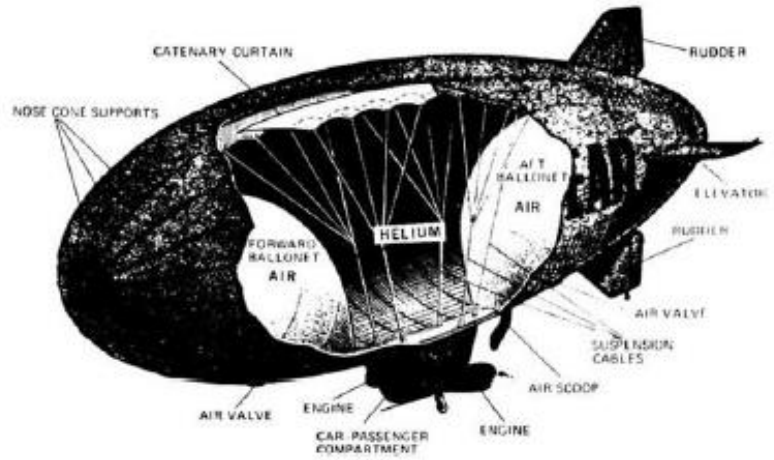

Figure 2.2: A typical non – rigid airship design (Liao & Pasternak 2009)

For a non – rigid airship, the hull material is an important component as it contains the lifting gas necessary for the airship flight and maintenance of its own aerodynamic shape. Due to this, the hull of an airship deserves the highest attention while designing and manufacturing an airship (Miller & Mandel 2000). Great advancements have been made in the past few decades, but a perfect airship still demands improvements. It can be said that developing a light weight yet strong material, capable of containing and lifting gas and resistant to the environment of the stratosphere is a huge challenge.

The strength-to-weight ratio of the hull material is the most important factor that significantly affects the possible size of a non – rigid airship. It is the requirement of a non – rigid airship to have a large diameter to bear the aerodynamic and hoop stress due to the pressure difference. It is also suggested that the diameter of the airship should be large enough to resist the hull bending moments and accommodate good amount of gas for providing sufficient lifting force. (Jamison, Lewis; Sommer, Geoffrey; Porche III 2007).The volume of the airship must be maintained even when the temperature of the lifting gas changes. These temperature variations influence the

pressure difference maintained. Hence, the hull material should be strong and flexible enough at the same time to bear the stresses raised due to variation in the pressure. 90% of the earth's ozone is concentrated in stratosphere. Therefore, the hull material must be resistant to intense UV radiations and ozone concentrations in the stratosphere, as the intense UV radiation and high concentration of ozone can deteriorate hull material, resulting in a loss of strength and permeability over time. The deterioration must be avoided as the airship has to survive in that atmosphere for months to years (Zhai & Euler 2005).

The airship hull should also avoid the leakage of the lifting gas from within the airship into the atmosphere. The lifting gas cannot afford leak as it provides buoyancy. Initially hydrogen gas was used as lifting gas but in past few years helium gas has replaced it. Helium gas will lend to leak over the period and hence prevention of the leakage is altogether another challenge (Islam & Bradley 2012). The loss of lifting gas is not desired as it will result in loss of operational capability and increased operational cost. At the height where airship hovers, the surrounding is cold, and can cause the airship hull laminate to lose its flexibility and become brittle. The airship cannot simply afford to lose its flexibility. High tear resistance is necessary to prevent catastrophic tear propagation. High flexibility and low creep is required to maintain the dimension stability of the airship for is long life in stratosphere. Joints in the hull material are as important as the hull itself. The seam should demonstrate good tensile, peel, and permeability properties. The Table 2.1 shows the design considerations of a stratospheric airship hull materials (Zhai & Euler 2005).

Table 2.1: Design consideration of stratospheric airship hull material (Zhai & Euler 2005)

Requirements	**Criteria**
Structural	Pressure load, Safety factor • Tensile and shear strength • Tear resistance • Strength-to-weight Ratio
System	Service life • Environmental resistance (UV, ozone, temperature, etc.) • Lifting gas permeability
Material Performance	Flexing (unaffected by folding), Blocking, Inter-layer bonding
Material Producibility	Repeatable process control (consistency) Yield percentage
Envelope Manufacturability	Bondabiliy Handling
Thermal Control	Solar absorptivity, α Infrared emissivity, ε

It has been a task to accommodate all these considerations in making a single hull material.

The modern time materials have seen multi-layer composite laminate material as an airship hull material. The multi-layered laminated structure can try accommodating most of the airship design consideration due to its multi-functional nature. Therefore, every layer of the multi-layered laminate must be selected by putting a lot of thought to it. The hull must possess good strength-to-weight ratio, tear resistance, and gas retention properties. It should be UV and ozone resistant, flexible, and durable.

To achieve all these properties, the multi-layered laminate should consist of a load bearing layer that will provide maximum strength to the non-rigid airship hull structure, gas retention layer to prevent the leakage of the gas and to protect the load bearing component and other components from UV and ozone degradation. The environmental/ weathering protection layer will also protect

from environmental degradation. Previously, hull material was made using polyester and polyurethane films which were formed by polymers to which additives were added for UV stability, microorganism resistance, and hydraulic stability (Hart-Smith 2002).

Figure 2.3 gives the layout of the layers on a multilayered laminate. The environmental/ weathering protection layer is the most outer layer to protect the inner layers from degradation due to weathering. The gas retention layer is sandwiched between the load bearing component and environmental/ weathering protection layer. The inner most layer is exposed to the lifting gas and pressure. It is observed that the airship hull laminate is made up of high performance polymer, fiber, film substrates, and/or fabrics(Islam & Bradley 2012). The critical review of the materials that can be used for producing the airship hull material are discussed in the next section.

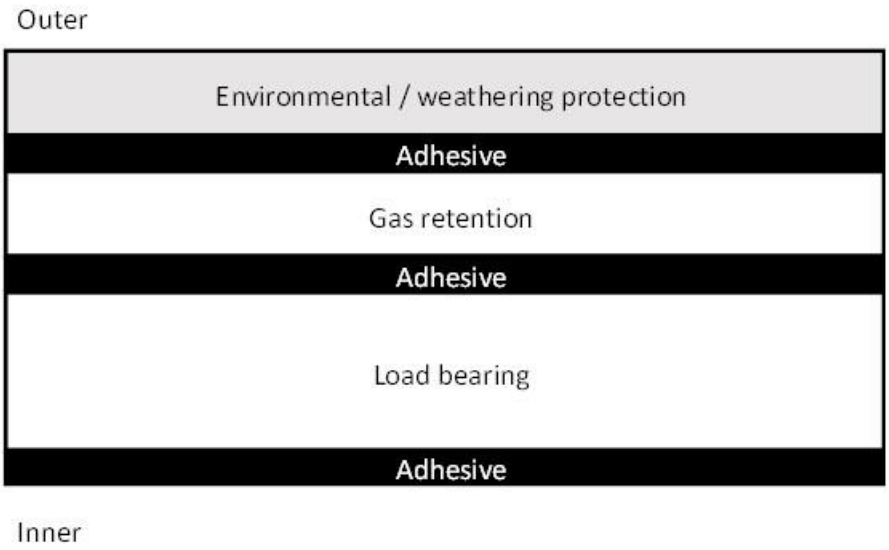

Figure 2.3: Layout of a multi – layered laminate (Islam & Bradley 2012)

2.3. Critical Evaluation of Materials for Airship Envelop

Almost all the airship hull laminates require the most important basic materials discussed in the previous section to sustain in the conditions of stratosphere. There have been only rare cases where the above-mentioned materials have been replaced with multifunctional materials to achieve similar properties. The following sections will evaluate the materials that have been used in the past and will also identify the most suitable materials depending on their properties.

2.3.1. Load Bearing Layer

A typical airship hull laminate material is a woven fabric, either single layered or multi-layered. Identification of a suitable fiber for the woven structure is a challenging aspect. With the development of the textile fibers, the selection of the fibers used for airship envelop have undergone many changes (Zhai & Euler 2005). Many synthetic fibers are now available, out of which few potential suitable candidates are given in the Table 2.2.

Table 2.2: Comparison between potential load bearing fibers (Zhai & Euler 2005)

MATERIAL		STRENGTH, g/d	PROs	CONs
M5®	PIPD	> 40	Strong, good compressive properties, excellent weatherability	Limited technical data and not commercially available
Zylon®	PBO	42	Strong	Low flex resistance, poor UV, visible light, and moisture resistance
Spectra®	PE	25-40	Strong, flexible, and good weatherability	Low melting point, poor creep resistance, and difficult to bond
Thornel®	Carbon	30	Strong, high temperature resistance, excellent weatherability	Stiff , low flex resistance, processing difficulty (weave), and very low stretch
Vectran®	LCP	23	Good overall properties and excellent cut resistance	Not as strong as Spectra® or Zylon®, poor UV Resistance
Kevlar®	Aramid	22	Strength comparable to Vectran®	Poor folding and abrasion resistance
Kosa®	PET	7-9	Tough, durable, inexpensive, fully evaluated LTA fiber	low strength

The largest non – rigid airship ever built had a load bearing component made up of two plies of polyester fabric. Even after 35 years, polyester remains the preferred fabric. This is because it has good combination of the required properties like high strength-to-weight ratio, low creep, low moisture regains and improved hydrolysis resistance (Islam & Bradley 2012). Nylon and Polyester fibers were commercialized in 1940 and 1950 respectively and the high-performance fibers became available in late twentieth century. They are defined as high tenacity (over 20g/den) and high modulus fibers (over 300 g/den). Currently, the strongest commercially available fibers are Zylon®, Vectran®, Spectra®, and Kevlar. M5® is a new developing fiber, however it is not commercially available. These new and developing commercially available fibers have drawbacks too. The cost of these fibers is high resulting in limited availability, research, and technical information. Spectra® has concerns such as stress concentration due to low extension, creep characteristics and Zylon® has concerns such as poor moisture and UV resistance (Zhai & Euler 2005). The competing fibers now have excellent properties compared to the polyester but still fail to achieve all the desirable combination of properties and in some instances have major drawback (Islam & Bradley 2012). Figure 2.4 compares the high-performance fibers.

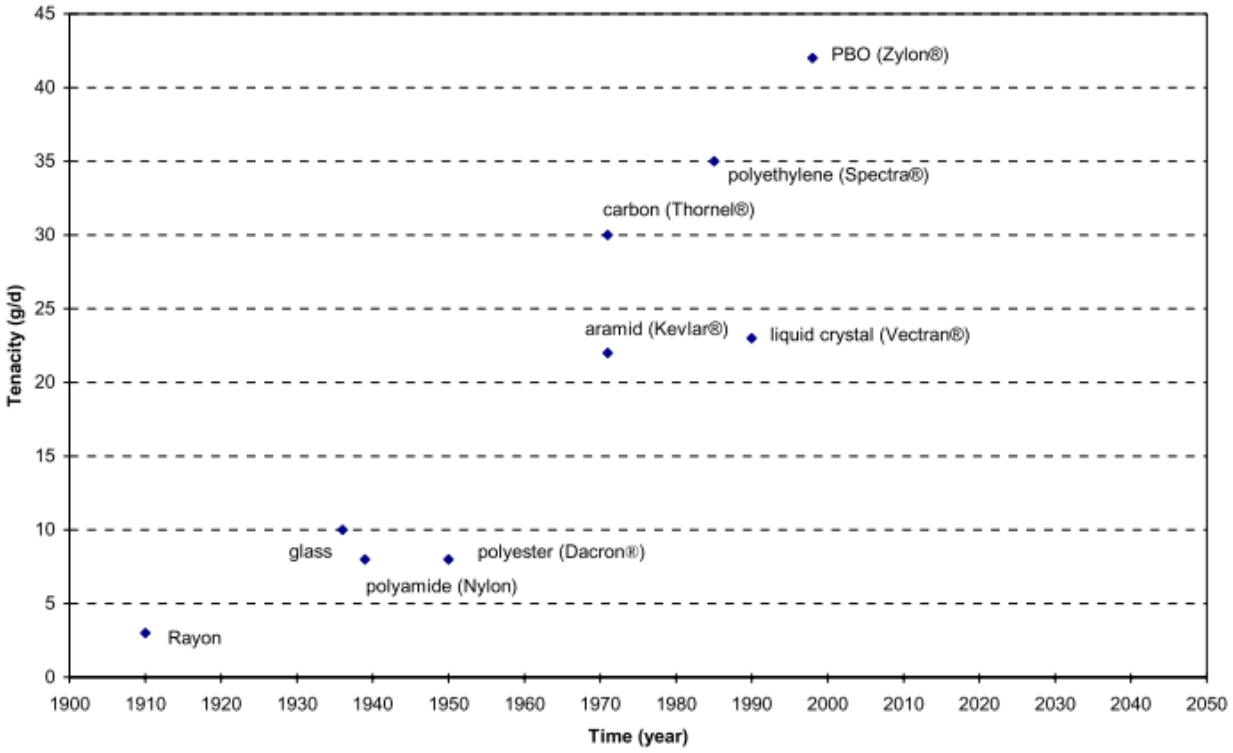

Figure 2.4: Fiber comparison over the period (Zhai & Euler 2005)

2.3.1.1. High Performance Fibers

Zylon®

Toyobo Company produces Zylon®, the strongest fiber with highest tensile strength (42 g/denier) and tensile modulus (2000 g/denier). It is a heterocyclic lyotropic polymer. It is also known as PBO (polybenzaxole) and is produced from an air – gap wet spinning process in the coagulation bath with a low spinning rate. Prolonged exposure of the Zylon® to UV or light degrades the fiber over the period (Said et al. 2006). Zylon® fiber is also expensive and show poor abrasion and flex fatigue performance, which are crucial to the inflatable aerospace applications (Islam & Bradley 2012).

Vectran®

Kuraray Company produces Vectran® fiber which is a fully aromatic polyester. They produce it by melt spinning from thermotropic liquid crystal polymers which have tensile strength of 27 g/denier and tensile modulus of 600 g/denier. Vectran® fiber is not easy to process and requires prodigious process design to weave a fabric free of faults (Islam & Bradley 2012). Still, Vectran® is an excellent choice for airship application because it has excellent abrasion resistance and flex-fatigue performance as airships need to inflate and deflate frequently for long period (Mcdaniels et al. 2009).

A high – tenacity polyallylate fiber, Vectran HT provides excellent combination if properties which are critical for airship development, structure, and performance. Vectran HT filament yarn, 1500D/300 with T97 spin finish would outperform the competing fibers like Kevlar®, Zylon®, Spectra®, or Dyneema® in dry – state testing. They provide high strength and modulus, high creep, and chemical, and abrasion resistance, with low moisture regain (Islam & Bradley 2012). Vectran® still does not provide strength as high as Zylon®

Spectra® and Dyneema®

These fibers are made from high-modulus polyethylene (HMPE) and are comparatively different than the materials familiar as polythene. In polythene generally, the long polymer chains are curled up which allows the material to stretch before failing. However, in the new fibers, the long chains have been straightened and have been placed along the fiber length. This has given these fibers much more strength but less failure strain. They are too new to have built up any long – term use but have the potential to produce the lightest fabrics with greater strength (almost half the weight

of polyester or polyamides) (Islam & Bradley 2012). The low melting point also restricts them, with a heat resistance of only up to ~150 °C. Ultra-high-modulus polyethylene (UHMWPE) fibers under the trade name of Dyneema® are very resistant to moisture and UV light (DSM 2008). This makes them better than Zylon® and Vectran®. The tradeoff of Dyneema® being with less than ideal creep, but excellent UV performance may be easier to design than the materials with opposite trade-offs. Unfortunately, there is no research yet done to develop laminated envelope material with Dyneema® fabrics for airship applications (Mcdaniels et al. 2009). These are not considered as structural materials as they are not compatible with epoxy resin, which is widely used in this industry (Islam & Bradley 2012).

Kevlar®

Kevlar® is a fully aromatic polyamide fiber. It has high specific strength, greater modulus, and much lower failure strain. It was originally developed as a cheaper alternative to carbon fibers as reinforcement for resins. They could significantly reduce the weight of an envelope, considering only strength. The only disadvantage they have is that they are subject to chemical degradation when exposed to UV radiation from sunlight. It appears that a para-aramid laminate is not able to disperse the stress concentrations, which are inevitably introduced during the manufacturing of large structures. According to conventional knowledge, the tensile deformation of para-aramid fiber is dominated by rotation of its crystallites toward the fiber axis. Tensile load application induces an immediate elastic rotation and a time-dependent creep rotation. Crystallite rotation stiffens the fiber, reducing elastic and creep compliance. Thus, the stress concentrations cannot be relieved effectively in a timely manner. The unrelieved stress concentrations can then initiate

catastrophic tear propagation. Before this problem is solved or eliminated, there will not be any further development of stronger and lighter aramid envelopes (Islam & Bradley 2012).

2.3.1.2. Load Bearing Textile Structure

During the development of the load bearing structure of the hull, maximum of the theoretic yarn strength should be transferred to the finished material. The weave patterns, processes, and other textile technologies significantly affect this component. Another factor that significantly affects the load bearing component is the load sharing between the yarns within the laminate. This factor is critical as the high modulus fibers have low elongation. Plain weave is generally chosen as it is a basic simple interlaced weave pattern that allows a lot of variations like the plain weave scrim that can be woven with various yarn sizes and counts. This can modify the tensile strength and openness of the finished fabrics. Another variation that can be done in the plain weave is the basket weave, and this provides rip-stop which improves the tear resistance of the structure (Zhai & Euler 2005). Twill and satin provide less crimp to primarily improve the in-plain properties like drape and comfort and hence are rarely used in the high-performance applications like aerospace. Usually various weave patterns are combined to give an optimized fabric performance. Bi-component, hybrid or coated yarns give unique potential to further engineer the fabric structures (Islam & Bradley 2012). Weft insertion warp knit fabric can also be used as a structure for load bearing. In this structure, the warp and weft yarns are laid over each other and are not interlaced. Hence, these fabrics do not have crimp in their structure. This structure provides improved tear resistance compared to the woven fabric (Mcdaniels et al. 2009). See Figure 2.5.

Mostly all the hull laminates with medium strength use single layer woven fabric as the structural load bearing layer. A multi-layer fabric would be required if the structure demands high strength or if multi-axial properties are required. The various layers in the multi-layer fabric can either be adhesively bonded or stitched depending upon the properties desired. These are thicker, stronger, stiffer, and heavier compared to the single layered structure (Zhai & Euler 2005). A multi-layer, multi-axial Teflon® was developed for inflatable military applications. It strength was determined to be 2000 lb./in in warp, weft, and both 45° axes. New machineries and technologies are continuously being developed in the textile industry (Zhai & Euler 2005).

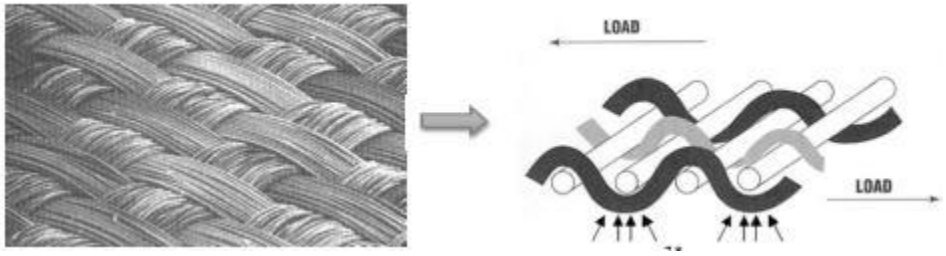

Figure 2.5: Magnified image of woven polyester and crimp diagram (Mcdaniels et al. 2009)

2.3.2. Gas Retention Layer

This component can either be a coating or a film. Early materials used coating as the gas barrier component but now, film is incorporated as a gas barrier component. A good gas retention film would give high tensile properties, ultimate elongation, low gas permeability, and excellent adhesion to other films and fabrics. The gas retention component has more than one function. In addition to low permeability, it possesses shear stiffness to enhance the overall stiffness of the laminate. It also allows bonding with the other components as it is sandwiched between them. Poor

bonding to either could result in delamination. Polyester is the preferred. High modulus polyester film (like Mylar; DuPont – Teijin) is the most common component as it has low permeability and is relatively strong and stiff (Islam & Bradley 2012).

2.3.3. Weathering Layer

Gas retention component can also behave like a weathering layer. This layer should possess properties like good shear stiffness, bonding properties, and thermal reflective and emissive properties (Zhai & Euler 2005). The environment at this altitude (20 km) closely resemble the outer space then the sea level atmosphere. Some of the consideration that must be kept in mind are that the air at this altitude is very cold, averaging – 55 °C, the sir pressure is low, 3 – 5 % of the sea level. The density is 15 to 20 % lower than that at the sea level and solar radiations are 25 – 37 % higher than that at the sea level. UV radiation is more intense and the exposed surface temperatures can drop as low as 79 °C (Baird et al. 2014). Hence materials must be carefully chosen for this layer. Table 2.3 shows different candidates for this layer.

Table 2.3: Candidate Environmental/ Gar Holding Polymeric Materials (Zhai & Euler 2005)

Material	Permeability	Weatherability	Flex Fatigue	Adhesion to Fabric/Film	Heat Sealability
PVF (Tedlar®)	Good	Excellent	Good	Poor	No
PTFE (Teflon®)	Good	Excellent	Good	Poor	Yes (> 500 °F)
Polyurethane	Fair	Good	Excellent	Excellent	Yes
Silicone Rubber	Poor	Excellent	Excellent	Poor	No
PVC	Fair	Good	Good	Excellent	Yes
Low Density Polyethylene	Fair	Fair	Excellent	Poor	Yes
PVDC (Saran®)	Excellent	Poor	Fair	Fair	Yes
Nylon	Excellent	Poor	Excellent	Fair	Yes
Polyester (Mylar®)	Good	Fair	Fair	Fair	No

2.3.3.1. Weathering Resistant Materials

Tedlar®

Polyvinylfluoride (PVF) film also known as Tedlar® (DuPont) has proven to be inert at ambient temperatures to wide range of acids, alkalis, and solvent had has resistance to degradation than most other materials (Islam & Bradley 2012). Hence, it will protect the load bearing component under it. Tedlar® also has toughness and flexibility over wide range of temperature (-72 to 102 °C) and has gas retention properties (Zhai & Euler 2005).

Teflon®

DuPont's FEP fluorocarbon film called Teflon®, offers excellent optical properties and outstanding weathering resistance. It can be heat sealed, thermos foamed, welded, metallized, and laminated to other materials. It also shows low permeability and low temperature toughness making Teflon® film a very good candidate for airship hull envelop (Zhai & Euler 2005).

Polyurethane

Polyurethane is available in many formulations and has balanced properties. It possesses high toughness, tensile, and tear strength. It provides abrasion resistance, requires much less coating weight, low temperature flexibility, good gas permeability and handling properties, crease, and weathering resistance. Thermoplastic polyurethane can be heat sealed, adhesive bonded, and laminated (Zhai & Euler 2005). TPU film is very versatile. The wide range of application of TPU films require great understanding of the surface properties and aging characteristics. That improves the stability and weatherability, which are the two important prerequisites in aggressive environments (Liu et al. 2014).

Others

Few other candidates for the weathering layer are silicone rubber, plasticized polyvinyl chloride (PVC), low density polyethylene (LDPE), and vinylidene chloride/ vinyl chloride copolymers. Silicone rubber has low temperature flexibility but does not provide low gas permeability, toughness, and abrasion resistance. PVC is used in commercialized coated fabrics. It provides resistance to weathering (5 years) and is heat sealable, but few of its disadvantages are that it gives low temperature flexibility and is expensive. LDPE is flexible and heat sealable polymer which is normally coextruded with other films to improve the gas permeation. It has been reported in the literature that lightweight LDPE/ Mylar®/ polyester fabric laminate has been used in super pressure balloon applications in the past. Vinylidene chloride/ vinyl chloride polymers are also good barrier materials and have their application in the packaging industry. However they are not recommended for use in the aerospace application as they have poor flex life, specially at low temperatures (Zhai & Euler 2005).

Triton Oxygen Resistant (TOR) polymers are thermoplastic polymers that have potential as weather resistant films or coatings in stratosphere. They are resistant to atomic oxygen, ozone, and ultra – violet radiation. These polymers are currently being tested at NASA. TOR have unique ability to form outer oxidized layer which has the potential to protect against abrasion and will reform if any surface damage occurs (Zhai & Euler 2005).

2.3.3.2. Weathering Treatments

UV Radiation

For an airship to stay in stratosphere for long durations, it should be able to resist the intense radiations. The airship hull material must not only be resistant to UV radiations, but should also be able to block the radiations from transmitting through. Airships have started using high performance fibers, to build the load bearing layer, which are mostly UV radiations and visible light sensitive. Significant reduction in strength is observed in high performance fibers when exposed to UV radiations (Said et al. 2006). Therefore, this can be a major issue in development of an airship. Researchers have been investigating ways to resolve this issue. In one study, sheath structure containing UV inhibitors were found to be highly effective in improving UV-visible resistance of PBO braids (Vallabh et al. 2016). Nakadate et al., Maekawa et al., Kurose et. al, and Kitida at al. investigated the long-term weathering characteristics on the high strength and light weight envelope material made from Zylon®. A two yearlong out door exposure was carried out on the material made with Zylon® fibers which was a long stratospheric platform airship. The results showed a unique seasonal effect on the tensile strength due to weathering. It was specifically observed that the substantial decrease in tensile strength occurred during late spring to early fall of the second year as well as the first year. Negligible decrease took place in other seasons. This suggested that the high humidity and/or temperature during these seasons were/was the cause of decrease in tensile strength. A six month long supplemental outdoor exposure test was conducted to evaluate the separate humidity effect from temperature effect. See Figure 2.6.

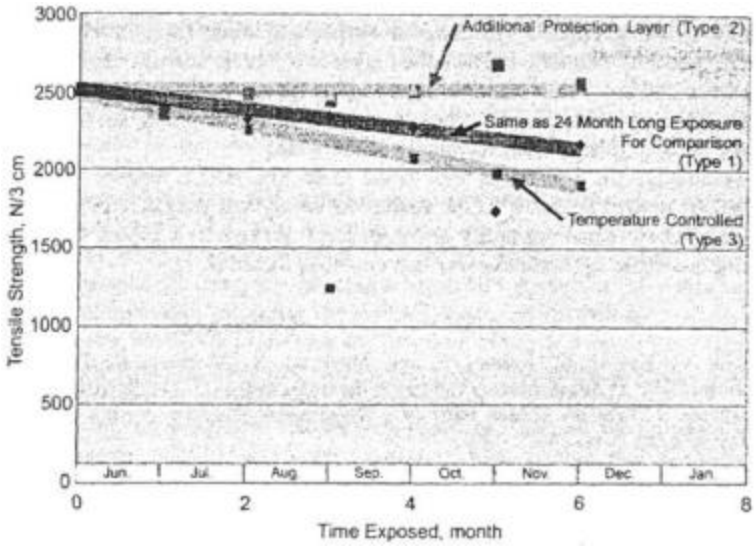

Figure 2.6: Summary of supplemental outdoor exposure test, effects of an additional protection layer, humidity, and temperature (Mcdaniels et al. 2009)

The test results suggested that humidity was the primary factor causing the decrease in tensile strength. The tensile strength of the material with an additional protection layer, which was the evaporated Aluminum Tedlar®, decreased as negligibly for months as that with humidity controlled (Type 4). The added layer to the outer surface might have reduced the overall permeability of the material and might have blocked the humidity from penetrating. However, since the primary effect of the aluminum evaporated Tedlar® protection layer, the effect of light should be separated from other factors in the future. This study concluded that dried air needs to be filled in final airship assembly before launching to the stratosphere where there is no moisture. This was to keep the strength and shape maintained. Moreover, it was also recommended that the addition of one thin layer or two for example, aluminum coating, with low permeability to gas and vapor could be effective in resisting the moisture.

Ozone and Atomic Oxygen Degradation

The airship materials bear a long time high – low temperature cycle, UV radiation, and ozone ageing and other environmental factors near space. All these factors affect the airship materials not leaving behind the ozone. Ozone is a strong oxidant and catalyst and hence could accelerate the ageing and brittleness of envelop materials. Maekawa et al. and Takegaki et al. studied 24 hours ozone ageing at 50 ppm ozone concentration on Zylon® fabric composite and found that the strength decreased by 10 %. Lin et al. and Tan et al. studied the ozone ageing of PE – EVOH (ethylene – vinyl alcohol copolymer) at 600 ppm ozone concentration (Lin & Tan 2011). It was concluded that the ozone had significant influence on the mechanical properties. The tensile strength decreased by 43.5 % and the Young's modulus decreased by 76.9 % after 144 hours of ozone exposure (See Figure 2.7). FTIR spectra of PE – EVOH showed that there was some chemical reaction that occurred between the film and ozone. New functional groups were generated. AFM films showed "etching" occurred on the surface of the film due to ozone (Lin & Tan 2011).

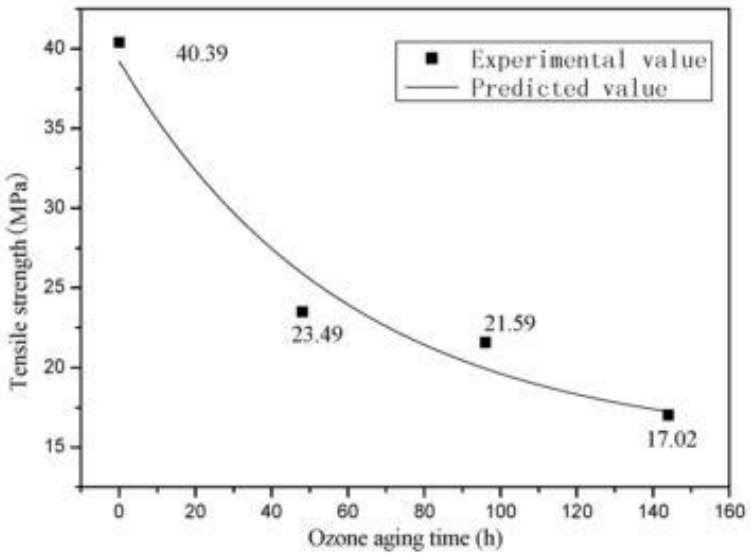

Figure 2.7: Tensile strength of PE – EVOH film under different ozone ageing time (Lin & Tan 2011)

Temperature Cycle

Managing the thermal balance of the lifting gas within the airship is the key to a successful airship. The atmosphere winds affect the stratospheric winds as well as the stratospheric temperature. The difference between the monthly maximum and minimum temperature in winter can exceed 50 K, whereas in summer, the variability is small at the poles typically plus minus 10 K in midlatitudes as well as the tropics throughout the year (Baird et al. 2014). Changes in the airship diurnal temperature system significantly affect the vehicle altitude control, power consumption as well as the airship ballonet materials. To minimize the system thermal control, a low solar absorptivity with a high infrared emissivity, that is low α / ε ratio, is desirable. A white non – metallic surface would be good, but a better choice would be transparent non – metallic surface with a shiny metallic backing. Table 2.4 below compares several material combinations. According to Table

2.4, metallic finished lab coupons demonstrated excellent thermal control parameters (Zhai & Euler 2005).

Table 2.4: Material Surface Thermal Properties (Zhai & Euler 2005)

	α	ε	α/ε
White Tedlar®	0.3	0.85	0.35
Silvered Teflon®	0.08	0.6	0.13
Quartz over Silver	0.077	0.79	0.10
LTA hull coupon	0.07	0.75	0.09

Maekawa et al. investigated the effect of temperature on Z2929T-AB airship envelop material. The strength of the laminates and seams were tested at low and high temperature levels. The results of this test are shown in Figure 2.8. It is clearly observed that the strength of the laminate as well as the seams degraded with increase in temperature. Hence, it is important to have a thermal control to maintain the airship material at a comparatively lower temperature to prevent strength degradation of the laminate or seams due to high temperature (Maekawa et al. 2008).

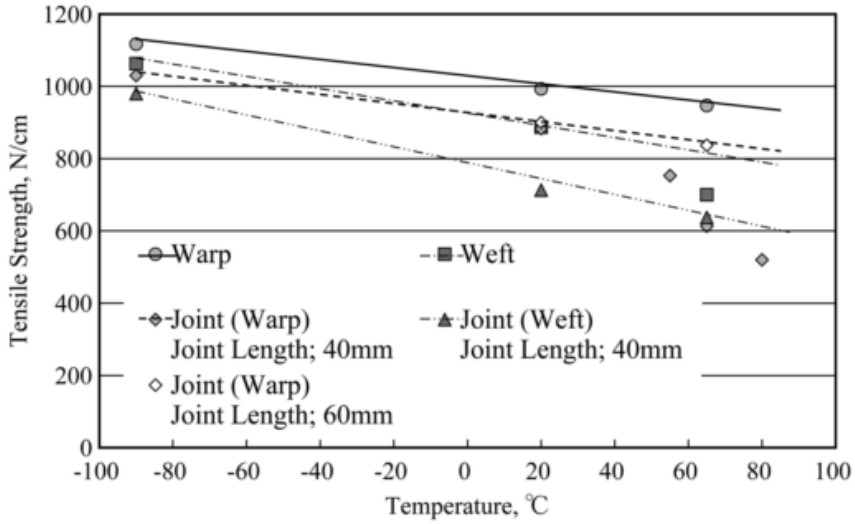

Figure 2.8: Tensile strength of Z2929T-AB and its seams in warp and weft directions (Maekawa et al. 2008)

2.3.4. Adhesive

Adhesive is the bonding agent that holds the layers within the laminate itself as well as it is the agent responsible to make joints It is an aid in manufacturing of the material and also reliability to make good joints/ seams (Islam & Bradley 2012). Adhesives are tougher and more ductile compared to the resin systems used and consistency in bond line thickness is important. There are different forms of adhesives. There can be epoxy films, or epoxy films with fiber scrims within it, or in the form of microbeads. A god bond will be formed when the adhesive can wet the surface and when the surface roughness allows mechanical interlocking of the adhesive (McConnell 1999). The choice of adhesive with such capabilities is very limited, Hytrel®, polyester elastomer manufactured by DuPont is one of the successful materials. It acts as a bonding agent and also reduces the permeability of the laminate (Islam & Bradley 2012).

Adhesives require aggressive solvents to be used during the manufacture of the laminate. This has cause some problem in the past as few solvents could not be used due to health and safety regulations. This has caused the need for using expensive replacements. Figure 2.9 below shows butt joint. This joint as heated and cooled under pressure. The butt joint was made with a special tape called the butt strap. This strap carries the load across the joint, where the outer strip behaves as the environment/ weather resistant which protects the joint against the environment. The butt strap tape is woven to have high strength across the width. When it comes to the polyurethane-coated materials, the joints made of the laminates are stronger than the laminates itself. In testing, a normal failure should be found in the base material and not the seam (Islam & Bradley 2012).

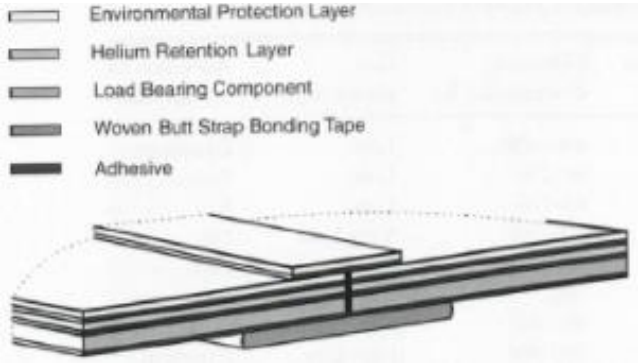

Figure 2.9: Section through a typical laminate material joint (Islam & Bradley 2012)

Multi-layered structures can achieve the desired properties the most. The only disadvantage of multi-layered structure is the addition of the weight of every layer used. New machines and technologies like co-extrusion is helping in eliminating the use of adhesive to bond the different layers, thus reducing the overall weight but maintaining crucial properties like adhesion, gas retention, and weatherability. Other technologies like polymer blending can combine the characteristics of multilayered fabric into a single layer. Polymers containing inorganic adhesives

and surface coatings (plasma) can reduce the gas leak. All these new technologies are currently being used in the packaging industry (Zhai & Euler 2005).

2.4. Airship Seam Component

Adhesive bonding is a material joining process in which an adhesive is placed between the two surfaces. The adhesive solidifies to produce an adhesive bond. Adhesively bonded joints are alternatives to the mechanical joints in engineering applications. The advantages of adhesive bonded joints are lower structural weight, lower fabrication cost, improved damage tolerance (Zhai & Euler 2005), high corrosion and fatigue resistance, crack retardance, and good damping characteristics (Tsai et al. 1998). They also have advantages like the good strength-to-weight ratio, design flexibility, and ease of fabrication. The application of these joints has increased significantly in recent years (Banea & da Silva 2009). Adhesive bonding has found applications in various areas such as aeronautics, aerospace, electronics, and automotive to construction, sports, and packaging. Structures can be made by using different fiber and its architectures, weaves, and resins (Banea & da Silva 2009). Adhesive bonded joints are expected to sustain static or cyclic loads for long period without having any adverse effect on the structural integrity (Chamis & Murthy 1991) and on the load-bearing capacity (Banea & da Silva 2009).

2.4.1. Seam Properties

Development of seam is as critical as development of base hull material. The airship envelope carries the load, and hence the seam should be able to transfer load from one part of the base material to the other part. There are various types of forces acting on the seam like the tensile and shear forces. The seam should be able to absorb stresses and have high fracture strength at the

operating temperature. The tensile strength of the seam should be equal or greater than the strength of the base hull laminate to give the airship envelope a structural efficiency and overall integrity (Zhai & Euler 2005).

In addition to the strength requirement, the seam should also be able to withstand the low temperatures cycles so that the joint integrity and durability is not affected. Thermal cycling effects and internal stresses are other important factors that affect the seam. Different coefficient of thermal expansion and thermal conductivity between the adhesive and the base material can result in residual stresses. Adhesive polymer bulk properties play a major role here. It is a fact that above Tg, the flexibility and toughness increases, whereas, the tensile strength and the elastic modulus decreases. Therefore, it is extremely important to predict the relationship between the Tg of the polymer and the service temperature for predicting the performance of the polymer. Trapped gases and volatiles evolved during the bonding process can also give rise to stress concentration in the joint structure. The effect of these internal stresses gets magnified at low temperatures and this can lead to seam failure (Zhai & Euler 2005).

2.4.2. Seam Types

In adhesive type joints, two materials, also known as adherends, are bonded together by an adhesive. Generally, epoxies are used, but adhesives like bismaleimides can also be used (McConnell 1999). There are basically two ways of seaming the airship hull laminate, one is lap seam, and the other one is butt seam. The Figure 2.10 shows the difference between the two. The lap seam is a simpler design than the butt seam, but for this type of seam, the base material should structurally be bondable from both the sides (Zhai & Euler 2005). The other types of adhesive

joints are, bevel joint, step joint, single strap joint, and scarf joint shown in Figure 2.11. Bevel, scarf, and double lap are irrelevant to airship seam. When the resin flows inside the joint a small fillet is often made. This fillet should not be removed as it reduces the stress concentration (McConnell 1999).

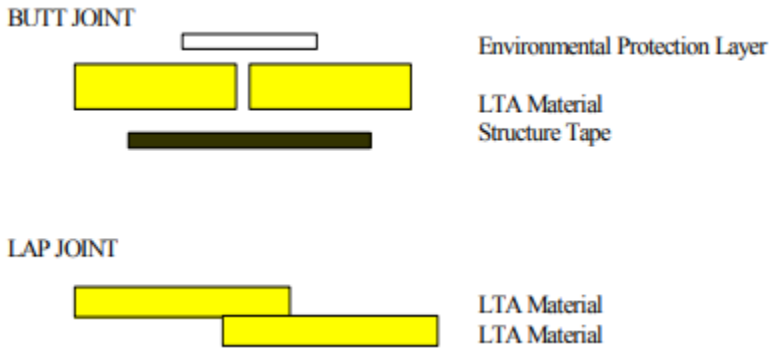

Figure 2.10: Typical joint designs (Zhai & Euler 2005)

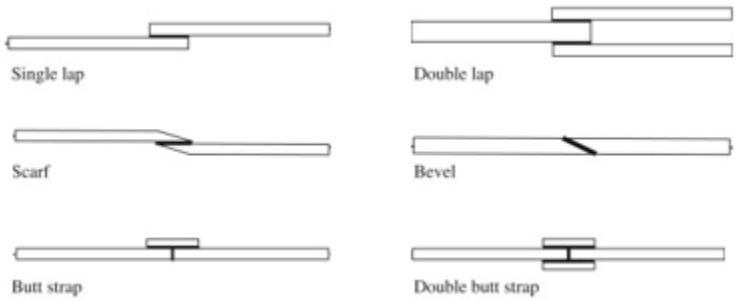

Figure 2.11: Various joint designs (He 2011)

The most common type of adhesive joints are the lap joints. One major disadvantage of the lap seam is the bending effect. This disadvantage can be overcome by incorporating double lap design (Figure 2.11).

2.4.3. Seam Fabrication Techniques

There are several different methods for fabrication of the airship envelop. Every fabrication technique has some key parameters that after the seam quality.

The ultrasonic welders produce a continuous/ static weld in the thermoplastic materials. In this technique, the material is fed by a feeding mechanism, and a series of rollers subject the material to ultrasonic vibrations that heats the materials while being under pressure (Zhai & Euler 2005). The parameters that affect the process are sealing temperature, amplitude of the ultrasonic vibrations, and the sealing force. The sealing time can be from a few milliseconds to several hundred milliseconds. The advantages of this technique are short sealing time, less exposure to the heat, and cooling under pressure. However, this is not the best technique to fabricate seams (Bach, Sascha; Thurling, Karsten; Majschak 2010). This requires relatively thick coated peel media (Ernest 1994). RF welders produce static and semi – continuous welds in the thermoplastic materials (Zhai & Euler 2005). Thermal welders produce a seal using an external heat source and pressure on the material (Zhai & Euler 2005). HF (high – frequency) dielectric heating technique has been used many times in the past for welding joint (Yang et al. 2015a).

Adhesive bonding applies a structural adhesive such as polyurethane, epoxy, acrylic, etc to bond two surfaces with or without applying pressure (Zhai & Euler 2005). This technique is most suitable to the fibrous composite structures because of their brittleness. Some remarkably efficient bonded composite joints have been developed in the past out of which the most notable was the stepped-lap carbon-epoxy-to-titanium joint at the wing-root of the F/A-18 Hornet aircraft. Adhesive bonding needs precision while manufacturing it but couple of its advantages are that it

is cheap and has got trouble-free service record (Hart-Smith 2002). It gives more uniform load distribution, resistant to fatigue and vibrational stresses, can bond thin, irregular surfaces, and give negligible weight penalty (McConnell 1999). Joining stronger materials is much more challenging than joining the medium strength materials (Zhai & Euler 2005).

Airships traditionally are 'ellipsoidal' with circular cross – section and elliptical or streamline profile. The traditional method to make airship envelope is to form long identical longitudinal panels called 'gores' extended all the way from nose to tail. The seams are then the lines from nose of the airship to the tail being the poles. The more number of gores, the smoother the surface of the airship would be when inflated and pressurized. Less number of gores are not recommended as the seams would wrinkle at the flat gores and will try to accommodate to the double curvature of the ellipsoidal form. Also, care must be taken while cutting the gores. Any inaccuracy in the gore would later get multiplied by the number of gores in an airship. Figure 2.12 shows wrinkle at the seam due to lack of care taken during cutting the gores (Sherwood 2006). Also, once the design of the joint is finalized, the strategically selected experiments should be performed to verify the joint design (Chamis & Murthy 1991).

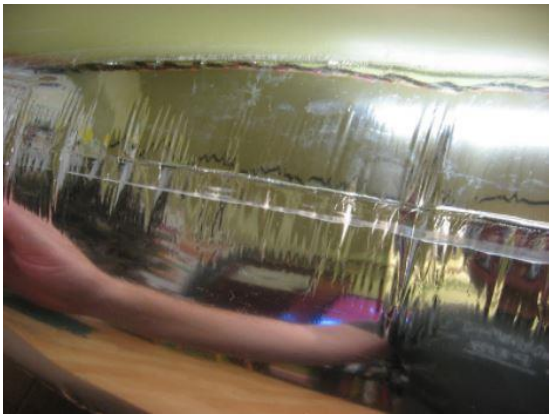

Figure 2.12: Wrinkled lap seam demonstration (Sherwood 2006)

Therefore, design and development of seam with an appropriate seaming technology is a major challenge for high strength airship envelope material.

2.4.4. Adhesive and Failure Modes

Polymers with low Tg are more resistant to low temperatures. Several adhesives can work well at low temperatures like, Polyurethane which has the best low temperature properties compared to the other commercially available adhesive. It can also be easily processed and bonds well with other materials. Silicon adhesives too have good properties over wide range of temperatures. Silicon joints are good when the peel property is the primary loading compared to tensile or lap shear properties. Rubber based adhesives also demonstrate useful properties at low temperatures. These include butyl, neoprene, and polysulfide rubbers. These adhesives generally retain their flexibility between – 50 $^{\circ}$C and 60 $^{\circ}$C. Modified epoxies are selected when then silicone and urethane adhesives are not suitable. Thermosetting acrylic resins are generally considered excellent adhesives at temperature as low as 40 $^{\circ}$C (Zhai & Euler 2005).

Figure 2.13 shows various types of failure modes. Unacceptable failure modes mean that the poor bonding is due to poor adhesive itself. This section of the failure modes includes adhesion failure of adhesive at the adhesive – adherend interface. The adhesive does not bond at all to one of the adherends. The second type of unacceptable failure mode of adhesive is the adhesive peel. This type of failure is observed due to excessive out – of – plane loads. And the last type in this category is the adhesive creep type. Here the two adherends just come off and separate from each other demonstrating poor bonding. The acceptable failure modes do not conclude that the adhesion between the adherends is poor or the adhesive properties are not good. These type of failure modes are obtained when the adhesion between the two adherends is good. One type of failure mode here is the cohesive type of failure. Here, the adhesive has bonded well to the adherends but failure occurs as the adhesive is not able to bear the load that is applied to it during testing or in the real scenario. The second type is the delamination type. Here too, the adhesive is bonded well to the adherends and failure occurs within the adherend, demonstrating poor adherend property. Adherend itself failing would show that the seam is good and can transfer load from one adherend to the other without failing (McConnell 1999).

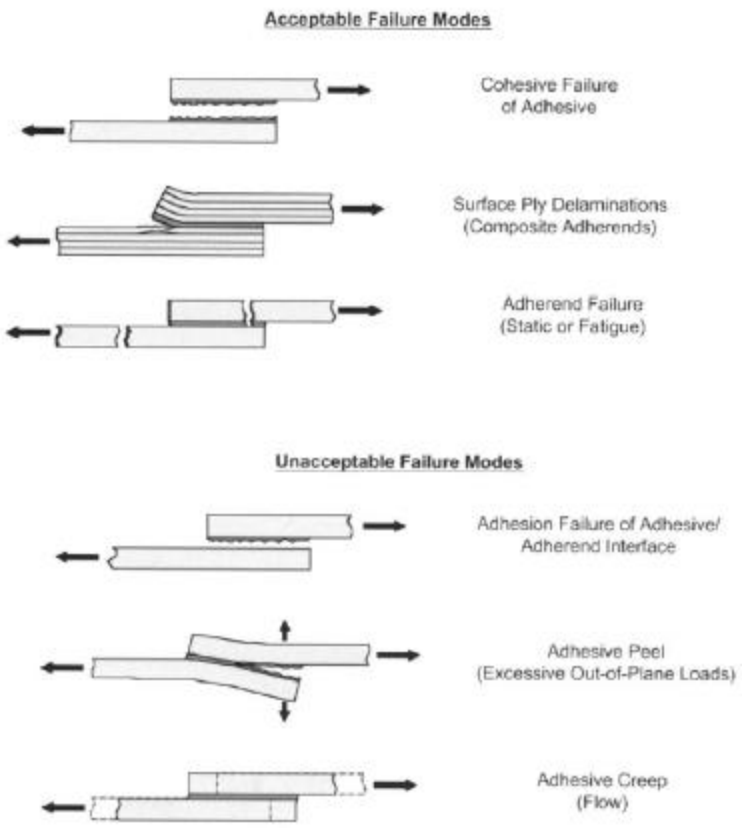

Figure 2.13: Acceptable and unacceptable failure modes (McConnell 1999)

2.4.5. Method of Seam Performance Evaluation

This section gives a few examples of how the seams or joint structures were tested and what test methods were used.

2.4.5.1.Tensile Property

Tang et al. and Keefe et al. tested the tensile property of the double tape polyester seam. This seam was composed of two polyester base laminates, a polyester structural tape, and a polyvinyl fluoride cover tape. The structural tape itself was a laminated fabric, and this tape was heat bonded to the base laminate. The other side of the base laminate was bonded to the cover tape using a polyester

urethane adhesive. The base laminate consisted of a plain weave polyester fabric (1000 denier, 81 x 21 count), a layer of polyester film, polyvinyl fluoride film with several other adhesive layers.

They compared the strength of the seam to its base laminate. The testing was carried out on Instru-Met machine based on the ASTM standard test method D5035-95 for breaking force and elongation of textile fabrics. This test method was also recommended for determination of the breaking force and elongation of coated fabrics. The width and the length of the specimen were 50.8 mm and 152.4 mm with the testing speed of 50 mm/min (Tang & Keefe 2003).

Under tension, the seam specimens failed due to the tension and bending in produced in the base laminate. See Figure 2.14. It was evident that there was degradation in the strength of the seam (average breaking force: 2389.1 N) compared to the strength of the base laminate (average breaking force: 2787.3 N). Out of the total 42 seam samples, 41 failed at the edge between the structural tape and the base laminate, and the remaining one failed in the outer base laminate (Tang & Keefe 2003). The tensile strength in the seam was determined by the magnitude of actual stress in the base laminate and the stress concentration factor. The lower the stress concentration of the seam, the higher the strength of the seam (the strength of the seam will be closer to the strength of the laminate). This research considered two structural modification (geometric change and material change) to improve the tensile property of the seam. One was to increase the width of the cover tape (mitigate the stiffness and geometrical discontinuity at the edge of the structural tape), and the other was to replace the polyester structural tape with nylon structural tape (reduced stiffness, more extensible material). The material modification improved the strength of the seam

from 86% to 94% of the strength of the base laminate. This was one of the example of how a seam was tested for its tensile property.

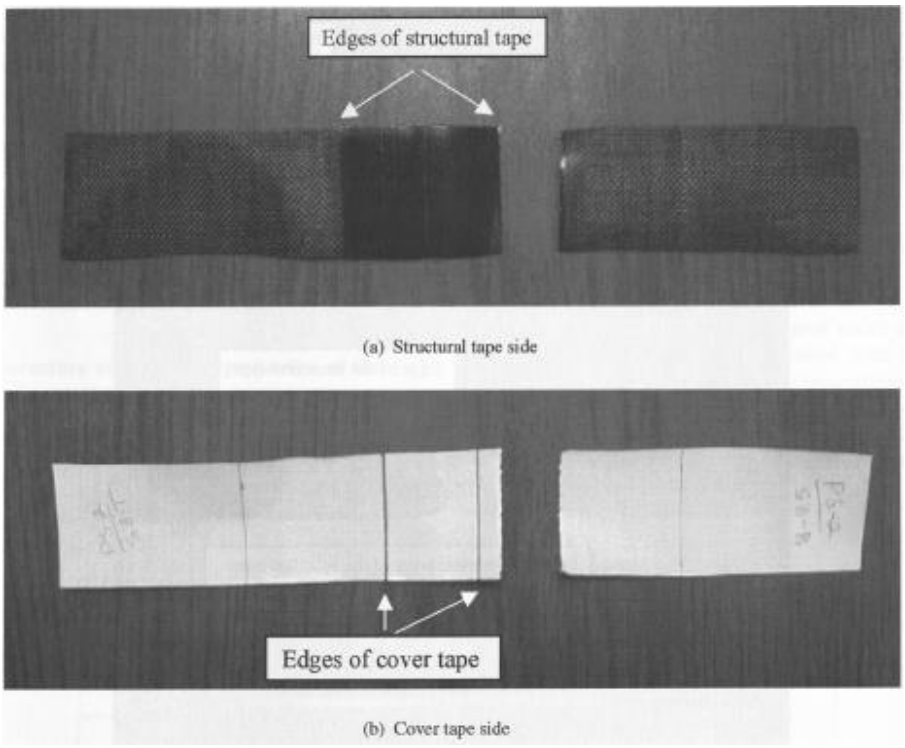

Figure 2.14: Two typical seam failure ((b)giving higher values than (a)) (Tang & Keefe 2003)

2.4.5.2. Peel Property

Yang et al., Zeng et al, and Lei et al. studied the T – peel behavior of coated fabric films used in inflatable structures. The materials used for this study were plain weave nylon fabric coated on both the sides with thermoplastic polyurethane (TPU) elastomer (0.6mm thick) as this material is widely used to fabricate inflatable materials. HF (High -Frequency) dielectric heating apparatus was used to weld the samples together with various setting of welding parameters (Yang et al. 2015b). The test specimen is shown in the Figure 2.15.

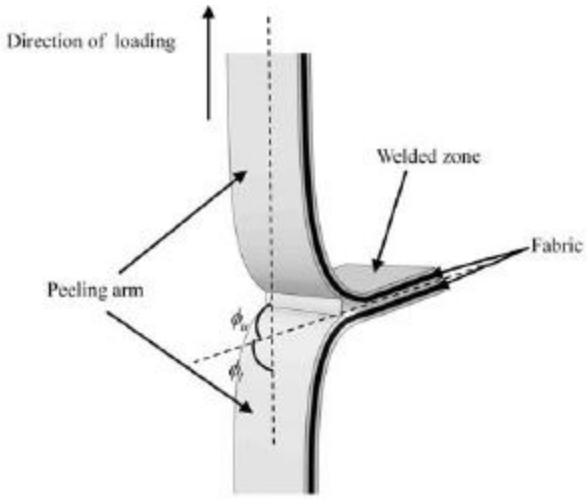

Figure 2.15: T – peel Test (Yang et al. 2015b)

Three different failure modes were observed with the change in welding parameters. In the first failure mode, the joined TPU coatings were torn away. This was known as intralaminar fracture. For this type of failure mode, the heat produced at the welding interface was not sufficient to make the TPU coatings mix adequately, and hence the fracture force was very low (Yang et al. 2015b). The second mode was observed when the melted TPU coatings were mixed with each other more adequately under the pressure. Fracture took place at the interface of the coating and the fabric. This type of fracture was called interlaminar fracture. The third mode was the strength of the welded zone exceeded that of the parent material, with a failure mode in which the parent material itself. This mode gave the highest fracture force among all and was called fiber fracture (See Figure 2.16). Figure 2.13 shows the different failure modes (Yang et al. 2015b).

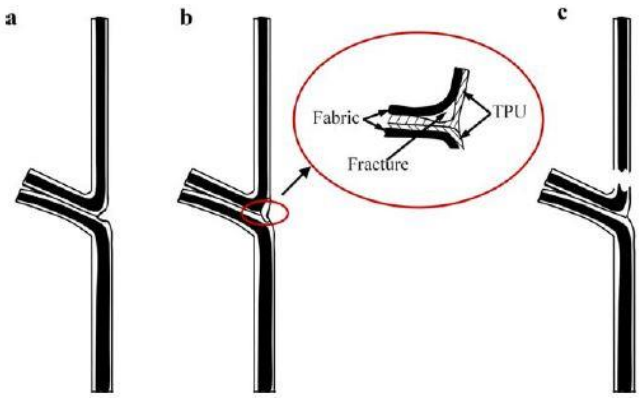

Figure 2.16: Failure modes in T – peel test. (a) intralaminar fracture, (b) interlaminar fracture, and (c) fiber fracture (Yang et al. 2015b)

Farris et al. investigated through the design of experiments the influence of temperature, dwell time, and bar pressure on the heat seal strength of oriented polypropylene films which were coated with gelatin – based thin layer. This study's approach allowed understanding of the effect of every factor on the two responses, namely, maximum force, and strain energy. The factor that affected both the responses negatively was the bar pressure. Whereas the temperature affected positively. Dwell time did not give any significant effect as a main factor (Farris et al. 2011). For responses see Figure 2.17.

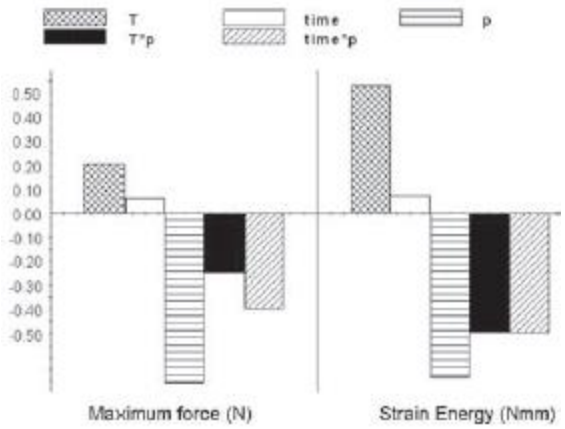

Figure 2.17: Coefficient overview plot for the two responses (maximum force and strain energy)

(Farris et al. 2011)

3. MOTIVATION AND OBJECTIVES

Considerable work has been done in the past to develop airship hull materials which were resistant to stratospheric weathering conditions and at the same time provided high strength-to-weight ratio. However, the literature lacks in developing high performance airship hull seams and its evaluation. The objective of this research was to conduct seam optimization by using experimental design and considering three different overlap seam lengths, and low and high seaming temperature, pressure, and speed. This experimental design would help evaluate the effect of varying overlap seam lengths, and seaming temperature, pressure, and speed on seam tensile strength. Another experimental design was used considering just the low and high seaming temperature, pressure, and speed, keeping overlap seam length constant. This would evaluate the effect of varying seaming, temperature, pressure, and speed on the seam peel strength. Weathering of seam has not been conducted so far. Therefore, this study will also focus on evaluation of effect of ozone concentrations and temperature cycles on seam tensile strength.

Solar cap fabric and harness are some recent developments seen in airship manufacturing. The objective of this research was also to expose the solar cap fabric, harness A, and harness B to UV radiations and ozone concentrations separately, and only solar cap fabric to both UV radiations and ozone concentrations. This would evaluate the degradation in the strength of the solar cap fabric and harness A and B after exposing them separately to UV radiation and ozone concentrations. It would also evaluate the combined effect of UV radiations and ozone concentrations on the solar cap fabric.

4. EXPERIMENTAL

This chapter would give detailed information about the materials and methods used to prepare seam samples, and equipment and standard test methods used to test them. It comprises of materials, design of experiments conducted for testing the tensile and peeling properties of the seam, and details of seam fabrication. This chapter will also give information about the protocol followed for weathering of solar cap fabrics, harness A, and harness B and the equipment and standard test methods used to test them.

4.1. Materials

4.1.1. Airship Hull Laminate

The laminate used as the airship's hull component was supplied by an industry. NCSU/SCEYE research team has designed the structure of the laminate along with the material selection except for the adhesive, which is the industry proprietary material. The structural design of this laminate is given in the Figure 4.1. This laminate had a multi-layered structure with the load bearing layer made of Zylon® (PBO) fibers. Industry proprietary adhesive was used for bonding the gas retention layers within the laminate. The first gas retention layer was made of a thin Polyethylene Terephthalate (PET) film, also known as Mylar®, with a Vacuum Deposited Aluminum (VDA) coating applied over it. The second gas retention layer (the weathering layer), was made of Polyimide (PI) film, also known as Kapton®, with VDA coating applied on both sides. The Corrosion Resistant Coating (CRC) is the outer most coating of the weathering layer to protect it from any degradation. Thermoplastic Polyurethane (TPU) adhesive film was used to seam the laminate. Further details of the materials are given in the following sections.

Figure 4.1: Laminate Structure

4.1.1.1. Load Bearing Layer - Zylon® fabric

The load bearing layer within the airship hull material was made using high – performance Zylon® produced and supplied by Toyobo Co. Ltd and a fabric was woven from these yarns by Textum Inc per NCSU team construction design. Zylon® was used as it is the strongest commercially available fiber with high modulus and tenacity. The specifications of the Zylon® fabric are given in the Table 4.1. It shows that the load bearing component of the laminate was made using plain weave of twisted Zylon® yarns with a liner density of 150 denier.

Table 4.1: Specifications of Zylon® Fabric used in industry proprietary laminate

Warp Yarn	150 Denier/ 99 fil/ 2.7 tpi/ Zylon®
Weft Yarn	150 Denier/ 99 fil/ 2.7 tpi/ Zylon®
Warp Density	38 epi
Weft Density	38 ppi
Weave Type	Plain Weave
Area Density	52.6 GSM
Thickness	120 µm
Crimp (Warp/ Weft)	1%/ 2.3%

4.1.1.2. Industry Proprietary Adhesive

Industry propriety adhesive was used to bond the load bearing Zylon® fabric to the gas retention films, Mylar® and Kapton®.

4.1.1.3. Gas Retention Polymer Films

Two polymer films were bonded to the Zylon® fabric using the industry proprietary adhesive. Kapton® film was bonded to the outer side if the Zylon® fabric, whereas the inner side was bonded to Mylar® film.

Mylar®

Mylar® is a PET film used as the inner gas retention layer of the airship hull laminate. Its properties like high tensile strength, shear strength and low permeability makes it a perfect layer to be placed at the innermost side of the airship laminate structure. However, few of its disadvantages are that it is stiff with least tear resistance compared to another polymer films. It is also difficult to bond.

Kapton®

Kapton® is a PI film used as the outer gas retention layer of the airship hull laminate, which is coated with VDA on both the sides. This layer is further coated with CRC on the side that would be exposed to weathering. Kapton® has high modulus and gas barrier properties and is highly resistant to weathering.

4.1.1.4. Vacuum Deposited Coating (VDA) and Corrosion Resistant Coating (CRC)

The purpose of using VDA coating is to protect load bearing layer, made of Zylon® fiber, from degradation due to UV radiations, Ozone, visible light, and varying heat. CRC also provides resistance to degradation and corrosion due to weathering. Zylon® fiber is sensitive to visible light, UV radiations, and moisture, and hence these coatings are important for a good airship laminate.

4.1.2. Thermoplastic Polyurethane (TPU)

The adhesive film used to make seams out of the laminate was Thermoplastic Polyurethane (TPU) film. Some properties that make TPU film a good adhesive are, outstanding toughness with high tensile strength, tear strength, and abrasion resistance. It has less coating weight, low temperature flexibility, fair gas permeability, good handling properties, and good resistance to weathering. EXF-951 adhesive film was used to seam the laminates. EXF-951 is a single layer of solvent free thermoplastic ether based polyurethane adhesive polymer extruded onto a paper release liner and supplied in various widths and thicknesses. The general and mechanical properties of this adhesive are given in Table 4.2.

Table 4.2: Specifications of EXF-951 adhesive film

	Method	**Value**
GENERAL		
Composition		Polyurethane
Shore Hardness A		83
Specific Gravity		1.105 g/cc
Thickness		50.8 µm
Taber Abrasion H-18 Wheel, 1000-g load, 1000 cycles		30 mg Loss

Table 4.2 (continued).

Bayshore Resilience		45%
MECHANICAL		
Tensile Strength		4500 psi (31 Mpa)
Tensile Stress (100% elongation)		800 psi (5.5 MPa)
300% elongation		1200 psi (8.3 Mpa)
Ultimate Elongation		670%
Melt Point	Gradient Heat Bar	-135 °C – 145 °C
Tg	DMA	-46 °C
Appearance	Visual	Water clear

4.2. Seam Experimental Design

Experimental design aims at predicting the outcome by introducing change of pre-conditions, which can be represented by one or more 'independent variables' (input variables). The change in these variables is hypothesized to result the changes in one or more 'dependent variable' (response variable). Experimental design is conducted to determine the effect of independent variable on the response variable. Therefore, in this study, multiple independent variables will be investigated simultaneously to evaluate their effect on the response variable. The independent variables considered to optimize the seams were, seaming temperature, pressure, speed (dwell time) and overlap seam lengths. Two levels were selected for every independent variable based on pre-trials (see Appendix A). 155 °C and 185 °C for temperature, 100 kPa and 400 kPa for pressure, and 3 m/min and 6 m/min for speed, and 2.54 cm, 7.62 cm, and 12.07 cm for seam overlap length.

4.2.1. Experimental Design for Seam Tensile Property

Table 4.3 gives the details of the first experimental design developed to evaluate the tensile property of the seam. The independent variables selected were low and high levels of seaming

temperature, pressure, speed, and three different overlap seam lengths. The response variable was tensile strength of the seams.

Table 4.3: Experimental design to evaluate the tensile property of seams

Variables	Levels
Temperature (°C)	155 °C and 185 °C
Pressure (kPa)	100 kPa and 400 kPa
Speed (m/min)	3 m/min and 6 m/min
Overlap Seam Length (cm)	2.54 cm, 7.62 cm, and 12.07 cm
Total Runs = 2 x 2 x 2 x 3 = 24	

4.2.2. Experimental Design for Evaluation of Peeling Property

Table 4.4 gives the details of the second experimental design developed to evaluate the peeling property of the seam. The independent variables selected were low and high levels of seaming temperature, pressure, and speed, keeping the overlap seam length variable to 2.54 cm. The response variable was peeling strength of the seams.

Table 4.4: Experimental design to evaluate the peel property of seams

Variables	Levels
Temperature (°C)	155 °C and 185 °C
Pressure (kPa)	100 kPa and 400 kPa
Speed (m/min)	3 m/min and 6 m/min
Total Runs = 2 x 2 x 2 = 8	

4.2.3. Experimental Design for Seam Weathering

Table 4.5 gives the details for the third experimental design developed to evaluate the effect of weathering on the seam strength. 50.8 µm thick TPU adhesive was used with the interface being PI – TPU – PI. Seaming was carried out on Kannegiesser GmbH & Co. D– 4973 VLOTHO fusing machine to evaluate the seam tensile strength after weathering. Seaming pressure and speed was set to 400 kPa and 6 m/min, respectively.

Table 4.5. Experimental design to evaluate the effect of weathering on seam tensile strength

Variables	Levels
Temperature (°C)	155°C, 185 °C
Overlap Seam Length (cm)	7.62, 12.7
Ozone Levels (ppm)	100 ppm 1 day, 10 ppm 10 days
Total = 2 x 2 x 2 = 8	

This experimental design was designed according to the results obtained after evaluating the tensile strength of seams at 3 levels of overlap seam length (2.54, 7.62. 12.7 cm), two levels of each temperature (155°C, 185°C), pressure (100, 400 kPa), and speed (3, 6 m/ min). The results showed that the seaming speed did not have any effect on the seam tensile strength. The connecting letters report showed high pressure (400 kPa) worked better than the low pressure (100 kPa). It was also observed that 7.62 cm overlap seam length showed the highest strength followed by 2.54 cm overlap length. 12.7 cm overlap length showed the least strength and therefore was not taken into consideration while evaluating the effect of weathering on seam tensile strength. Both high and low levels of temperature showed good seaming and therefore they were included in Table 4.5. This is the justification for the variables and their levels chosen for this experimental design.

4.3. Seam Fabrication

A lap seam was prepared with PI – TPU – PI interface as shown in the Figure 4.2. This interface is selected as PI and TPU adhere well compared to PET and TPU. Hence PI – TPU – PI forms a stronger interface than PI – TPU – PET.

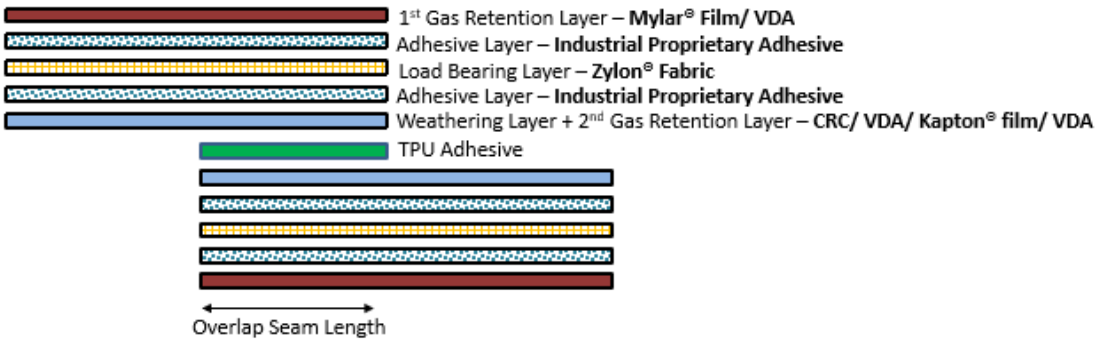

Figure 4.2: A schematic of lap seam

Two pieces of laminates are seamed using the Kannegiesser GmbH & Co. D – 4973 VLOTH fusing machine (Figure 4.3). The machine consists of a fusing chamber with a continuous belt. There is a switch on the machine that controls the heating chamber. The two pressure rollers are placed inside the fusing chamber and the pressure is produced by spring and pneumatic power. There are separate switches to control the temperature of the top and the bottom roller, whereas, there is only one switch to control the pressure and speed of both rollers. A schematic of the machine is shown in the Figure 4.4.

Figure 4.3: Kannegiesser GmbH & Co. D – 4973 VLOTHO fusing machine, (a) Input, (b) Output

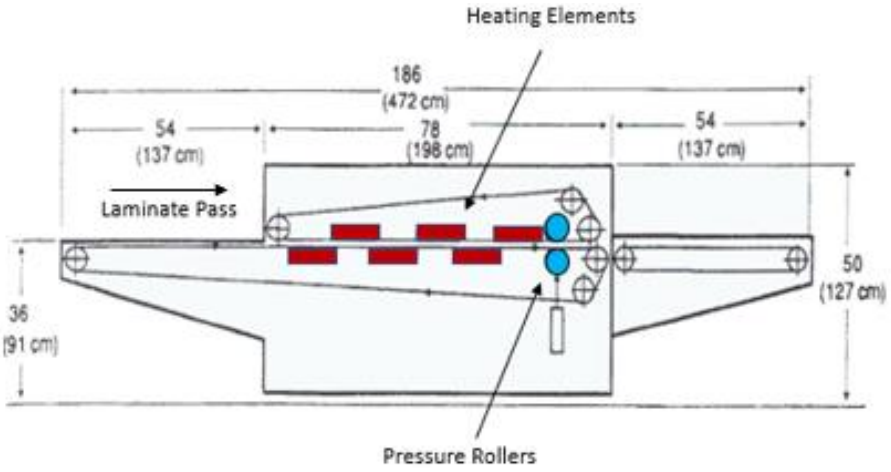

Figure 4.4: Schematic of continuous fusing machine

To seam sample, the laminates and the TPU films were placed in the apropriate order, that is PI side of both the laminates facing the TPU film, in the middle of two teflon sheets (to prevent any stickying). The desired seaming parameters (high or low seaming tempraure, pressure, and speed)

had to preset before seaming to maintain accuracy of these parameters. To check the exact temperature at the nip of the pressure rollers, IR gun was used.

4.4. Testing and Evaluation of Seam

Two tests were carried out on the seams, tensile test, and T-peel test according to the two experimental designs. This section discusses the procedure used to prepare sample/ specimens for these tests, the standard test methods followed, and the way of evaluating the results.

4.4.1. Seam Tensile Test

ASTM D5035 standard was carried out to determine the strength of the laminate in warp and weft direction. The tensile test was carried out on MTS Landmark servo hydraulic 250 kN testing machine. Five specimens were prepared in warp direction and weft direction. Each specimen had 7.62 cm gauge length and was 2.54 cm wide. All the tabs used in this thesis had 5.08 cm length and 3.81 cm width. Additional 5.08 cm space had to be left in every sample to attach the tabs for better grip.

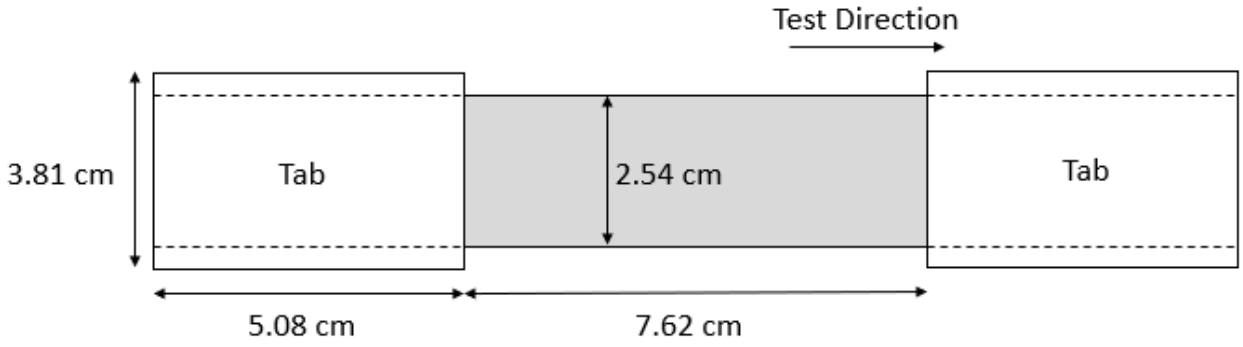

Figure 4.5: Schematic of a laminate specimen for tensile test

This test was carried out to evaluate the tensile strength of the specimens with three different overlap seam lengths seamed at high and low levels of temperature, pressure, and speed as discussed in the experimental design.

4.4.1.1. Sample Preparation

Laminate was placed on the cutting table and observed for the alignment of yarns within the laminate. The area with the most aligned yarns was selected. To prepare a lap seam sample, two identical laminates were cut. TPU adhesive was cut according to the overlap seam lengths. The adhesive film for every sample was cut a little longer, in length and width, than the overlap seam area, to make sure that the entire area was evenly bonded. The laminates and adhesive cuttings were arranged to get a PI – TPU – PI interface. This arrangement was kept in between two Teflon® sheets to avoid the sticking of the TPU film to the belt of the fusing machine. After seaming, five specimens were cut from every seamed sample. The Figure 4.6 shows the schematic of the specimens with 2.54 cm, 7.62 cm, and 12.07 cm overlap seam lengths. The width of all the specimens was kept constant, that is 2.54 cm. Every specimen had additional 7.62 cm on either side of the seamed area. Therefore, the gauge length of 2.54 cm, 7.62 cm, and 12.07 cm seam specimens were, 17.78, 22.86, and 27.94 cm, respectively.

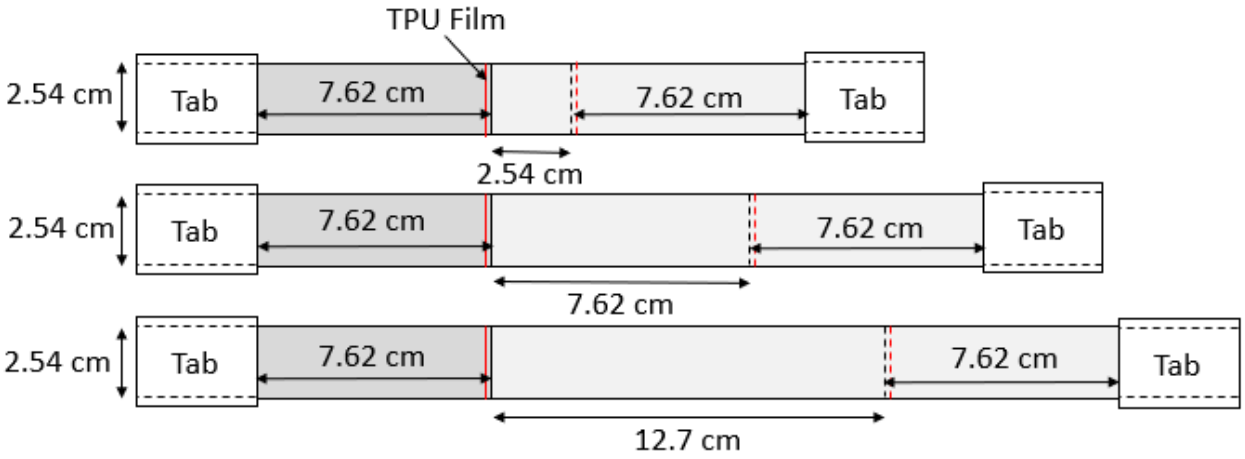

Figure 4.6: 2.54 cm, 7.62 cm and 12.70 cm test specimens

4.4.1.2. Testing and Evaluation

ASTM standard D5035 was followed to evaluate the tensile property of the seams. The primary objective of this method was to determine the tensile strength of the seam under high load (250 kN). The best seam would break at the laminate (that is the base material known as fiber fracture failure modes), away from the seamed area This would indicate a strong seam. A bad specimen would show seam failure, delamination, or breaking of the laminate at the edge of the seamed area. The MTS Landmark servo hydraulic 250 kN testing machine (Figure 4.7) was used to evaluate the tensile property of the seams. The specimens were evaluated by recording the strength (N/ cm) values obtained after the completion of the test.

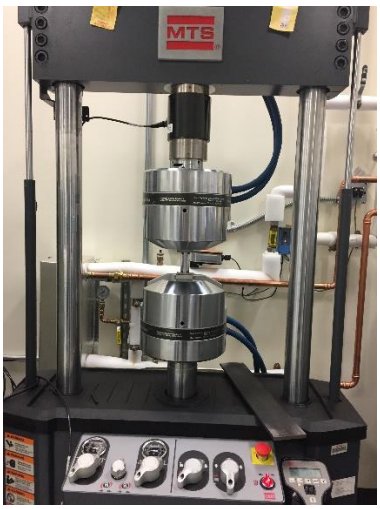

Figure 4.7: MTS Landmark servo hydraulic 250 kN testing machine

4.4.2. T-Peel Test

The T-peel test was carried out to evaluate the peel strength of the adhesive bonded laminate seams after seaming them at different parameters discussed in experimental design for testing the peeling property.

4.4.2.1. Sample Preparation

According to the ASTM D1876 standard, the specimens were prepared in the way shown in the Figures 4.8 and 4.9. Every sample had 5 specimens, 30.48 cm long and 2.54 cm wide. Out of the 30.48 cm, only 22.86 cm was bonded by the TPU adhesive by keeping it in between the two laminates (making PI – TPU – PI interface). This arrangement was placed in between two Teflon sheets and taped together improve the stability of the seams during seaming.

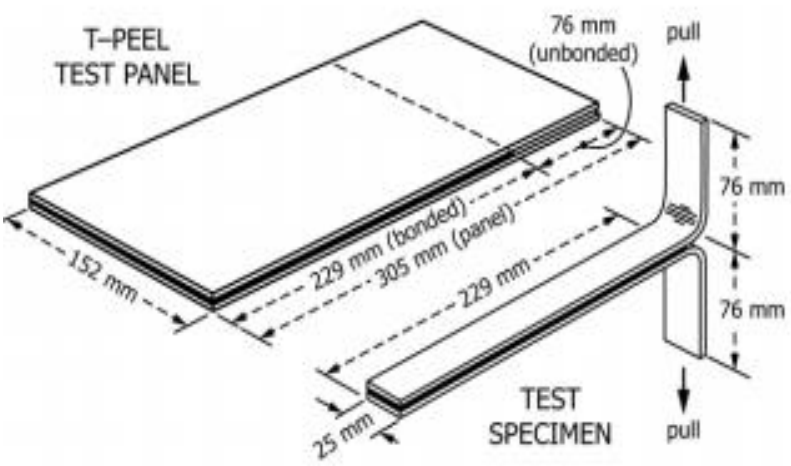

Figure 4.8: Test specimen preparation according to the ASTM D1876 standard

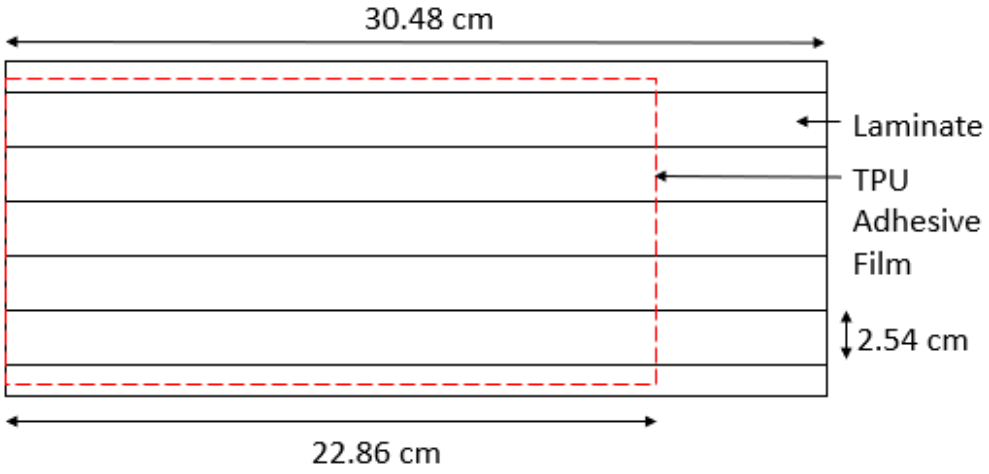

Figure 4.9: Schematic of sample preparation for T – peel test

4.4.2.2. Testing and Evaluation

The standard ASTM D1876 was followed to evaluate the peeling property. The primary objective of this method was to determine the peel resistance of the adhesive bond between the flexible adherents by the means of a T – type specimen. This test was carried out on the MTS Q – Test/ 5 Universal Testing Machine shown in the Figure 4.10.

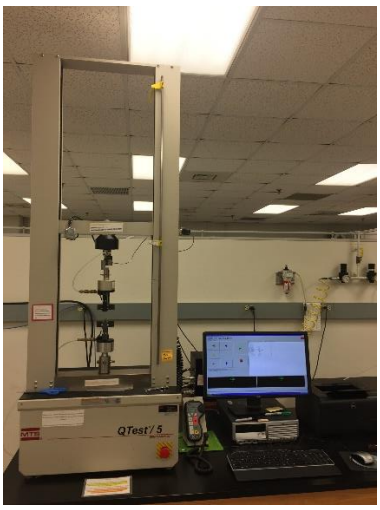

Figure 4.10: MTS Q – Test/ 5 Universal Testing Machine

The specimens were evaluated by determining the average peeling load (N/ cm) from the autographic curve for the first 12.70 cm of peeling after the initial peak. Figure 4.11 shows a typical T-peel curve.

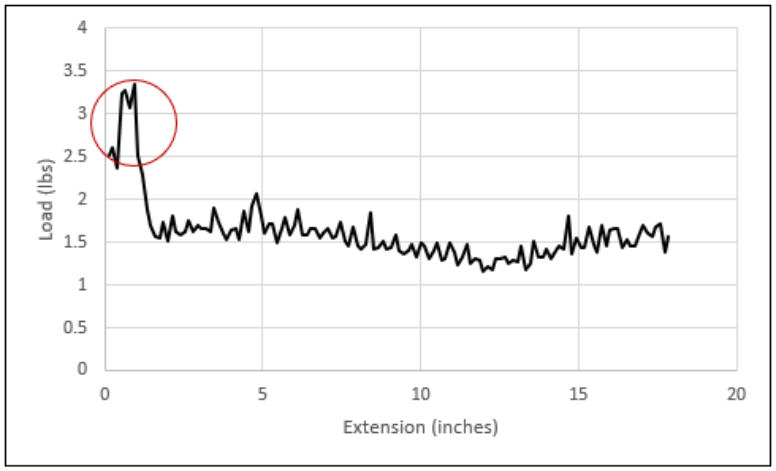

Figure 4.11: Typical T-peel curve highlighting the initial peak

4.4.3. Seam Weathering

The base laminates were seamed in the same way as they were seamed while evaluating the seam tensile property initially, as indicated previously in section 4.3 Seam Fabrication, but keeping in

mind the new experimental design. The weathering treatment included ozone treatment (100 ppm for 1 day and 10 ppm for 10 days), and this was followed by high and low temperature cycles (+20°C to – 40°C) as shown in Figure 4.12.

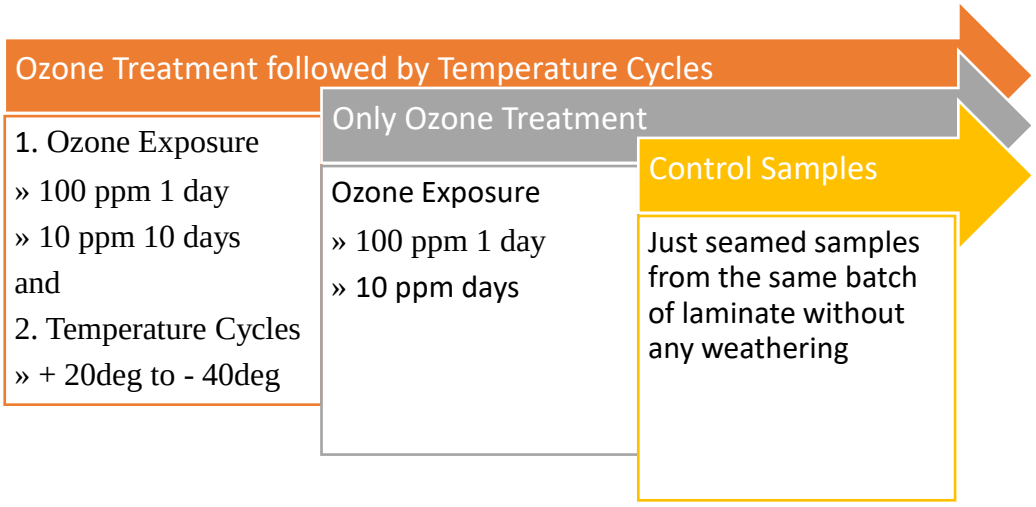

Figure 4.12: Protocol followed to test the effect of weathering on seam tensile strength

Airships that hover in stratosphere would experience these weathering effects, but to evaluate just the effect of ozone, specimens were tested after only ozone exposure. To evaluate the effect of high and low temperature, the seamed specimens were first treated for ozone and then this ozone treated samples were put in the Instron CEAST 9000 series machine weathering chamber (Figure 4.13) to expose them to high and low temperature cycles to evaluate the cumulative effect of ozone followed by temperature cycles.

4.4.3.1. Testing and Evaluation

Five specimens were tested for each sample and samples were prepared as mentioned in the above section. Out of the three sets for three different treatment, one set was considered as control which was not exposed to weathering condition. These samples were tested on the MTS Landmark servo

hydraulic 250 kN to evaluate the seam tensile strength (control samples). The second set was exposed to ozone at 100 ppm for 1 day and 10 ppm for 10 days in CH – 2 Ozone Chamber by Oxidation Technology, LLC. The ozone exposed set was then tested to evaluate the effect of ozone exposure on the seam tensile strength. The last set of samples were exposed to different concentrations of ozone (100 ppm for 1 day and 10 ppm for 10 days) and then was placed in Instron weathering chamber for high and low temperature cycle. Figure 4.13 shows the Instron machine. The samples were treated at – 40 °C for 11 hours, then at room temperature (+20 °C) for 10 hours, then again at – 40 °C for 3.7 hours, and at 27 °C for 11.3 hours.

Figure 4.13: Instron machine with ozone treated seam samples placed in it

As there were too many samples, every sample was given a specific samples ID. The nomenclature of the IDs was, overlap length _ temperature – ozone treatment – temperature weathering.

4.5. Solar Cap Fabric and Harness

Solar cap fabric and harnesses were exposed to UV radiation and different levels of ozone concentrations to evaluate the effect of weathering on their strength. The objectives of this test were, (a) to establish exponential relationships to predict degradation at any desired time (b) to verify if 100 ppm concentration of ozone for 1 day was equivalent to 10 ppm concentration of ozone for 10 days, and (c) to know the loss in strength of the solar cap fabric (already exposed to UV radiation for 6 days), after 100 ppm ozone concentration for 1 day.

4.5.1. Materials

4.5.1.1. CT1E.08/KM7 Dyneema Composite Fabric (Solar Cap Fabric)

This was a Dyneema® fabric (see Figure 4.14) which had a metallized polyester film – 0^0/ 90^0 and Dyneema® fiber – Polyester film. It was composed of 100% Dyneema® Polyethylene fiber, with a front coating of 100% metallized polyester and a back coating of 100% polyester. The fabric received was 137 cm wide with areal density of 32 g/ m^2. This fabric was already tested to evaluate the strength, elongation, tear strength, puncture, and water resistance. The values for these properties are mentioned in Table 4.6.

Table 4.6: Test methods used to test the given properties of CT1E.08/KM7 Dyneema Composite Fabric and their values

Property	**Test Method**		**Value**
Tensile Strength	ASTM D3039	Warp	63 lb/ in (552N/ 5cm)
		Weft	63 lb/ in (552N/ 5cm)
Elongation	ASTM D3039	Warp	2.7%
		Weft	2.7%

Table 4.6 (continued).

Tear Strength	Mil-C-21189 10.2.4	Warp	16 lb (71N)
		Weft	16 lb (71N)
Puncture	ASTM F1342 Probe B		2 lb (8.9N)
Water Resistance	AATCC TM127		15,000 mmH_2O

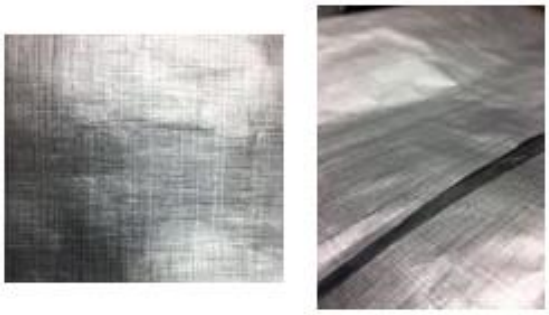

Figure 4.14: CT1E.08/KM7 Dyneema Composite Fabric

4.5.1.2. TiO_2 coated Vectran & Silicon fiber warp knitted fabric (Harness A)

This is a warp knit fabric (labelled 'Harness A' for convenience purpose) (see Figure 4.15). The specifications of this fabric are given in Table 4.7.

Table 4.7: Specification for Vectran and Silicone fiber harness

Vectran & silicone fiber harness (TiO_2 coated)	
Construction	Warp knit
Weft yarn density	16,00 threads/ cm
Weft yarn linear density, Vectran (44,9%)	120 dTex
Warp yarn density	1.48 threads/ cm
Warp yarn 1 linear density, Silicone/ PA6.6 (34,7%)	1000 dTex

Table 4.7 (continued).

Warp yarn 2 linear density, Vectran (20,4%)	120 dTex
Textile material composition (without TiO_2 coating)	Vectran = 65,3%, Silicone = 34.7%, PA 6.6. = 7,6%
App. m^2-weight (without TiO_2 coating)	66 grams
App. m^2- weight (including TiO_2 coating)	88 grams

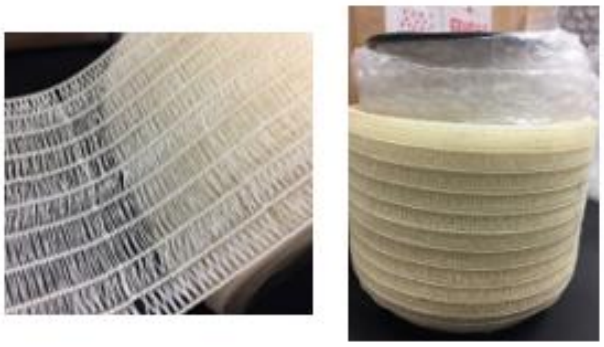

Figure 4.15: TiO_2 coated Vectran & Silicon fiber warp knitted fabric (Harness A)

4.5.1.3. Dyneema SK75 & Silicon Fiber Warp Knitted Fabric (Harness B)

This is another warp knit fabric (see Figure 4.16) with identification 'Harness B'. The specifications of this fabric are given in Table 4.8. The structure of this fabric contains wires (for power supply), which are removable when the fabric is cut. This fabric was tested without wires.

Table 4.8: Specification for Dyneema SK7 harness

Dyneema SK7 harness	
Construction	Warpknit
Weft yarn density	8,00 threads/ cm

Table 4.8 (continued).

Weft yarn linear density, Dyneema (55,9%)	165 dTex
Warp yarn density	1.43 threads/ cm
Warp yarn 1 linear density, Silicone/ PA6.6 (30,6%)	1000 dTex
Warp yarn 2 linear density, Dyneema (13,5%)	165 dTex
Textile material composition	Dyneema = 69,4%, Silicone = 23,9%, PA 6.6. = 6,7%
App. m^2-weight (Without AWG 20 FEP insulated wires)	58 grams

Figure 4.16: Dyneema SK75 & silicone fiber warp knitted fabric

4.5.2. Protocol

A protocol was followed to achieve the objectives of this study. This section will provide information about the protocol that was followed to treat the above samples to UV radiation and ozone concentrations. The protocol was necessary to determine the degradation in strength of the solar cap, harness A, and B fabrics after treating them with UV radiations and ozone concentration (See Figure 4.17).

4.5.2.1. UV Radiation Treatment

The solar cap fabric and harness A and B were exposed to the UV radiation for total 6 days. 7 samples of each solar cap fabric, harness A, and harness B were prepared. One of each fabric was the control sample that was untreated. The remaining 6 samples were put into the UV chamber all at one time. One sample was taken out of the UV chamber every day. This gave solar cap, harness A, and harness B fabrics 0,1, 2, 3, 4, 5, and 6 days of UV exposure.

4.5.2.2. Ozone Concentration Treatment

Depending on results of the previous study by NCSU/SCEYE team, after 24 hours of 100 ppm ozone exposure on the PI and PET films, visible cracking or degradation was observed around the edges of the laminate sample. The PET side appeared to have damaged more compared to the PI side. Microscale degradation was observed on the PI side. Hence, for this study 100 ppm concentration for 1 day was considered. The protocol of this study was to determine if 100 ppm concentration of ozone for 1 day was equivalent to 10 ppm of ozone concentration for 10 days. The objective was to understand if higher concentration for less time gave same amount of degradation in strength as compared to low concentration at prolonged period. The samples exposed to ozone concentrations were, the solar cap fabric without laminate backing, solar cap fabric with laminate backing, harness A fabric, and harness B fabric, and the laminate.

4.5.2.3. UV and Ozone Treatment

The protocol for determining the combined effect of UV radiation and ozone concentration was to cut a solar cap fabric sample and expose it to UV radiations for 6 days. The same sample then had to be exposed to 100 ppm ozone concentration for 1 day.

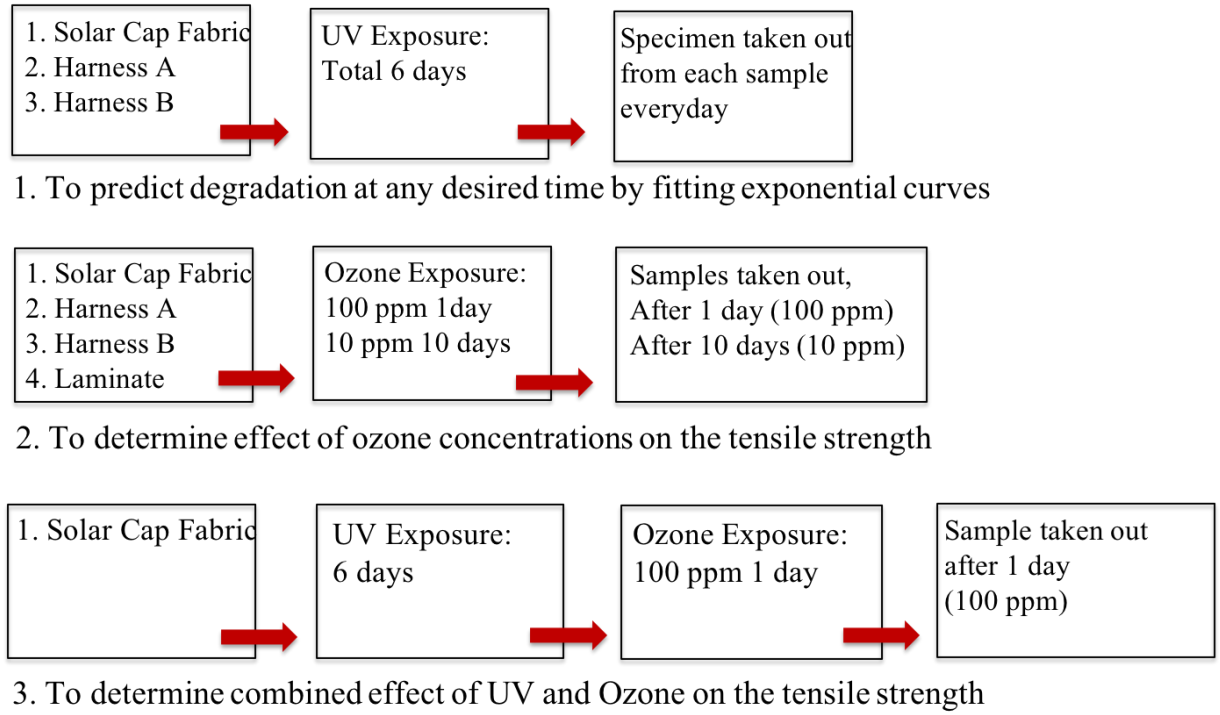

Figure 4.17: Protocol followed for weathering of solar cap fabric, harness A, and B

4.6. Harness and Solar Cap Fabric Testing and Evaluation

This section is divided in two parts, first part comprises of the solar cap fabric and harness fabric A and B exposed to the UV radiations. The second part comprises of treating the solar cap fabric with and without laminate backing, harness fabrics A and B, and laminate with 100 ppm ozone concentration for 1 day and 10 ppm concentration of ozone for 10 days.

4.6.1. UV Radiation Treatment

Since significant number of samples had to be prepared for weathering, each sample was given a unique ID. Solar Cap Fabric was labelled as ‘I’, harness fabric A as ‘II’, and harness fabric B as ‘III’. Numbers were assigned for the number of days of UV exposure. For example, ‘I-1UV-0OZ’ meant, solar cap fabric exposed to 1 day of UV exposure and no ozone treatment.

4.6.1.1. Sample Preparation

Seven solar cap fabric samples were cut with a length and width of 20.32 cm (See Figure 4.18). All the seven samples were labelled with appropriate sample IDs.

Figure 4.18: Solar cap fabric sample for UV exposure

Twenty-one harness A samples were cut with a length of 20.32 cm (See Figure 4.19). The width of the harness A was short and hence 3 strips were considered as one sample. All the seven samples were labelled with appropriate sample IDs. These samples attached to a piece of hull laminate for stability of the sample inside the UV chamber, and to imitate the placement of harness A on an actual airship.

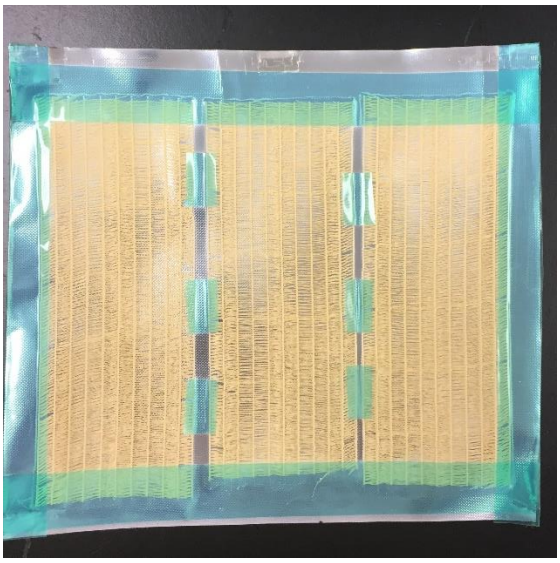

Figure 4.19: Harness A sample for UV Exposure

Seven harness B samples were cut with length and width of 20.32 cm (See Figure 4.20). All the seven samples were then labelled with appropriate sample IDs. These samples attached to a piece of hull laminate for stability of the sample inside the UV chamber, and to imitate the placement of harness B on an actual airship.

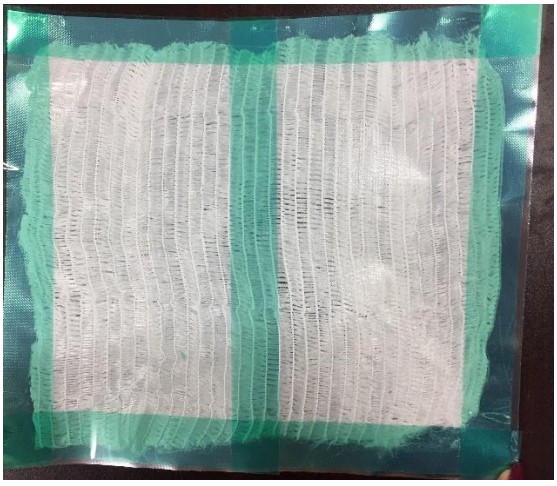

Figure 4.20: Sample preparation of Harness (Fabric B) for UV Exposure

4.6.1.2. Weathering

Out of the seven samples prepared, six samples were clipped inside the ATLAS Ci3000+ Xenon Fade-Ometer (See Figure 4.21). The seventh sample being the control sample was not placed inside the chamber. The samples were exposed to UV irradiance at 340 nm, 1.09 W/ m^2 for 24 hours. Relative humidity was adjusted to 57% with chamber temperature adjusted to 45.5° C.

Figure 4.21: ATLAS Ci3000+ Xenon Fade-Ometer

Due to limitation of space inside the chamber, the maximum number of samples that could fit inside the chamber were placed. After the weathering of a sample was complete, it was replaced with another sample. A test matrix was prepared to keep track of the number of days of UV exposure completed for a sample. Figure 4.22 shows the placement of solar cap fabric sample inside the ATLAS Ci3000+ Xenon Fade-Ometer.

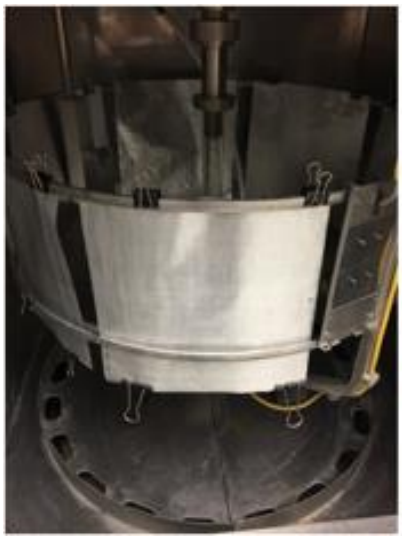

Figure 4.22: Solar cap fabric samples placed inside the ATLAS Ci3000+ Xenon Fade-Ometer

4.6.2. Ozone Treatment

The samples that were decided to expose to the 100 ppm concentration of ozone for 1 day and 10 ppm concentration for 10 days were, solar cap fabric without laminate backing, solar cap fabric with laminate backing, harness A, and B, and the laminate. The samples that were supposed to be exposed to 100 ppm concentration of ozone for 1 day were labelled '100 ppm 1 day', whereas the samples which were supposed to be exposed to 10 ppm concentration for 10 days were labelled '10 ppm 10 days'.

4.6.2.1. Sample Preparation

The samples were prepared exactly the way samples were prepared for UV exposure. 2 samples were cut for individual fabric, one for 100 ppm ozone concentration for 1 day, and the other for 10 ppm ozone concentration for 10 days. Total 4 solar cap fabrics were cut with length and width of 20.32 cm. Out of these 4 samples, 2 were backed with a laminate and 2 were not. The laminate

was attached to the solar cap fabrics with a masking tape. Figure 4.23 shows the prepared solar cap fabric samples.

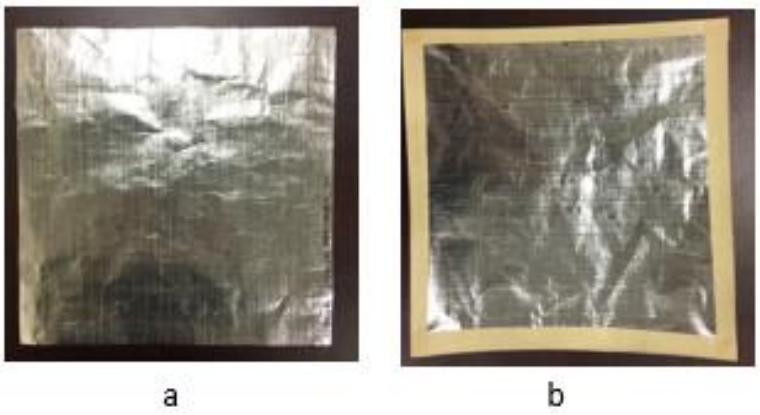

Figure 4.23: (a) Solar cap fabric sample without laminate, (b) solar cap fabric sample with laminate

Six harness A samples (3 small strips considered as one sample due to narrow width) were cut with the length of 20.32 cm. Two samples of each, harness B and laminate, were prepared with length and width of 20.32 cm. Figure 4.24 shows the prepared samples. All the samples were labelled before the weathering.

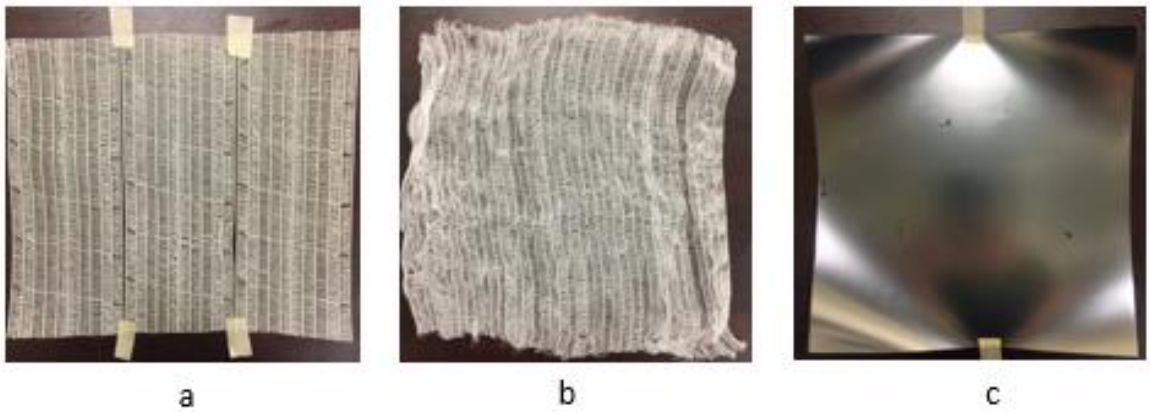

Figure 4.24: (a) Harness A, (b) harness B, and (c) laminate samples for ozone exposure

4.6.2.2. Weathering

All the samples were attached on a frame, and this frame was kept inside the ozone chamber. Weathering was carried out at 100 ppm ozone concentration for 1 day, and 10 ppm concentration for 10 days continuous at 25 °C. Figure 4.25 shows the frame with samples attached to it before exposing them to ozone.

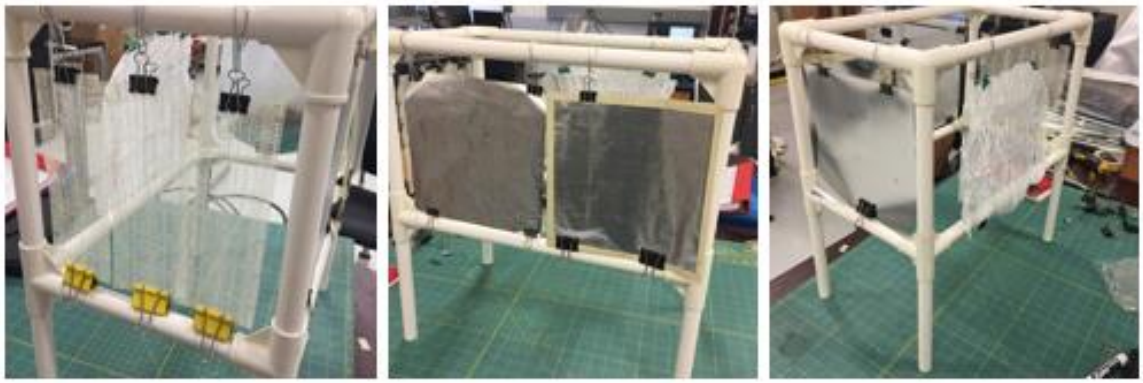

Figure 4.25: Different view of samples attached to the frame for ozone exposure

4.6.3. UV and Ozone Exposure

Five solar cap fabric samples were cut with a length and width of 20.32 cm. These were first exposed to UV radiation for total of 6 days in ATLAS Ci3000+ Xenon Fade-Ometer. After exposure, the same samples were then placed in Ozone chamber at 100 ppm concentration for 1 day. Tensile test was then carried out on the weathered samples to evaluate the effect of weathering on tensile strength.

4.6.4. Mechanical Testing and Evaluation

ASTM standard D5035 was followed to evaluate the tensile property of all the samples. MTS Landmark servo hydraulic 250 kN testing machine was used to carry out the tensile test of the

solar cap fabric. All the solar cap fabric specimens were prepared with 7.62 cm gauge length and 2.54 cm width.

MTS Q – Test/ Universal Testing Machine was used to carry out tensile test on the harness A and B. Four strands of harness A could be tested in a 2.54 cm wide specimen strip. The gauge length of harness A was 7.62 cm. Harness B was challenging to test as all the 4 strands, fitting in 2.54 cm width, could not be broken at a time, and hence the software tends to give low load values. Due to this, it was decided to test one strand of the harness B at a time, and then calculate the strength of 4 strands. The gauge length of the strands was kept constant to 7.62 cm.

Tensile test was carried out on the treated samples to check the strength of the solar cap fabric, harness A, and B, by fitting an exponential relationship. Degradation due to weathering was evaluated by plotting the time – strength and time – strength loss relationship.

5. RESULT AND DISCUSSION

This section will provide in detail the results and discussion of two major parts, one was the seam optimization, and second being the weathering of solar cap, harness A, and B fabrics. The critical effects of various seaming parameters and their combination on the seams were investigated and analyzed statistically using Analysis of Variance and Tukey Kramer HSD to compare means. The second part of this chapter is going to focus on the results and discussion of the effect of weathering by UV radiation and ozone concentration on solar cap fabric, harness A, and harness B. A significance level of 5% was selected to reject the null hypothesis. Any outliers were removed before the statistical analysis of the data.

5.1. Laminate Evaluation

The industry proprietary laminate was tested in both direction (warp as well as weft). It was observed that the strength of the laminate in weft direction was higher compared to strength in warp direction since the warp yarns are subjected to more stresses and abrasion during weaving compared to weft yarns. The average strength in the weft direction was as high as 772.15 N/ cm, whereas the average strength in warp direction was 762.69 N/ cm. Table 5.1 shows the individual observations long with the average tensile strength of the laminates was seamed in the weft direction to obtain maximum strength. The ends per inch and picks per inch of this laminate were 38 and 38, respectively. The areal density of the laminate was 109 g/m^2. The thickness of the laminate was measured using a digital micrometer. The thickness of the laminate was 120 µm.

Table 5.1: Strength of laminate in weft and warp direction

#	Warp	Weft
1	761.48	762.60
2	764.42	786.79
3	760.54	767.07
4	762.81	780.17
5	764.22	765.87
Mean Strength (N/ cm)	762.69	772.50
CV (%)	0.19	1.21

5.2. Laminate Seam Evaluation

The adhesive bonded seams were evaluated for their tensile property and peel property This part of the results and discussion chapter will determine the effects of best seaming parameters and their combination on the above-mentioned properties of the seam.

5.2.1. Seam Tensile Property

As per the experimental design, the factors considered to evaluate the tensile property of the seams were, low and high levels of temperature, pressure, speed, and three different overlap seam lengths. 2.54 cm, 7.62 cm, and 12.70 cm overlap seam samples were seamed using low and high seaming temperature (155 °C, 185 °C), pressure (100 kPa, 400 kPa), and speed (3 m/min, 6 m/min). Specimens were prepared according to chapter 4 and tested on the MTS Landmark servo hydraulic 250 kN testing machine. Five specimens of every sample were tested.

Figure 5.1 shows the result of the seam strength of 24 samples per the experimental design. For 2.54 cm overlap seam lengths, the high strength was given by the samples which were seamed at

higher temperature and higher speed. Pressure did not seem to have a significant effect on these seams. Even though 2.54 cm did not give strength equal to, or higher than the laminate itself, the seams failed away from the seamed area. This can be an acceptable failure as the seam was strong enough to bear the load and did not fail at high load values. The average value that 2.54 cm seam specimen gave at 185 °C and 100 kPa pressure and 6 m/min was 701.75 N/ cm. This was the highest strength observed in the specimens seamed with 2.54 cm overlap seam length.

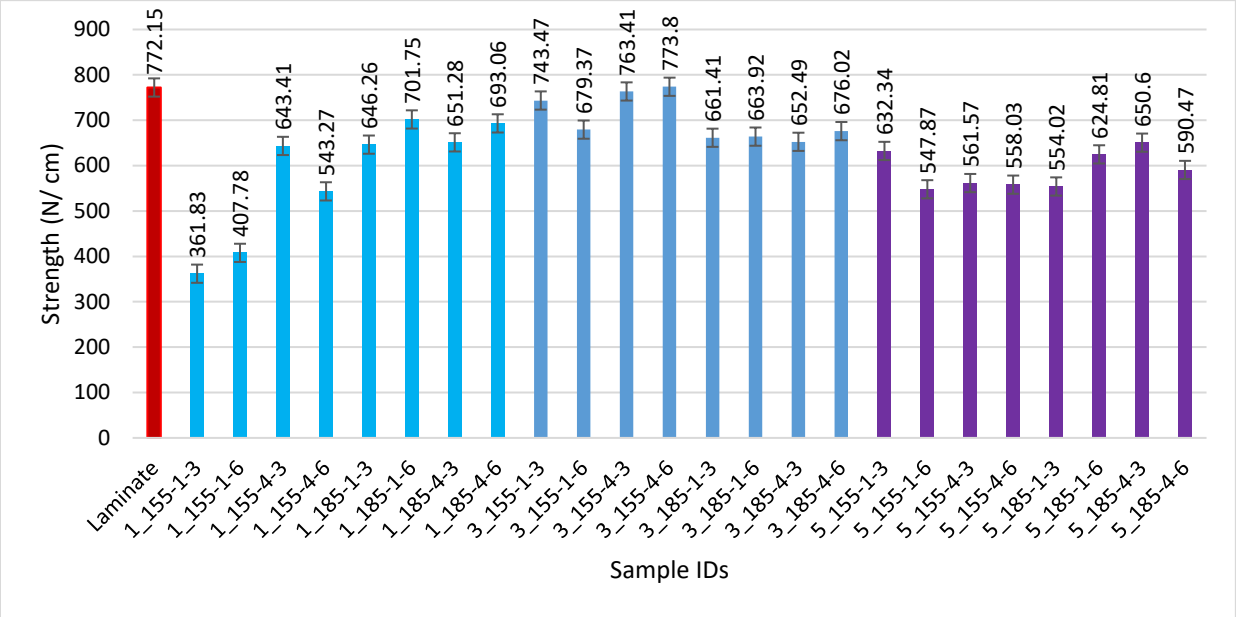

Figure 5.1: Seam tensile strength

Table 5.2: Seam tensile strength

Sample IDs	Overlap Seam Length (cm)	Temperature (°C)	Pressure (kPa)	Speed (m/min)	Average Strength (N/ cm)	CV (%)
1	2.54	155	100	3	361.83	2.25
2	2.54	155	100	6	407.78	4.55

Table 5.2 (continued).

3	2.54	155	400	3	643.41	3.55
4	2.54	155	400	6	543.27	3.32
5	2.54	185	100	3	646.26	3.51
6	2.54	185	100	6	701.75	5.78
7	2.54	185	400	3	651.28	2.73
8	2.54	185	400	6	693.06	3.83
9	7.62	155	100	3	743.47	2.00
10	7.62	155	100	6	679.37	5.62
11	7.62	155	400	3	763.41	1.60
12	7.62	155	400	6	773.80	3.00
13	7.62	185	100	3	661.41	2.09
14	7.62	185	100	6	663.92	2.20
15	7.62	185	400	3	652.49	3.15
16	7.62	185	400	6	676.02	4.91
17	12.70	155	100	3	632.34	2.63
18	12.70	155	100	6	547.87	1.96
19	12.70	155	400	3	561.57	2.68
20	12.70	155	400	6	558.03	1.75
21	12.70	185	100	3	554.02	1.36
22	12.70	185	100	6	624.81	2.27
23	12.70	185	400	3	650.60	3.30
24	12.70	185	400	6	590.47	3.22

Figure 5.2: Failure Mode – Base laminate breaks away from the seam, giving higher strength values for samples seamed at higher temperature and speed

Low temperatures gave lower seam strength values compared to higher temperature irrespective of the variation in the pressure and speed. However, for specimen seamed at 155 °C, and 400 kPas did give higher strength values compared to the samples seamed at 155 °C, and 100 kPa. It was observed that increase in speed did not increase the strength further. The sample seamed at 155 °C, 100 kPa pressure, and with speed of 3 m/min and 6 m/min failed at the seam. It was observed that the adhesive did not bond the two base laminates well at these seaming conditions (See Figure 5.3). The two base laminates partially separated at the seamed area giving strength as low as 361. 83 N/ cm and 407.78 N/ cm, respectively.

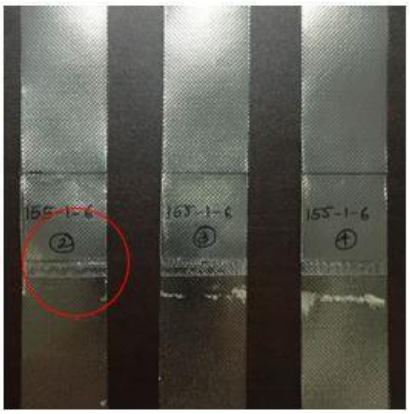

Figure 5.3: Failure Mode – Seam failure, separating two base laminates, giving lower strength values for samples seamed at 155 °C

The samples that were seamed at 155 °C, 400 kPa pressure (higher pressure), and with speed of 3 m/min and 6 m/min also failed at the seam (See Figure 5.4). Higher pressure did give higher strength values compared to the lower pressure, but these values were still very low compared to the strength of the laminate base material. These samples also failed at the seam but in a slightly different way. It was observed that the seamed area was either damaged (wrinkled) or slight peeling had started initiating at the edges of the seamed area. It was also observed that all yarns did not equally bear the load. This might be the reason why peeling and wrinkles were observed on the 2.54 cm seamed area. Observing the tested specimens more closely, it could be said that the TPU film was not able to bond the base laminates well at lower temperature. Even the small overlap seam length might not be able to bear the load when seamed at lower temperature.

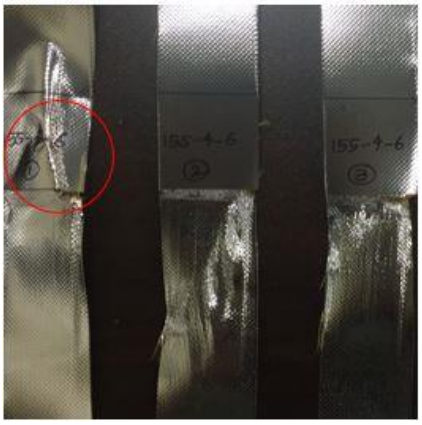

Figure 5.4: Failure Mode – Seam failure, giving lower strength values for samples seamed at 155 °C, 400 kPa

Samples with 7.62 cm overlap seam length gave much higher strength values compared to 2.54 cm overlap. 185 °C with 400 kPa seaming pressure gave highest seam strength among all the specimens. Average strength as high as 773.80 N/cm was seen in the sample seamed at 185 °C, 400 kPa pressure, and 6 m/min speed. This was the only sample that gave average seam strength higher than the average laminate strength in weft direction. Almost all the 7.62 cm specimens failed at the base laminate away from the seamed area. This failure mode determines that the seam was strong enough and the adhesion between the laminates and the seam was good to be able to bear higher load. This can be considered the reason higher strengths were achieved. Some samples gave low values as the laminate broke half due to unequal contribution of yarns while bearing the load. The specimen in the Figure 5.5 a shows partial break in the laminate resulting in lower load values compared to the specimens that completely broke.

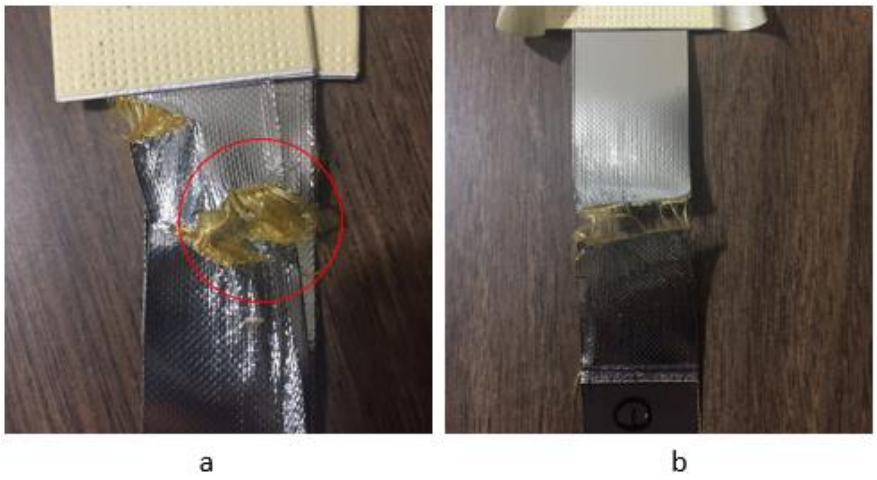

Figure 5.5: Failure Mode – (a) partial break of the base laminate (b) complete break of the base laminate away from the seam

As 7.62 cm overlap seam length gave higher strength values compared to 2.54 cm, the overlap area was further increased to 12.70 cm. After testing all the specimens of 12.70 cm overlap seam length, it was observed that the strength of the seam did not further increase. The strength values did not increase neither were they equal to the seam strength values of 7.62 cm overlap seam. The seam sample that gave the highest strength was seamed at 185 °C, 400 kPa pressure, and 3m/min speed. It was observed that, there was, to large extent, unequal load sharing by the yarns. Due to this, almost all the specimens broke partially at the edge of the seams due to high stress concentration. The failure mode observed is shown in the Figure 5.6.

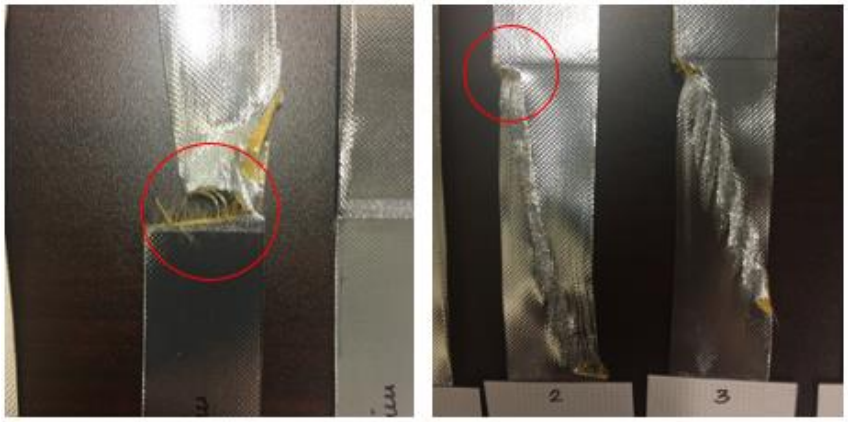

Figure 5.6: Failure Mode – Partial break of the base laminate at the edge of the seam

The entire data was analyzed using analysis of variance to determine the effect of low and high levels of seaming parameters, as well as the effect of 2.54 cm, 7.62 cm, and 12.70 cm overlap seam length on the strength of the seams. The results of analysis of variance was conformed using Tukey HSD (Honest Significance Difference) for all the 24 samples. Having it done for the entire data allowed to find the best seaming parameters that gave the best bonding resulting in higher strength values. The statistical analysis results are shown in Appendix B.

The regression report gave the summary of fit and the analysis of variance report. The RSquare in the Summary of Fit measures the proportion of variation explained by the model. The remaining variation is not explained by the model and is attributed to random error. The RSquare value for this data was 0.9523, which means that 95.25% of variation was explained by the model. The analysis of variance for regression partitions the total variation of samples into components, and these components are used to compute the F-ratio that evaluates the effectiveness of the model. The F-ratio for this model is 73.71, and the probability associated with it is <.0001, which very small. Hence, it can be said that this model is considered a better statistical fit for the data than the

response means alone. From Table B.4 of effect test it was found that the p-value of the parameter ‘speed’ was 0.2609, which is higher than 0.05, and therefore, the seaming variable ‘speed’ showed no effect on the seam strength. Whereas, on the other hand, overlap seam length followed by the seaming parameter ‘temperature’ showed maximum effect on the seam strength.

The Tukey HSD (Table 5.3) shows a test that is sized for all differences among the means. The connecting letters report shows that the levels that are not connected by the same letter are significantly different. This report showed that the samples prepared with 7.62 cm overlap seam strength, 155 °C, 400 kPa, with 3 m/min and the same variables with 6 m/min was not significantly different.

Table 5.3: Tukey HSD connecting letters report

Level	**Rank**								**Average strength (N/cm)**
7.6_155-400-6	A								773.80325
7.6_155-400-3	A								763.40620
7.6_155-100-3	A	B							743.46760
2.5_185-100-6		B	C						701.75025
2.5_185-400-6		B	C	D					693.05667
7.6_155-100-6			C	D	E				679.36520
7.6_185-400-6			C	D	E				676.02220
7.6_185-100-6			C	D	E				663.91800
7.6_185-100-3			C	D	E				661.40875
7.6_185-400-3			C	D	E				652.48940
2.5_185-400-3			C	D	E				651.27540
12.7_185-400-3			C	D	E				650.59980

Table 5.3 (continued).

2.5_185-100-3			C	D	E	F			646.25725
2.5_155-400-3			C	D	E	F			643.40800
12.7_155-100-3				D	E	F			632.33600
12.7_185-100-6					E	F			624.81050
12.7_185-400-6						F	G		590.47400
12.7_155-400-3							G		561.57260
12.7_155-400-6							G		558.07300
12.7_185-100-3							G		554.02320
12.7_155-100-6							G		547.87425
2.5_155-400-6							G		543.27220
2.5_155-100-6								H	407.78175
2.5_155-100-3								H	361.86300

Hence, it can be concluded that the 7.62 cm overlap seam seamed at 155 °C and 400 kPa, and 3 m/min or 6 m/min, gave the best seams. Following the 7.62 cm overlap seam was the 2.54 cm overlap seam seamed at 185 °C that gave good results. Unexpectedly, 12.70 cm overlap seams did not perform well compared to 2.54 cm and 7.62 cm overlap seams. The failure mode of the 12.70 cm seam was investigated and following could be the reasons for low strength values of 12.70 cm overlap seams. During the sample preparation, the area with most aligned yarns was selected for obtaining accurate results. It was observed that the weft yarns within the laminate were not straight and had some degree of curvature. It was easy to cut laminate pieces with aligned yarns for 2.54 cm and 7.62 cm overlap seams as their lengths were small. 12.70 cm overlap seams required long laminate pieces and hence, it was challenging to find an area on the laminate that had straight aligned yarns. Also, after the laminate pieces were cut, one of them had to be flipped to make a PI

– TPU – PI interfaced seam. This also changed the alignment of yarns after seaming. See Figure 5.7.

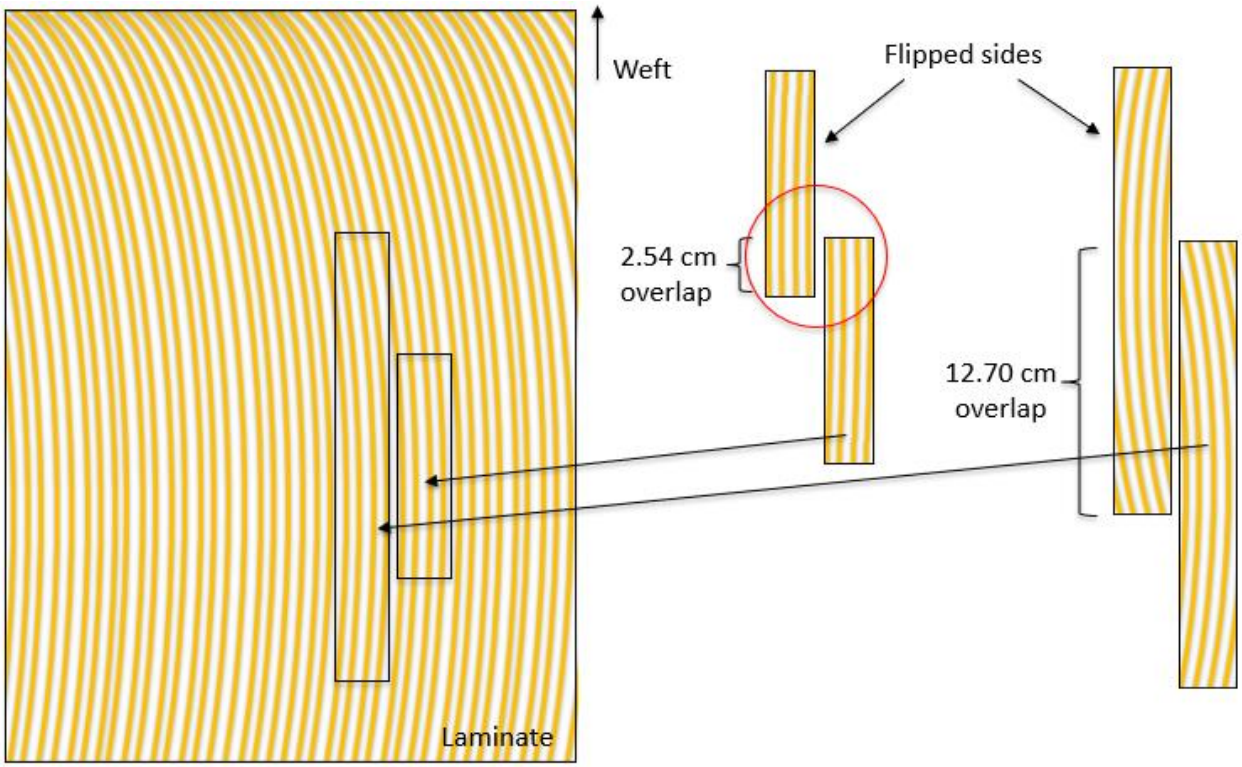

Figure 5.7: Diagram showing alignment of yarns in the laminate and 2.54 cm and 12.70 cm sample prepared from it

Therefore, misalignment of yarns was the major reason for getting such low values for the 12.70 cm overlap seam strengths. The misalignment of yarns was very much evident from the failure mode as well. See Figure 5.7.

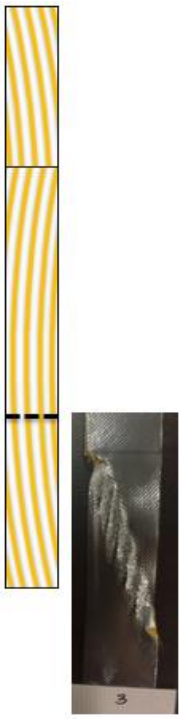

Figure 5.8: Failure mode: Base laminate fails at the edge of the of 12.70 cm overlap seam

5.2.2. Seam Peel Property

As per the experimental design, the factors considered to evaluate the peel property of the seams were, low and high seaming temperature (155 °C, 185 °C), pressure (100 kPa and 400 kPa), and speed (3 m/min, 6 m/min). To characterize the peel resistance, specimens were prepared according to chapter 4 and tested on the MTS Q – Test/ 5 Universal Testing Machine following ASTM D1876 standard. The samples and specimens were made according to the standard mentioned in chapter 4. Five specimens of every sample were tested.

In the samples subjected to the T – peel test, one typical significant failure mode was observed. It was observed that the failure initiated with the adhesive failure and then continued with VDA coating being peeled off from the PI side of the base laminate. Figure 5.8 depicts that the adhesive

film starts to break apart from the laminate as the peeling initiates. With further propagation of the peel, the failure mode changes to delamination of the VDA coating from the PI film. This exposes the PI film to the environment as shown in Figure 5.9. The yellow shiny surface is the PI film.

Figure 5.9: A tested T-peel specimen

Hence, it can be said that the peel strength of the adhesive adhered to the base laminate could not be effectively evaluated, instead the load values obtained determined the strength required to peel of the VDA coating from the PI film. This would fail to show a response significant to the change in seaming parameters. The load to displacement curves of these specimens were different from a typical T- peel test curve. Places where the adhesive peeled off from the laminate or when the adhesive film itself stretched, gave higher strength values (see Figure 5.10). Places where the VDA coating simply peeled away with the TPU, away from the PI film gave relatively low peaks. All specimens were peeled in different ways and there was significant fluctuation observed in the peaks after the initial peak. These peaks fail to reflect the true bonding strength of the adhesive

film adhered to the two laminate pieces. The adhesive tearing apart attributed to the inherent tensile strength rather than adhesive film bonding strength.

Therefore, the higher peaks cannot conclude that the seams were bonded well, it is just that the interface within the laminate, that is the VDA-PI interface is much weaker than the seam itself, and due to this, every time it is expected that the peeling would occur at VDA – PI interface. The Table 5.4 gives the T-peel test results of all the samples tested.

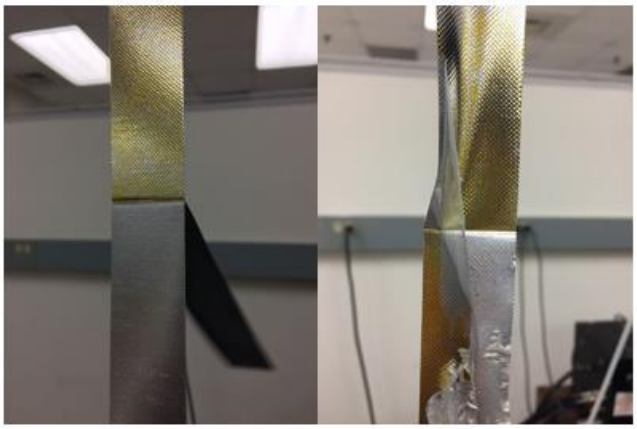

Figure 5.10: (a) Clean VDA peel away from the PI film, (b) TPU film stretch

Table 5.4: T-peel test result

Sample ID	**Temperature (°C)**	**Pressure (kPa)**	**Speed (m/min)**	**Average Strength (N/ cm)**	**CV (%)**
1	155	100	3	2.34	6.85
2	155	100	6	2.27	8.91
3	155	400	3	2.27	2.28
4	155	400	6	4.71	2.63

Table 5.4 (continued).

5	185	100	3	3.46	4.10
6	185	100	6	2.78	6.16
7	185	400	3	3.45	3.97
8	185	400	6	2.58	5.29

The results of the T-peel test were analyzed using analysis of variance to study the effect of seaming parameters on the peel strength of the seams. The statistical analyses of the T-peel test results are given in Appendix D.

The regression report gives the summary of fit and the analysis of variance report. The RSquare in the Summary of Fit measures the proportion of variation explained by the model. The remaining variation is not explained by the model and is attributed to random error. The RSquare value for this data is 0.9628, which means that 96.28% of variation is explained by the model. The analysis of variance for regression partitions the total variation of samples into components, and these components are used to compute the F-ratio that evaluates the effectiveness of the model. The F-ratio for this model is 107.07, and the probability associated with it is <.0001, which very small. Hence, it can be said that this model is considered a better statistical fit for the data than the response means alone. From the effect test it is found that the p-value of all the parameters is less than 0.05, and therefore, all the seaming parameters have effect on the seam strength.

The Tukey HSD (Table 5.5) shows a test that is sized for all differences among the means. The connecting letters report shows the levels that are not connected by the same letter are significantly different. This report showed that the samples prepared with 7.62 cm overlap seam strength, 155

°C, 400 kPa, with 6 m/min gave the highest peel strength value, which was significantly different from the rest. This does not indicate that these seaming condition gives maximum resistance to peeling. It was observed that in almost all the specimens seamed at these condition, the adhesive film stretched and tore apart with the VDA coating from the PI film, leading to higher strength values. The other samples seamed at 155 °C with high and low pressure and speed did not show any significant difference. These samples gave least peel strengths. Samples seamed at 185 °C and 6 m/min speed and 185 °C and 3m/min speed did not show any significant difference in strength when seamed at high and low pressure. Therefore, it can be concluded that, except for that sample seamed at 155 °C, 400 kPa, and 6m/min, higher seaming temperature and high speed seemed to have maximum significant effect on the peel strength compared to the other factors.

Table 5.5: Tukey HSD connecting letters report for T-peel test

Level	**Rank**				**Average Strength (N/cm)**
155-400-6	A				4.71
185-100-3		B			3.46
185-400-3		B			3.45
185-100-6			C		2.78
185-400-6			C	D	2.58
155-100-3				D	2.34
155-100-6				D	2.27
155-400-3				D	2.27

T-peel test was chosen to evaluate the peel property of the seam, but considering the failure modes, it can be said that T-peel test is not the best way to evaluate the effects of seaming parameter on the adhesion of the PI to PI interface of the seam using an adhesive film. VDA coating is just a

vacuum deposition of the aluminum on the surface of the PI, and hence PI – VDA is not a strong interface to bear the peeling load. When seams are made at different seaming conditions, it is the VDA coating that first encounters the TPU adhesive. Looking at the peeling mode, it is observed that the VDA adheres to the TPU film and separates from the PI film surface. This shows that the TPU – VDA bond is stronger than that VDA – PI bond. Hence, whenever a peeling test is carried out for this seam structure, the same failure mode is going to be observed irrespective of the seaming parameters. Thus, it can be concluded that T-peel test is not the best method to evaluate the effect of seaming parameters on the PI – TPU – PI interface adhesion, but still gives some important information about the effect of seaming parameters on the TPU – VDA bond and VDA – PI bond.

5.2.3. Weathering effects on seams

Tukey HSD test was follow on the entire data in conjunction with ANOVA. The statistical analysis show that ozone exposure and temperature cycles did not reduce or affect the seam strength. Table 5.1 shows the Tukey connecting letters report for seam weathering data. In Table 5.1 average strength values connected by the same letter are not significant. From this analysis it can be concluded that weathering does not affect the seam tensile strength. It is observed that seams without any weathering showed less strength. This could be because of the variation within the laminate. While cutting the laminate for preparing the seams, it was observed that the yarns within the laminate roll were not aligned throughout the laminate. This might have caused reduction in strength of the untreated seams. The variation in the strength is not due to weathering, but due to uneven yarn alignment. Table 5.6 shows the Tukey HSD connecting letters report.

Table 5.6. Tukey HSD connecting letters report for seam weathering results

Sample ID	Rank					Average Strength (N/cm)
2.5_185-10ppm-T	A					769.39
7.6_155-100ppm-T	A	B				757.52
7.6_185-10ppm-T	A	B	C			755.14
7.6_155-10ppm-T	A	B	C			754.16
7.6_185-100ppm-T	A	B	C			746.84
2.5_185-100ppm-T	A	B	C			745.79
7.6_155-100ppm	A	B	C			745.57
2.5_155-100ppm-T	A	B	C			741.43
Laminate	A	B	C	D		732.60
2.5_155-10ppm-T	A	B	C	D	E	723.34
2.5_155-10ppm	A	B	C	D	E	716.80
7.6_185	A	B	C	D	E	716.69
7.6_185-10ppm	A	B	C	D	E	716.38
7.6_185-100ppm	A	B	C	D	E	716.08
2.5_185-10ppm	A	B	C	D	E	714.23
2.5_155-100ppm	A	B	C	D	E	710.62
2.5_185	A	B	C	D	E	706.38
7.6_155-10ppm		B	C	D	E	695.85
2.5_185-100ppm			C	D	E	690.63
7.6_155				D	E	672.03
2.5_155					E	659.31

5.3. Weathering Effects on Harness and Solar Cap Fabrics

It was calculated that 1 day of exposure in the UV chamber is equal to 15 hours 14 minutes of real time exposure. The Table 5.7 gives the equivalent time of exposure to the UV at 20 km away from the earth's surface.

Table 5.7: Time of exposure to UV in the chamber with the equivalent time of exposure to UV at 20 km away from earth's surface and equivalent time of exposure to UV at 20 km from earth's surface (10 hours flight time – by SCEYE Inc.)

Time of exposure (hours)	**Equivalent time at 20 km from earth's surface (hours)**	**Equivalent time of exposure to UV at 20 km from earth's surface (days*)**
24	15.233	1.5
48	30.467	3.0
72	45.700	4.5
96	60.933	6.0
120	76.167	7.5
144	91.340	9.0

Solar cap, Harness A, and B fabric samples were exposed to UV in the ATLAS Ci3000+ Xenon Fade-Ometer for 6 days total exposure, with specimens taken out from each sample every day. Solar cap, harness A, and B fabrics and laminate were separately exposed to 100 ppm ozone concentration for 1 day, and 10 ppm for 10 days. One solar cap fabric sample was exposed to the UV for 6 days and then to 100 ppm ozone concentration for 1 day to evaluate the added effect of UV and ozone on its strength.

5.3.1. Tensile Strength Decay After UV Exposure

Despite of making sure that the solar cap fabric samples were sturdy inside the ATLAS Ci3000+ Xenon Fade-Ometer, some samples got wrinkled and folded due to heavy air cycles inside the chamber. Due to this, some specimens gave lower strength values. Uneven yarn spacing was also observed within the solar cap fabric. These imperfections resulted in non-uniform load sharing among the load-bearing yarns, which ultimately caused pre-mature rupture of specimens during the tensile test.

Six solar cap fabric samples were exposed to 1, 2, 3, 4, 5, and 6 days of UV, respectively. After UV exposure, the weight of each sample was measured and recorded (Table 5.8).

Table 5.8: Weights of solar cap fabrics after total 6 days of UV exposure

Fabrics	**Weight (g/m^2)**						
	Day 0	Day 1	Day 2	Day 3	Day 4	Day 5	Day 6
Solar Cap Fabric	32.50	32.44	32.38	32.36	32.32	32.30	31.98
Rank	A	A	A	A	A	A	A
Harness A	81.10	80.64	80.48	80.22	80.18	80.16	80.12
Rank	A	A	A	A	A	A	A
Harness B	62.60	62.54	62.38	62.38	62.28	62.24	62.12
Rank	A	A	A	A	A	A	A

The exposed sample were then tested on the MTS Landmark servo hydraulic 250 kN testing machine to evaluate their strength. Table 5.9 gives the strength and the CV values for the entire

data of the solar cap fabric samples. The CV (%) values show the variability in the specimen strength. About 17.71 % of variability is observed in the strength of the solar cap fabric specimens exposed to 5 days of UV exposure. This sample gives lower strength values compared to the sample that was exposed to 6 days of UV radiations.

Table 5.9: Strength and strength loss of solar cap fabric after exposure to UV radiations

Time (Days)	Strength (N/ cm)		Strength loss (%)
	Mean Strength (N/ cm)	CV (%)	
0	131.34	2.00	0.00
1	108.41	7.45	17.46
2	102.61	8.00	21.87
3	96.26	10.24	26.71
4	94.84	3.38	27.79
5	85.95	17.71	34.56
6	99.05	10.10	24.59

Figure 5.11 shows the exponential fit for the solar cap fabric, where time (days) was plotted on the x-axis and strength (N/ cm) was plotted on the y-axis. RSquare value shows that only 26. 06% of variability of the response data is explained by the model. The equation $y = 131.34e^{-0.075x}$ would predict the degradation of solar cap fabric at any desired time.

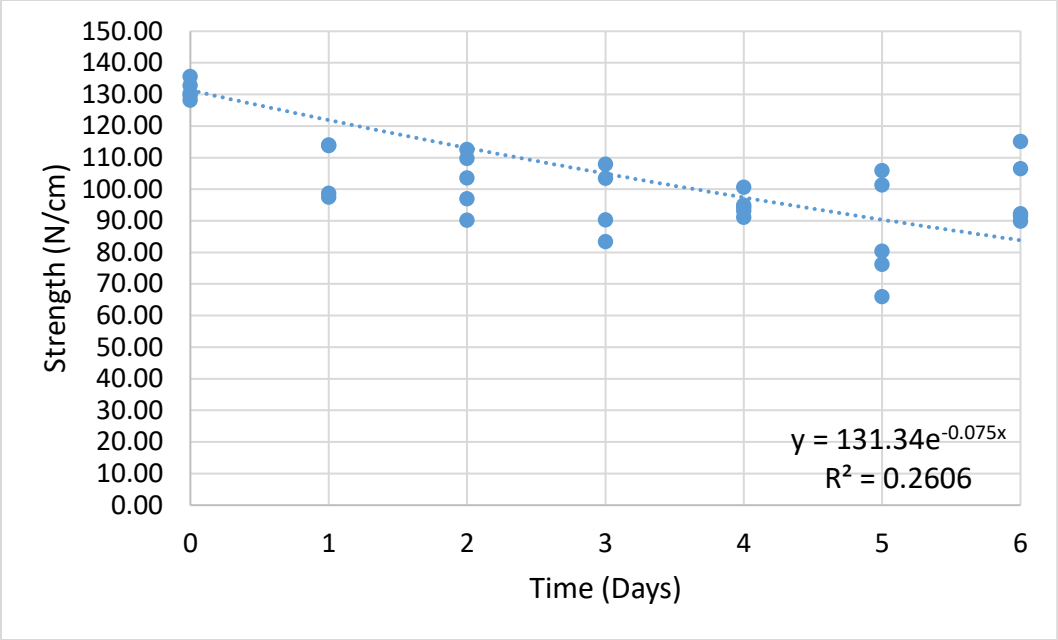

Figure 5.11: Strength vs time plot for solar cap fabric

Figure 5.12 shows the exponential fit for solar cap fabric, where time (days) was plotted on the x-axis and strength reduction (%) was plotted on the y-axis. It is observed that there was 25 % strength reduction after exposing the solar cap fabric samples for 6 days of UV radiations. The equation $y = 17.46e^{0.0994x}$ would predict the strength reduction (%) of solar cap fabric at any desired time.

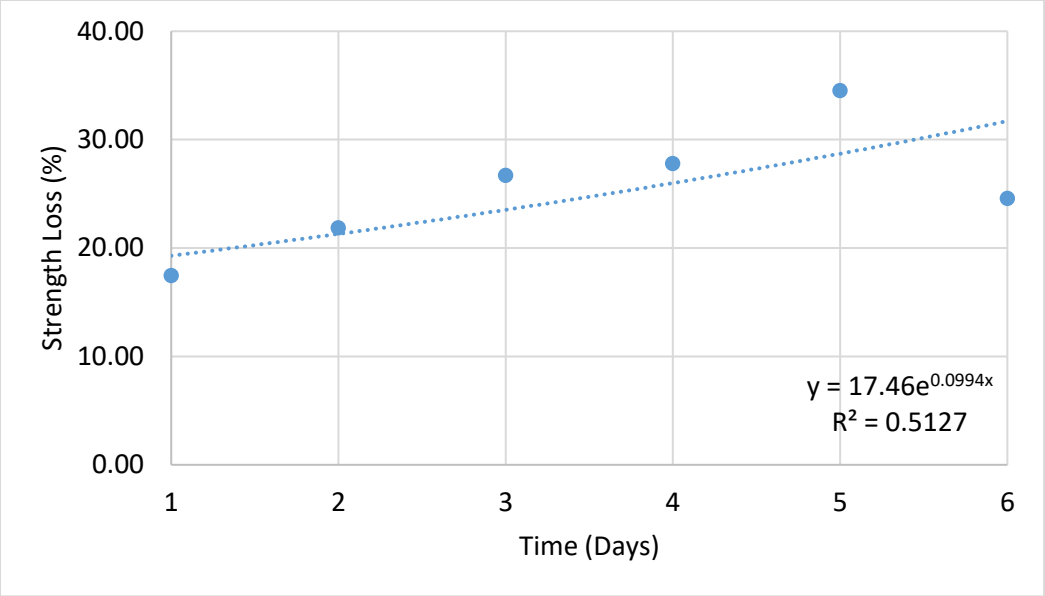

Figure 5.12: Strength loss vs time plot for solar cap fabric

The solar cap fabric samples were mounted inside the UV chamber without attaching laminate backing. By running a t-test, it was statistically observed that there was no significant difference in the strength of this fabric by attaching a laminate backing. Statistical analysis is shown in Appendix E.

Harness A was sturdy compared to the solar cap fabric and hence was easy to handle. The tensile test results for harness A gave the least variation. Eighteen harness A samples (3 for each condition) were exposed to 1, 2, 3, 4, 5, and 6 days of UV, respectively. After UV exposure, the weight of each sample was measured, and recorded. The exposed sample were then tested on the MTS Q – Test/ 5 Universal Testing Machine to evaluate their strength. Table 5.10 gives the strength and the CV values for the entire data of the harness A samples. The CV (%) value shows the variability in the specimen strengths.

Table 5.10: Strength and strength loss of harness A after exposure to UV radiations

Time (Days)	Strength (N/ cm)		Strength loss (%)
	Mean Strength (N/ cm)	CV (%)	
0	22.44	3.74	0.00
1	19.32	11.09	13.90
2	15.91	6.82	29.10
3	12.90	12.84	42.51
4	12.07	8.49	46.21
5	10.51	11.02	53.16
6	8.61	8.84	61.63

Figure 5.13 shows the exponential fit for the harness A, where time (days) was plotted on the x-axis and strength (N/ cm) on the y-axis. RSquare value shows that 90.49% of variability of the response data was explained by the model. The equation $y = 22.44e^{-0.161x}$ would predict the degradation of the harness A at any desired time.

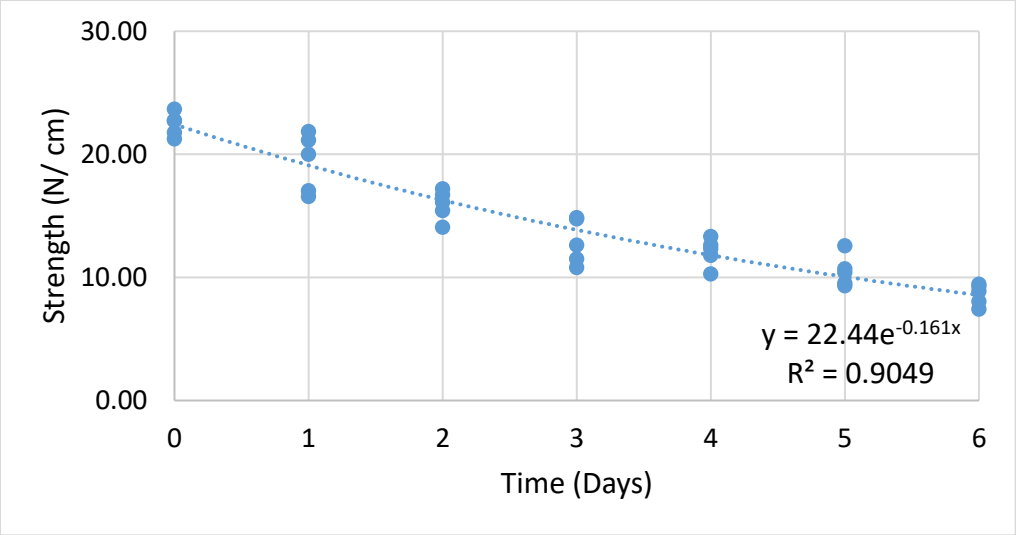

Figure 5.13: Strength vs Time plot for harness A

Figure 5.14 shows the exponential fit for the harness A, where time (days) is plotted on the x-axis and strength reduction (%) is plotted on the y-axis. It is observed that there is 61.63 % strength reduction after exposing the harness A samples for 6 days of UV. The equation $y = 13.9e^{0.2778x}$ would predict the strength reduction (%) of harness A at any desired time.

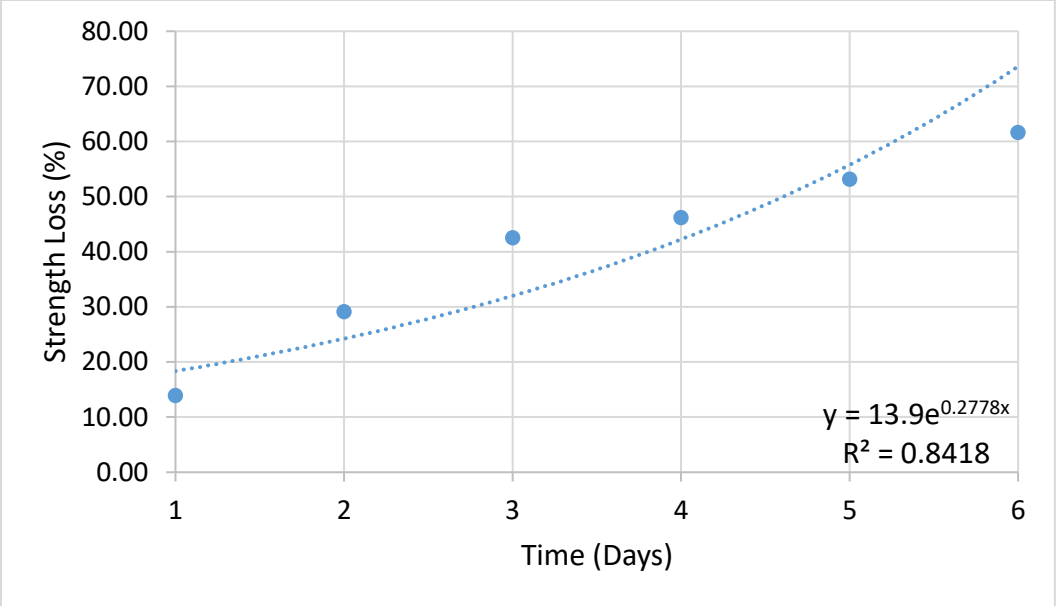

Figure 5.14: Strength loss vs time plot for harness A

Six harness B samples were exposed to 1, 2, 3, 4, 5, and 6 days of UV. After UV exposure, the weight of each sample was measured, and recorded. The exposed sample were then tested on the MTS Q – Test/ 5 Universal Testing Machine to evaluate their strength. Table 5.11 gives the strength and the CV values for the entire data of the harness B samples. The CV (%) value shows the variability in the specimen strengths.

Table 5.11: Strength and strength loss for harness B after UV radiations

Time (Days)	**Strength (N/ cm)**		**Strength loss (%)**
	Mean Strength (N/ cm)	**CV (%)**	
0	89.22	3.15	0.00
1	79.80	3.23	10.56
2	77.10	9.08	13.58

Table 5.11 (continued).

3	78.52	12.35	11.99
4	73.49	5.35	17.63
5	71.00	7.64	20.42
6	74.87	10.81	16.08

Figure 5.15 shows the exponential fit for the harness B, where time (days) was plotted on the x-axis and strength (N/ cm) on the y-axis. RSquare value shows that only 21.06% of variability of the response data was explained by the model. The equation $y = 89.22e^{-0.043x}$ would predict the degradation of the harness B at any desired time.

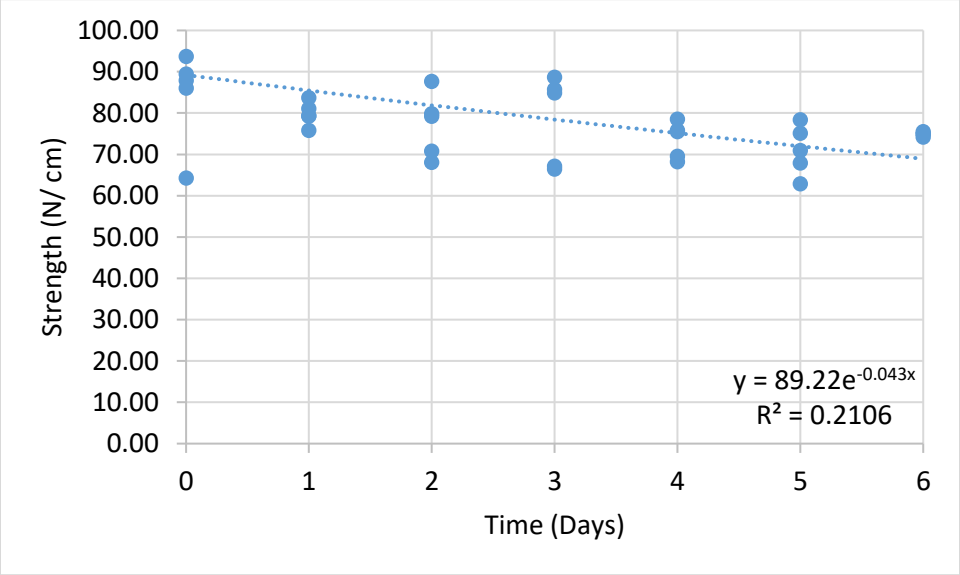

Figure 5.15: Strength vs time plot for harness B

Figure 5.16 shows the exponential fit for the harness B, where time (days) is plotted on the x-axis and strength reduction (%) is plotted on the y-axis. It is observed that there is 16.08 % strength

reduction after exposing the harness B samples for 6 days of UV. The equation $y = 89.22e^{-0.043x}$ would predict the strength reduction (%) of harness A at any desired time.

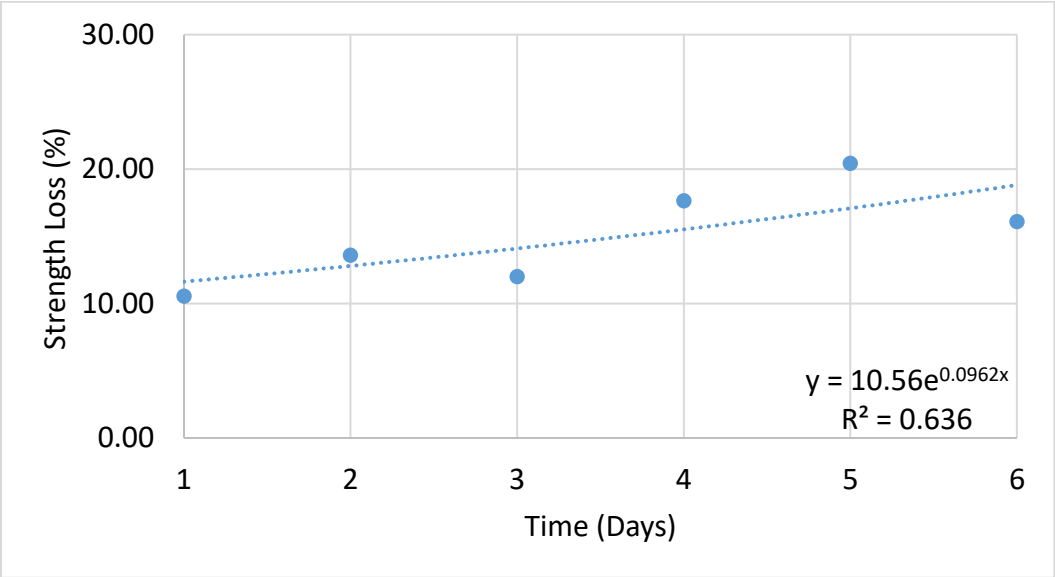

Figure 5.16: Strength loss vs time plot for harness B

The strength loss was calculated using the above exponential equations. The Table 5.12 shows the strength loss after one year.

Table 5.12: Strength loss in the fabrics after 1 year

Time (months)	**Strength Loss (%)**		
	Solar Cap Fabric	**Harness A**	**Harness B**
Month 1	90.22	99.33	75.21
Month 2	98.80	99.99	92.97
Month 3	99.89	99.99	98.26
Month 4	99.99	100	99.55
Month 5	99.99	100	99.89

Table 5.12 (continued).

Month 6	100	100	99.99
Month 7	100	100	99.99
Month 8	100	100	99.99
Month 9	100	100	99.99
Month 10	100	100	99.99
Month 11	100	100	99.99
Month 12	100	100	99.99

5.3.2. Tensile Strength Decay After Ozone Exposure

As per chapter 4, two ozone concentration were considered for carrying out weathering of the solar cap fabric with laminate backing, without laminate backing, harness A, harness B, and the laminate. These fabrics were exposed to 100 ppm ozone concentration for 1 day, and 10 ppm concentration for 10 days.

Weight of all the fabrics was measured before and after ozone exposure. Table 5.13 gives the average weight of the samples before weathering and after weathering at both levels of ozone concentration. Table 5.13 as well as the statistical analysis show that there was no significant weight loss after exposing the samples to 100 ppm ozone concentration for 1 day, and 10 ppm concentration for 10 days.

Table 5.13: Average weight of the samples before and after ozone treatments

		Solar Cap Fabric (with laminate)	**Solar Cap Fabric (without laminate)**	**Harness A**	**Harness B**	**Laminate**
Weight (gm)	Before	1.381	1.378	1.036	3.667	4.617
	100 ppm 1 day	1.384	1.381	1.039	3.674	4.616
	10 ppm 10 days	1.383	1.379	1.039	3.668	4.615
	Rank	A	A	A	A	A

Microscopic images of all the samples were taken before and after the weathering. There was no change in the images observed after exposing them to 100 ppm ozone concentration for 1 day, and 10 ppm concentration for 10 days.

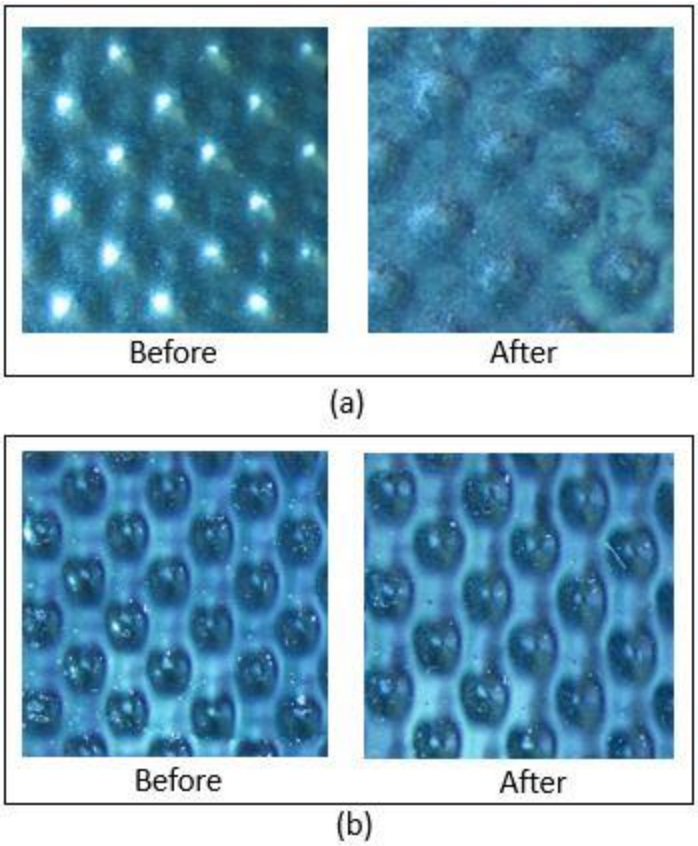

Figure 5.17: Microscopic images of laminate at 20X magnification (a) Mylar; (b) Kapton

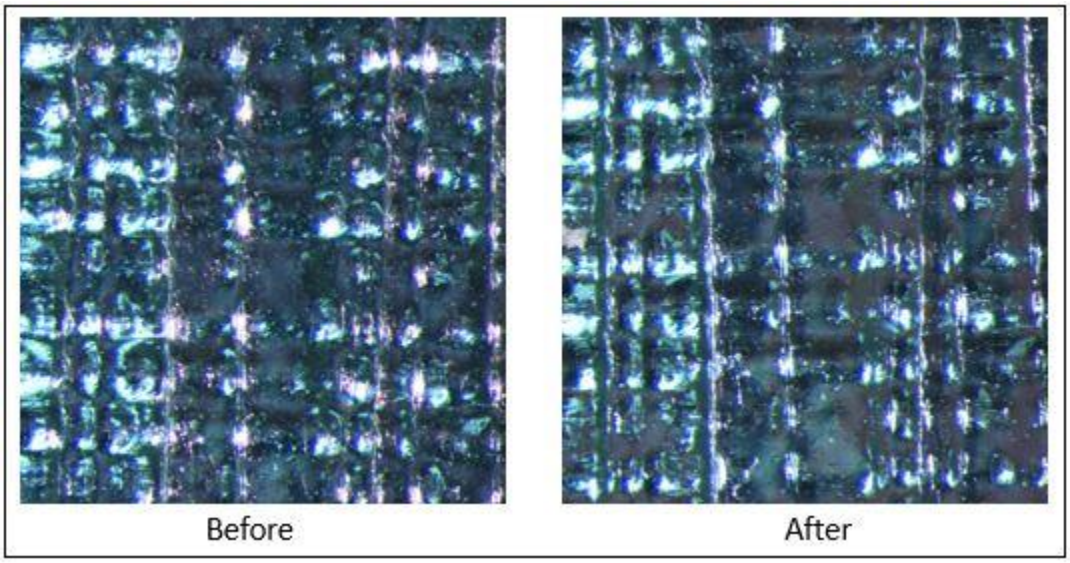

Figure 5.18: Microscopic images of solar cap fabric (with laminate backing on the non-metallized side) at 40X magnification

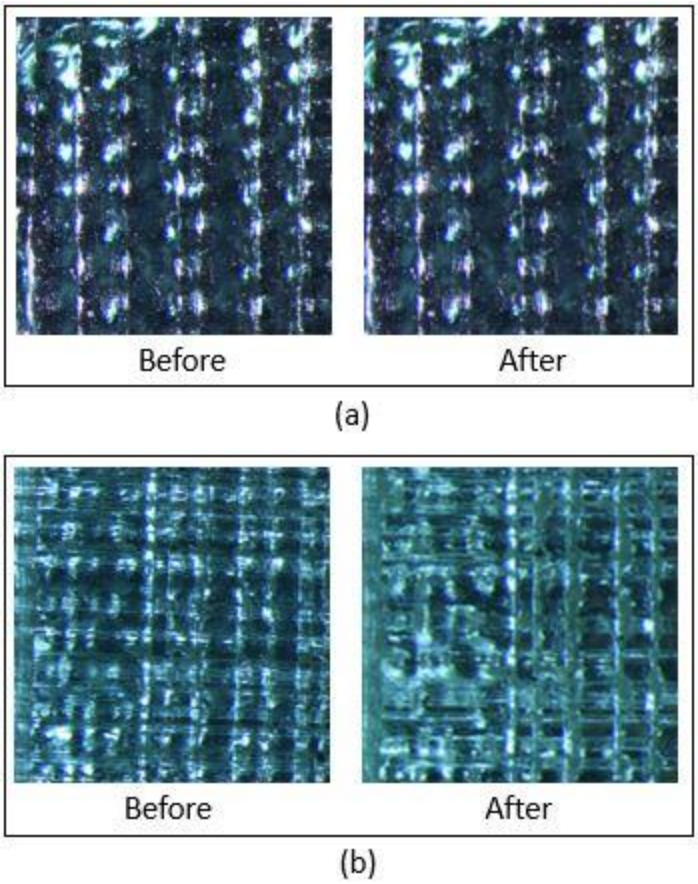

Figure 5.19: Microscopic images of solar cap fabric (without laminate backing) at 40X magnification (a) Metallized side; (b) Non-metallized side

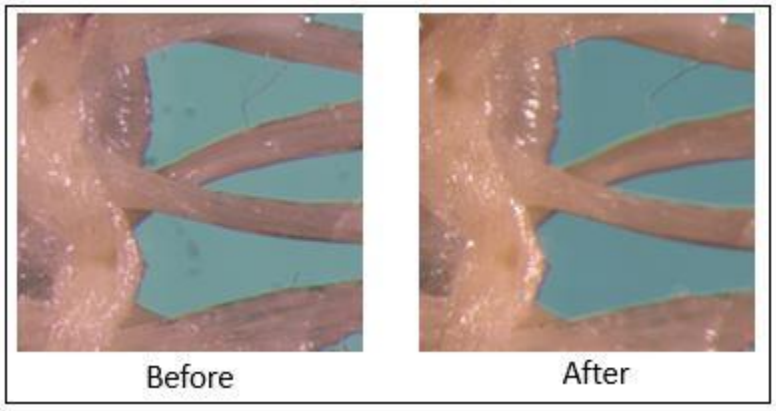

Figure 5.20: Microscopic images of harness A at 40X magnification

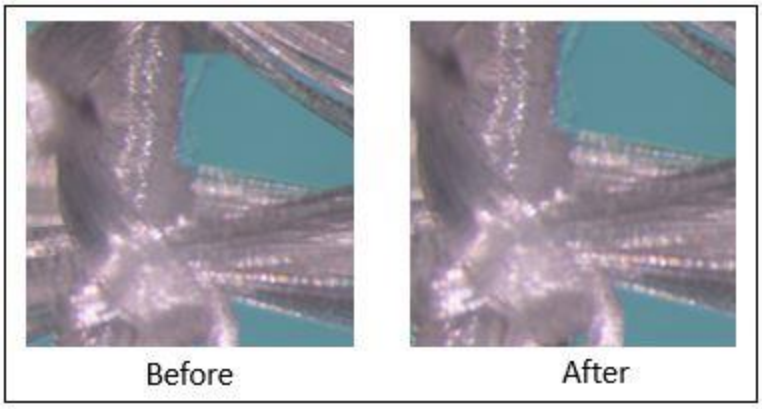

Figure 5.21: Microscopic images of harness B at 40X magnification

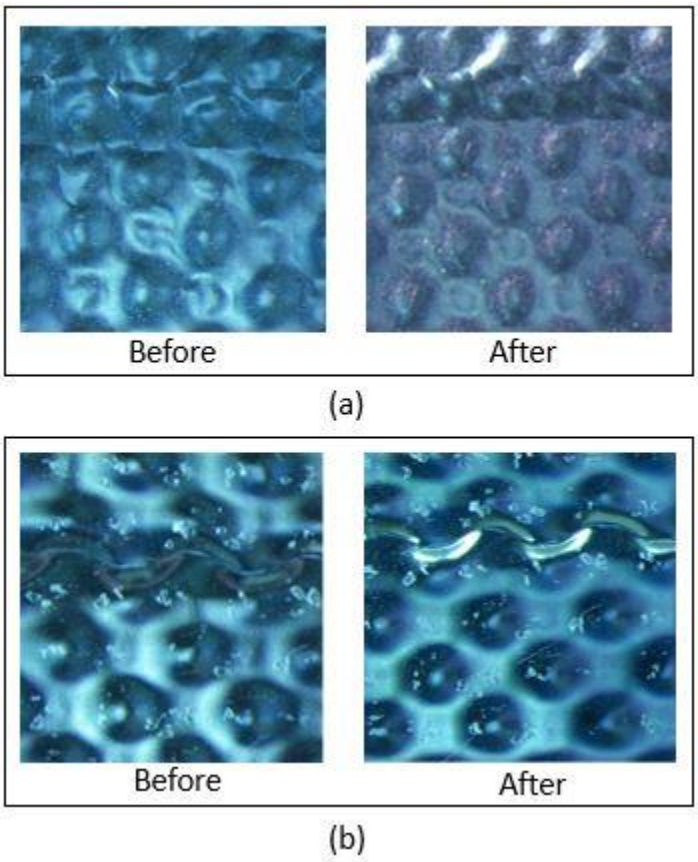

Figure 5.22: Microscopic images of laminate at 20X magnification (a) Mylar; (b) Kapton

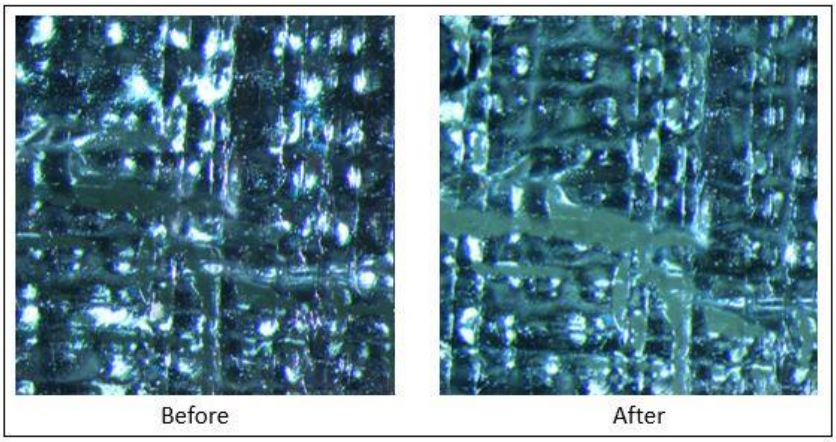

Figure 5.23: Microscopic images of solar cap fabric (with laminate backing on the non-metallized side) at 40X magnification

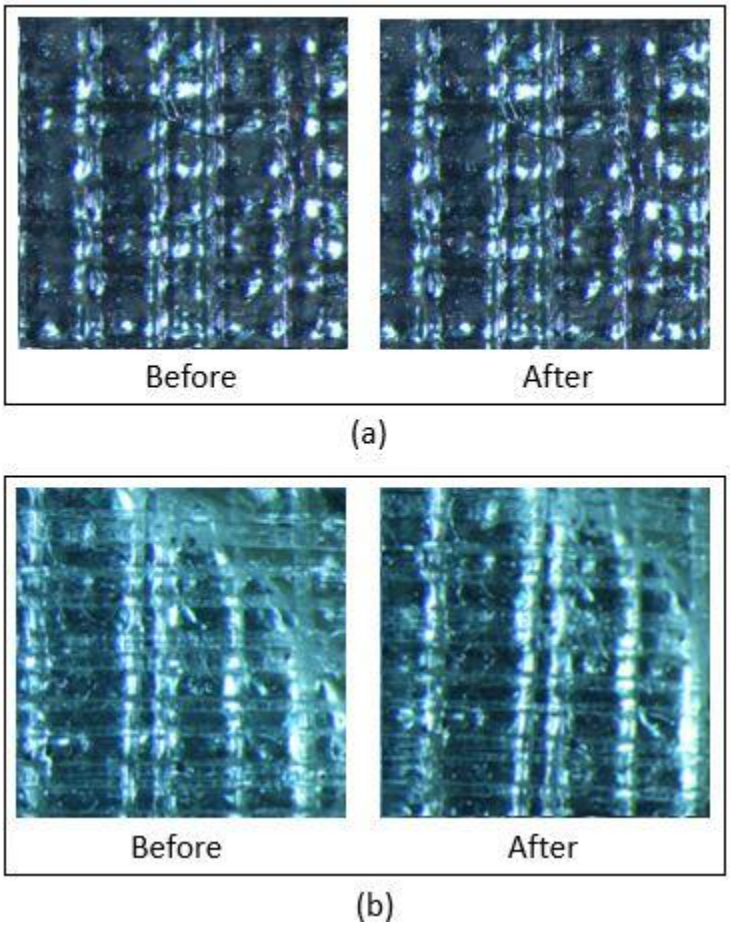

Figure 5.24: Microscopic images of solar cap fabric (without laminate backing) at 40X magnification (a) Metallized side; (b) Non-metallized side

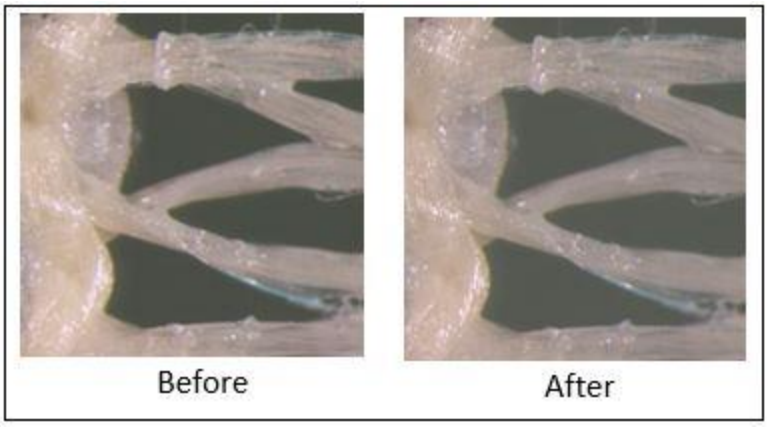

Figure 5.25: Microscopic images of harness A at 40X magnification

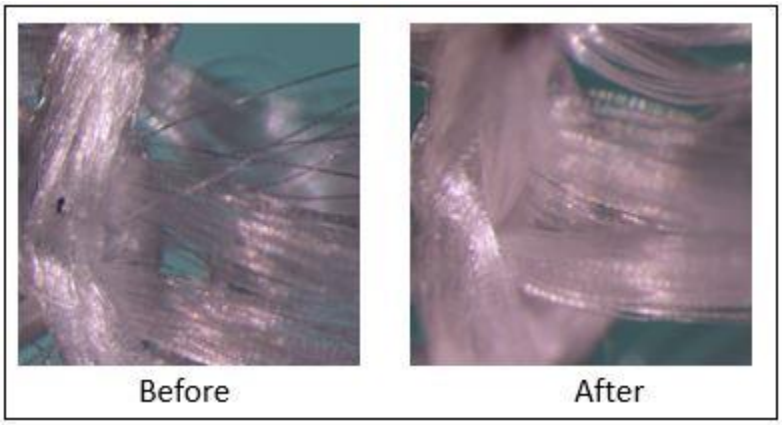

Figure 5.26: Microscopic images of harness B at 40X magnification

After the microscopic image were evaluated, specimens were cut from the samples according the specimen preparation discussion in chapter 4 and tested using MTS Landmark servo hydraulic 250 kN testing machine for the laminate and solar cap fabric, and MTS Q – Test/ 5 Universal Testing Machine for harness A and B. Table 5.14 shows the strength of all the samples before and after weathering done at 100 ppm concentration for 1 day and 10 ppm concentration for 10 days.

Table 5.14: Strength and CV values of all samples before and after weathering with 100 ppm concentration for 1 day, and 10 ppm concentration for 10 days

	Treatment	Average Strength (N/ cm)	CV (%)
Laminate	Untreated	772.16	1.36
	100 ppm 1 day	746.32	2.41
	10 ppm 10 days	747.14	1.88
Solar Cap Fabric (with laminate)	Untreated	131.34	2.00
	100 ppm 1 day	130.60	9.50
	10 ppm 10 days	137.62	5.15
Solar Cap Fabric (without laminate)	Untreated	131.34	2.00
	100 ppm 1 day	129.83	7.80
	10 ppm 10 days	121.44	4.81
Harness A	Untreated	24.49	3.74
	100 ppm 1 day	23.20	5.98
	10 ppm 10 days	23.40	6.05
Harness B	Untreated	82.71	3.15
	100 ppm 1 day	77.08	10.02
	10 ppm 10 days	89.19	6.29

Tukey HSD test was carried out of the entire date of each sample. The connecting letters plot of Tukey HSD test (Table 5.15) showed that there was not significant difference between the average strength of the samples before and after ozone exposure at different concentrations and period.

Hence, the variation seen in the strengths of all the samples might be because of variables other than the two-different ozone concentration.

Table 5.15: Tukey HSD connecting letters report of laminate, solar cap fabric with and without laminate backing, harness A, and harness B after total ozone exposure

Laminate	**Level**	**Rank**	**Mean**
	Untreated	A	772.15
	10 ppm 10 days	A	747.13
	100 ppm 1 Day	A	746.32
Solar Cap Fabric (with laminate)	Level		Mean
	10 ppm 10 days	A	137.61
	Untreated	A	131.33
	100 ppm 1 Day	A	130.60
Solar Cap Fabric (without laminate)	**Level**		**Mean**
	100 ppm 1 Day	A	134.72
	Untreated	A	131.33
	10 ppm 10 days	A	121.43
Harness A	**Level**		**Mean**
	10 ppm 10 days	A	23.40
	100 ppm 1 Day	A	23.20
	Untreated	A	22.43
Harness B	**Level**		**Mean**
	10 ppm 10 days	A	91.20
	Untreated	A	89.21
	100 ppm 1 Day	A	79.49

5.3.3. Tensile Strength Decay After UV and Ozone Exposure

The effect of UV radiation for 6 days and ozone concentration of 100 ppm 1 day on the solar cap fabric was evaluated. The average strength of the specimens turned out to be 94.91 N/ cm, which is less than 131.34 N/ cm (untreated). The result of the strength of unexposed sample was compared to the sample exposed only to the UV radiations, sample exposed only to 100 ppm concentration for 1 day, and sample exposed to both, UV radiation for 6 days and 100 ppm ozone concentration for 1 day. Comparison for all the pairs was done using Tukey HSD. There was a significant strength loss when the sample was exposed to UV radiations for 6 days There was no significant difference in the strength of the unexposed sample and samples exposed to 100 ppm ozone concentration for 1 day. This showed that ozone did not cause any strength reduction for the solar cap fabric. Also, there was no significant difference in the strength of sample exposed only to UV radiations and sample exposed to UV radiation plus ozone concentration. This proved that the ozone does not affect the strength of the solar cap fabric. See Table 5.16.

Table 5.16: Tukey HSD connecting letters report for solar cap fabric treated with ozone and UV

(Levels not connected by the same letter are significantly different)

Level	**Rank**		**Average Strength (N/cm)**
Untreated	A		131.33600
Only Ozone	A		130.60080
Only UV		B	99.05200
UV + Ozone		B	94.91875

6. CONCLUSION AND SUGGESTIONS FOR FUTURE STUDIES

This chapter would comprise of conclusions based on the results discussed on chapter 5. Tensile test on the seams was carried out using different variables like seaming temperature, pressure, and speed, and overlap seam lengths. Every variable had levels as mentioned in chapter 3. From the results obtained from the tensile test, it could be concluded that seam formed with 7.62 cm of overlap seam length, seamed at 155 °C, 400 kPa, and 6m/min speed gave the highest strength, even greater then the base hull laminate. The statistical analysis showed that the overlap seam length variable and the seaming temperature variable had the most effect on the strength of the seams, whereas low or high levels of seaming speed did not show any effect. The 2.54 cm overlap seam gave highest strength when seamed at 185 °C, 100 kPa, and 6m/min speed. 2.54 cm seams seamed at 155 °C did not give good results. Increase in the overlap length from 7.62 cm to 12.70 cm did not show increase in strength due to more number of defects observed as the length of the specimen increased.

Hence, in the future it is recommended that, while fabricating the hull laminate, it must be made sure that the load bearing yarns are equally spaced and at the same time well oriented. For a plain-woven fabric, it must be made sure that the weft and the warp yarns are perfectly perpendicular to each other. Load bearing layer is a crucial layer of an airship hull laminate, and therefore yarns must be well oriented to give high strength values, due to equal load sharing by all the yarns.

Peel test on the seams was carried out using different variables like, seaming temperature, pressure, and speed. Every variable had levels as mentioned in chapter 3. For the T-peel test it was observed that high load peaks were obtained at specimens prepared at 155 °C, 400 kPa, and 6m/min.

However, it cannot be concluded that the above-mentioned variables were good to give high peel resistance. The adhesive at these variables showed inherent failure rather than adhesive failure which tend to give high peaks. Any seam that gave high peaks failed the same way. Other than the above seaming variables, the T-peel specimens showed higher strength values at 185 °C compared to 155 °C.

The solar cap fabric, harness A, and harness B when exposed to total 6 days of UV exposure, gave 25%, 61.63%, and 16.08% reduction in the strength, respectively. No weight loss was observed. Exponential plots gave equations that would predict the degradation of solar cap fabric, harness A, and B at any desired time. The statistical analysis of the strength of the solar cap fabric with and without laminate, harness A, harness B, and laminate showed that the strength of these samples, after exposure to ozone at 100 ppm concentration for 1 day, and 10 ppm concentration for 10 days, were not significantly different that the strength of untreated samples. Therefore, there was no strength loss observed after ozone treatment. The sola cap fabric that was exposed to 6 days of UV and then 100 ppm concentration of ozone for 1 day showed reduction in strength. The statistical analysis proved that the loss in strength was due to exposure to UV radiations and not ozone concentration.

The weathering procedure followed in this research does not consider two treatments simultaneously, may it be weathering of seamed laminates or weathering of solar cap fabric. The solar cap fabric was treated with UV radiations first followed by ozone concentrations, whereas the seams were treated with ozone concentrations first and then exposed to low and high temperatures. This not the condition in stratosphere. All kinds of weathering take place

simultaneously and depending on day and night (UV and temperature level). Therefore, to know that actual effect of weathering on the seams and solar cap fabric, similar type of wreathing conditions need to be set for testing as well.

7. REFERENCES

Anon, 2012_cambridge_university_-_airship_technology_-_second_edition.pdf.

Bach, Sascha; Thurling, Karsten; Majschak, J.-P., 2010. Effect of high-pressure food processing on the mass transfer properties of selected packaging materials. *Packaging and Technology and Science*, 23(May), pp.253–266. Available at: http://onlinelibrary.wiley.com/doi/10.1002/pts.893/abstract.

Baird, G. et al., 2014. A I R S H I P S : , (February).

Banea, M.D. & da Silva, L.F.M., 2009. Adhesively bonded joints in composite materials: An overview. *Proceedings of the Institution of Mechanical Engineers, Part L: Journal of Materials: Design and Applications*, 223(1), pp.1–18. Available at: http://journals.sagepub.com/doi/10.1243/14644207JMDA219.

Chamis, C.C. & Murthy, P.L.N., 1991. Simplified Adhesively Procedures for Designing Bonded Composite Joints. *Journal of Reinforced Plastics and Composites*, 10(1), pp.29–41. Available at: http://jrp.sagepub.com/cgi/doi/10.1177/073168449101000102.

Colozza, A. & Dolce, J.L., 2005. High-Altitude, Long-Endurance Airships for Coastal Surveillance. *NASA Technical Report*, (February).

D'Oliveira, F.A., De Melo, F.C.L. & Devezas, T.C., 2016. High-altitude platforms — Present situation and technology trends. *Journal of Aerospace Technology and Management*, 8(3), pp.249–262.

Davey, L. et al., 2008. High altitude platform stations for Australia. *Telecommunications Journal of Australia*, 58(2–3), pp.1–8.

DSM, 2008. Technical brochure: Dyneema in marine and industrial applications. , 31(46), p.4.

Ernest, U., 1994. Peelable Seam Systems and their Production. , 7, pp.39–50.

Farris, S. et al., 2011. Effects of different sealing conditions on the seal strength of polypropylene films coated with a bio-based thin layer. *Italian Journal of Food Science*, 23(SUPPL.), pp.111–114.

Fesen, R.A., A High-Altitude, Station Keeping Astronomical Platform.

Fesen, R. & Brown, Y., 2015. A method for establishing a long duration, stratospheric platform for astronomical research. *Experimental Astronomy*, 39(3), pp.475–493.

Hart-Smith, L.J., 2002. Adhesive bonding of composite structures—progress to date and some remaining challenges. *Journal of Composites, Technology and Research*, 24(3), pp.133–151.

He, X., 2011. A review of finite element analysis of adhesively bonded joints. *International Journal of Adhesion and Adhesives*, 31(4), pp.248–264. Available at: http://dx.doi.org/10.1016/j.ijadhadh.2011.01.006.

Islam, S. & Bradley, P., 2012. Materials. In *Airship Technology*. pp. 113–148.

Jamison, Lewis; Sommer, Geoffrey; Porche III, I., 2007. *High-Altitude Airships for the Future Force Army*,

Li, Y., Nahon, M. & Sharf, I., 2011. Airship dynamics modeling: A literature review. *Progress in Aerospace Sciences*, 47(3), pp.217–239. Available at: http://dx.doi.org/10.1016/j.paerosci.2010.10.001.

Liao, L. & Pasternak, I., 2009. A review of airship structural research and development. *Progress in Aerospace Sciences*, 45(4–5), pp.83–96. Available at: http://dx.doi.org/10.1016/j.paerosci.2009.03.001.

Lin, G. & Tan, H., 2011. The influence of ozone on the property of envelop materials of near space vehicle. *Proceedings of 2011 International Conference on Electronic and Mechanical*

Engineering and Information Technology, EMEIT 2011, 3, pp.1413–1416.

Liu, Y. et al., 2014. Effect of accelerated xenon lamp aging on the mechanical properties and structure of thermoplastic polyurethane for stratospheric airship envelope. *Journal Wuhan University of Technology, Materials Science Edition*, 29(6), pp.1270–1276.

Maekawa, S. et al., 2008. Tear Propagation of a High-Performance Airship Envelope Material. *Journal of Aircraft*, 45(5), pp.1546–1553. Available at: http://arc.aiaa.org/doi/10.2514/1.32264.

McConnell, V.P., 1999. Joining composites. *Reinforced Plastics*, 43(6), pp.26–32.

Mcdaniels, K. et al., 2009. Fabrics for Aerospace Applications. *Cubic Tech Corp.*, pp.1–9.

Miller, T. & Mandel, M., 2000. Airship Envelopes : Requirements, Materials and Test Methods. *3rd International Airship Convention and Exhibition*, pp.1–5.

Reliable, P. & Airships, Q., Lighter-Than-Air.

Said, M.A. et al., 2006. Investigation of ultra violet (UV) resistance for high strength fibers. *Advances in Space Research*, 37(11), pp.2052–2058.

Sami, A. et al., 2015. OPEN ACCESS A Brief Study on Airship Using Aerospace , Electronic and Communication Applications. , 5(4), pp.34–46.

Seely, L.G. & Smith, M.S., 2002. A realistic view of the future of scientific ballooning. *Advances in Space Research*, 30(5), pp.1125–1133.

Sherwood, A., 2006. Making Mylar Envelopes. *Envelope Design*. Available at: https://www.rcgroups.com/forums/showthread.php?489372-Making-Mylar-Envelopes.

Smith, I. et al., 2011. HiSentinel80: Flight of a High Altitude Airship. *11th AIAA Aviation Technology, Integration, and Operations (ATIO) Conference*, (September). Available at: http://arc.aiaa.org/doi/10.2514/6.2011-6973.

Tang, W. & Keefe, M., 2003. Stress analysis and structural modificatoins of a polyester double-tape seam.pdf. *Proceedings of the Institution of Mechanical Engineers, Part L: Journal of Materials: Design and Applications*, 217, pp.101–112.

Tsai, M.Y., Oplinger, D.W. & Morton, J., 1998. Improved theoretical solutions for adhesive lap joints. *International Journal of Solids and Structures*, 35(12), pp.1163–1185.

Vallabh, R. et al., 2016. Improving high-altitude UV–Vis resistance of PBO braided tendons of NASA's super pressure balloons. *Journal of the Textile Institute*, 107(1), pp.136–143. Available at: http://dx.doi.org/10.1080/00405000.2015.1077021.

Yang, Y., Zeng, P. & Lei, L., 2015a. High-frequency dielectric heating and the strength of flexible polymer seams. *Journal of Materials Processing Technology*, 215(January), pp.105–113. Available at: http://dx.doi.org/10.1016/j.jmatprotec.2014.07.024.

Yang, Y., Zeng, P. & Lei, L., 2015b. Numerical simulation study of the T-Peel behavior of coated fabric films used in inflatable structures. *Journal of Applied Polymer Science*, 132(3), pp.1–9.

Zhai, H. & Euler, A., 2005. Material challenges for lighter-than-air systems in high altitude applications. *AIAA 5th Aviation, Technology, Integration, and Operations Conference (ATIO)*, (September), pp.1–12. Available at: http://arc.aiaa.org/doi/pdf/10.2514/6.2005-7488.

8. APPENDICES

Appendix A

Pretrials to set the levels of variable in the experimental design for seams

To set the two levels of the variable (temperature, pressure, and speed), a few pre – trials were carried out using hand peel test and T – peel test. Setting the pressure and speed constant, at 3 bars at 4m/ min, temperature was varied. Specimens were seamed at 135 ^{0} C, 145 ^{0} C, 155 ^{0} C, 165 ^{0} C, 175 ^{0} C, 185 ^{0} C, and 195 ^{0} C. 135 ^{0} C and 145^0 C made poor seam, whereas, the peeling strength required to peel increased tremendously for the sample that was seamed at 155 ^{0} C. 165 ^{0} C and 175 ^{0} C did not give higher strength than 155 °C, but specimen seamed at 185^0 C made the best seam. The strength required to peel was the highest at 185 °C, and no damage occurred to the laminate or the seam. 195^0 C also proved to be as good as 185^0 C. Based on this justification, 155^0 C was decided to be the low temperature, whereas 185^0 C was decided to be the high temperature.

For setting low and high-speed level, temperature and pressure was kept constant at 155^0 C and 3 bars, respectively. Seams were prepared from speed starting at 3 m/ min up to 10 m/min. It was found that 3 m/ min speed gave good strength. 4 m/ min and 5 m/ min did not show much difference. 6 m/ min speed gave significantly improved seam peeling property compared to 3 m/ min, 4 m/ min, and 5 m /min. Seams prepared at speeds higher than 6 m/ min did not significantly affect the seam quality. Based on this justification, 3 m/ min was decided to be the lower speed for seaming and 6 m/ min was decided to be the high speed. Faster speed gave even distribution of heat to the entire seam due to low dwell time.

For setting low and high pressure, temperature and speed were kept constant at 155^0 C and 4 m/ min, respectively. Seams were prepared at pressure 100 kPa, 2 bar, 3 bar, 400 kPa, and 5 bar. 100 kPa pressure gave moderate seam strength, at the same time, 2 bar and 3 bar did not make any great difference. 400 kPa pressure gave significantly better seam compared to the previous pressure. 5 bar did not make any difference and also damaged the seam a bit. Based on this justification, 100 kPa pressure was decided to be the lower pressure for seaming whereas, 400 kPa would be the high speed.

7.62 x 10.16 cm laminates were cut to prepare a seam of 1" overlap seam length. 50.8 µm TPU was the adhesive used to bond the two laminates with the interface being PI – TPU – PI. The laminates were seamed using the Fusing Machine. The Figure A.1 shows sample preparation.

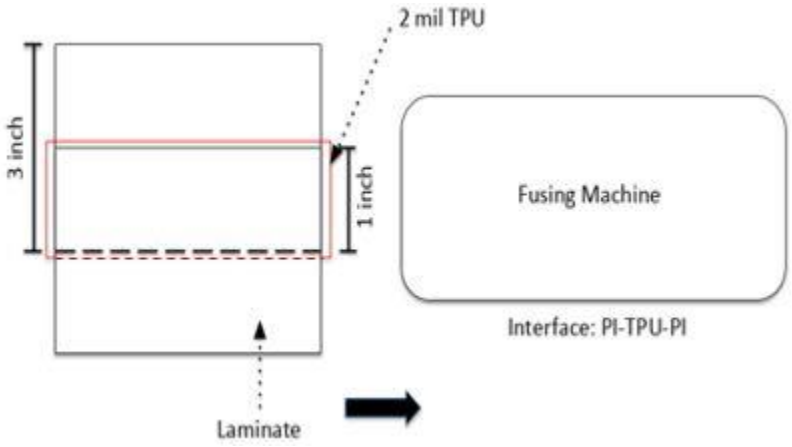

Figure A.1: Pretrial sample preparation

Appendix B

Statistical analysis of tensile test for seam optimization

Table B.1: Summary of fit for the seam tensile test

RSquare	0.952254
RSquare Adj	0.939335
Root Mean Square Error	23.5753
Mean of Response	625.7744
Observations (or Sum Wgts)	109

Table B.2: Analysis of Variance for seam tensile test

Source	**DF**	**Sum of Squares**	**Mean Square**	**F Ratio**
Model	23	942221.82	40966.2	73.7074
Error	85	47242.54	555.8	**Prob > F**
C. Total	108	989464.36		<.0001*

Table B.3: Parameter estimates for tensile test

Term	**Estimate**	**Std Error**	**t Ratio**	**Prob>|t|**
Intercept	624.26285	2.279143	273.90	<.0001*
Overlap Seam Length (in)[1]	-43.17979	3.284971	-13.14	<.0001*
Overlap Seam Length (in)[3]	77.472222	3.180501	24.36	<.0001*
Temperature (deg)[155]	-22.91093	2.279143	-10.05	<.0001*
Overlap Seam Length (in)[1]*Temperature (deg)[155]	-69.0909	3.284971	-21.03	<.0001*
Overlap Seam Length (in)[3]*Temperature (deg)[155]	61.186419	3.180501	19.24	<.0001*
Pressure (bar)[1]	-22.19154	2.279143	-9.74	<.0001*

Table B.3 (continued).

Overlap Seam Length (in)[1]*Pressure (bar)[1]	-29.47846	3.284971	-8.97	<.0001*
Overlap Seam Length (in)[3]*Pressure (bar)[1]	7.4963528	3.180501	2.36	0.0207*
Temperature (deg)[155]*Pressure (bar)[1]	-17.04575	2.279143	-7.48	<.0001*
Overlap Seam Length (in)[1]*Temperature (deg)[155]*Pressure (bar)[1]	-35.54311	3.284971	-10.82	<.0001*

Table B.4: Effect tests for tensile test

Source	**Nparm**	**DF**	**Sum of Squares**	**F Ratio**	**Prob > F**
Overlap Seam Length (in)	2	2	330177.52	297.0320	<.0001*
Temperature (deg)	1	1	56163.83	101.0514	<.0001*
Overlap Seam Length (in)*Temperature (deg)	2	2	300379.09	270.2249	<.0001*
Pressure (bar)	1	1	52692.17	94.8051	<.0001*
Overlap Seam Length (in)*Pressure (bar)	2	2	48440.26	43.5775	<.0001*
Temperature (deg)*Pressure (bar)	1	1	31088.75	55.9357	<.0001*
Overlap Seam Length (in)*Temperature (deg)*Pressure (bar)	2	2	80425.90	72.3522	<.0001*
Speed (m/min)	1	1	711.89	1.2809	0.2609
Overlap Seam Length (in)*Speed (m/min)	2	2	3954.55	3.5576	0.0328*
Temperature (deg)*Speed (m/min)	1	1	20212.13	36.3662	<.0001*
Overlap Seam Length (in)*Temperature (deg)*Speed (m/min)	2	2	1497.98	1.3476	0.2654
Pressure (bar)*Speed (m/min)	1	1	2422.35	4.3584	0.0398*
Overlap Seam Length (in)*Pressure (bar)*Speed (m/min)	2	2	18192.59	16.3663	<.0001*
Temperature (deg)*Pressure (bar)*Speed (m/min)	1	1	3286.29	5.9128	0.0171*
Overlap Seam Length (in)*Temperature (deg)*Pressure (bar)*Speed (m/min)	2	2	32178.27	28.9480	<.0001*

Appendix C

T-peel test graphs

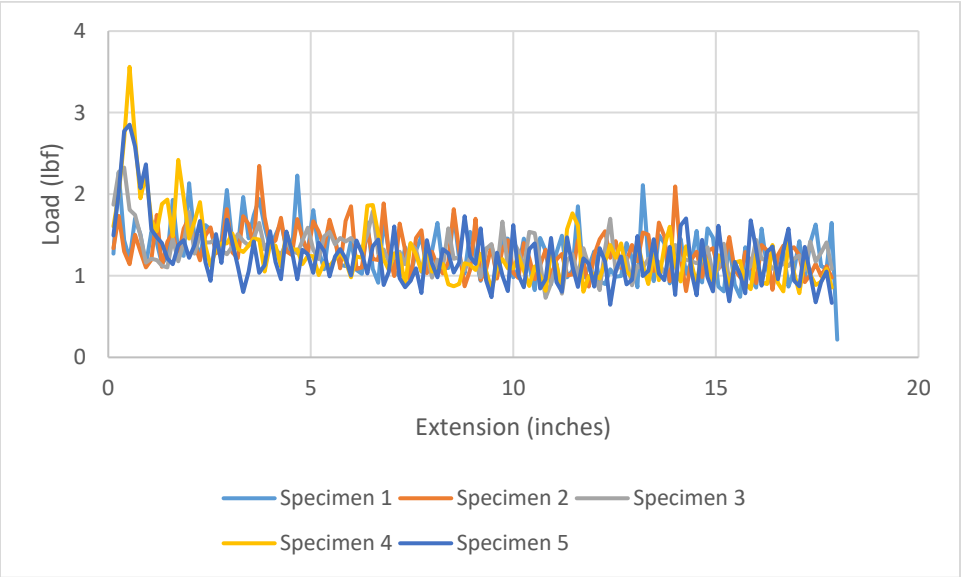

Figure C.1: T-peel test graph for seaming variables 155 °C, 100 kPa, 3 m/min

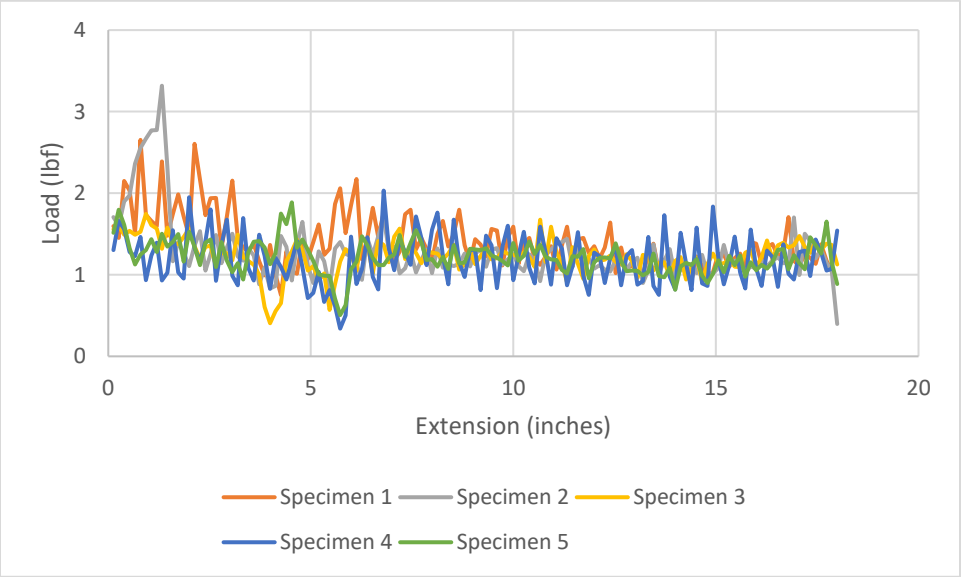

Figure C.2: T-peel test graph for seaming variables 155 °C, 100 kPa, 6 m/min

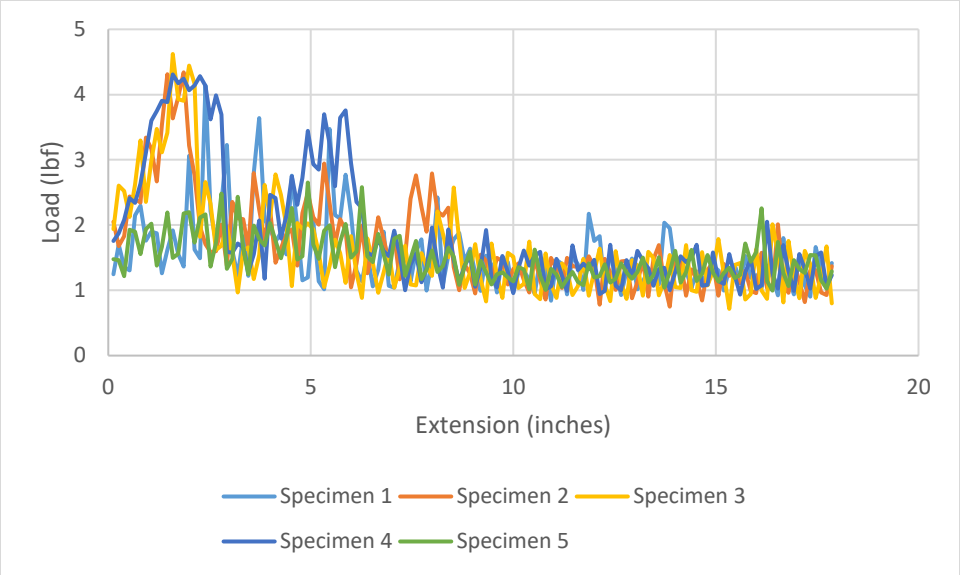

Figure C.3: T-peel test graph for seaming variables 155 °C, 400 kPa, 3 m/min

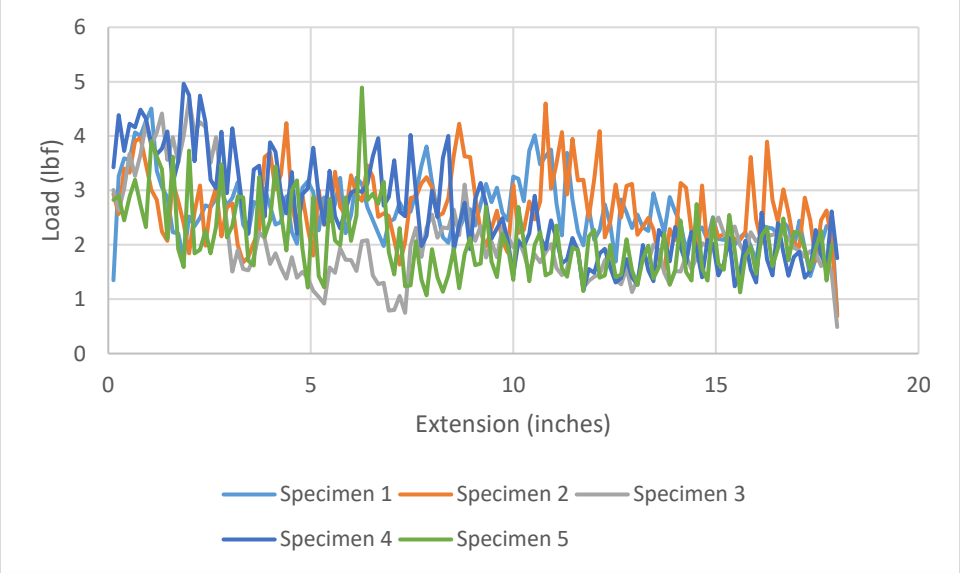

Figure C.4: T-peel test graph for seaming variables 155 °C, 400 kPa, 6 m/min

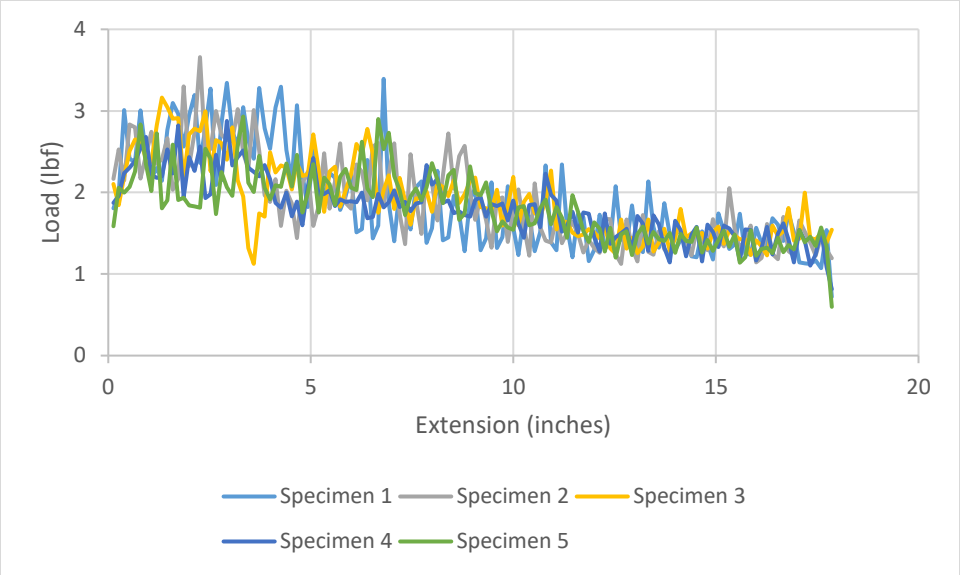

Figure C.5: T-peel test graph for seaming variables 185 °C, 100 kPa, 3 m/min

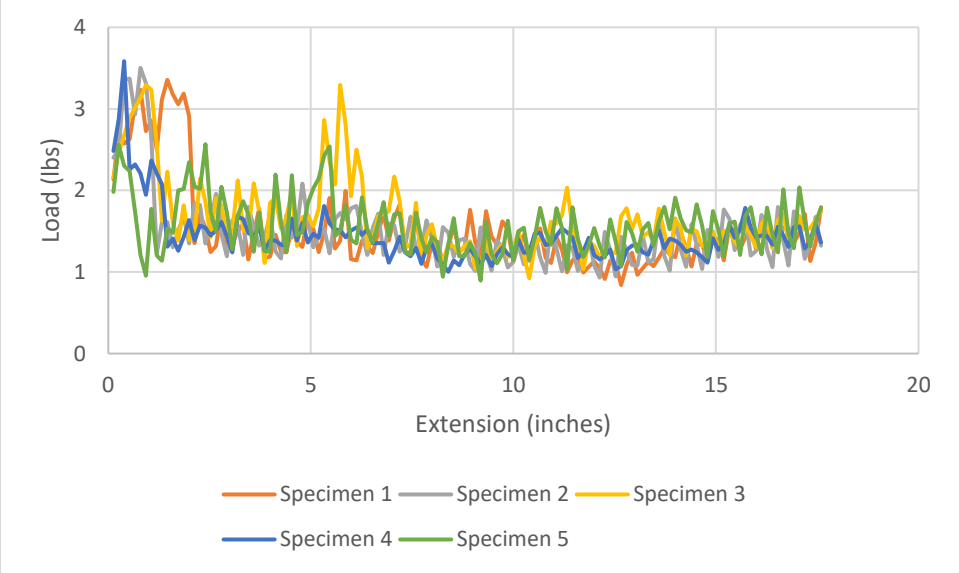

Figure C.6: T-peel test graph for seaming variables 185 °C, 100 kPa, 6 m/min

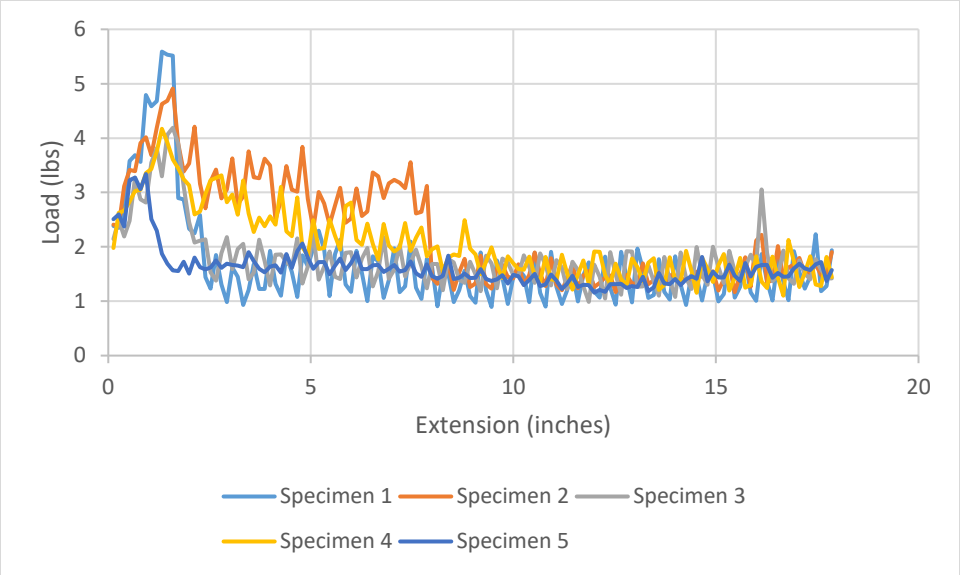

Figure C.7: T-peel test graph for seaming variables 185 °C, 400 kPa, 3 m/min

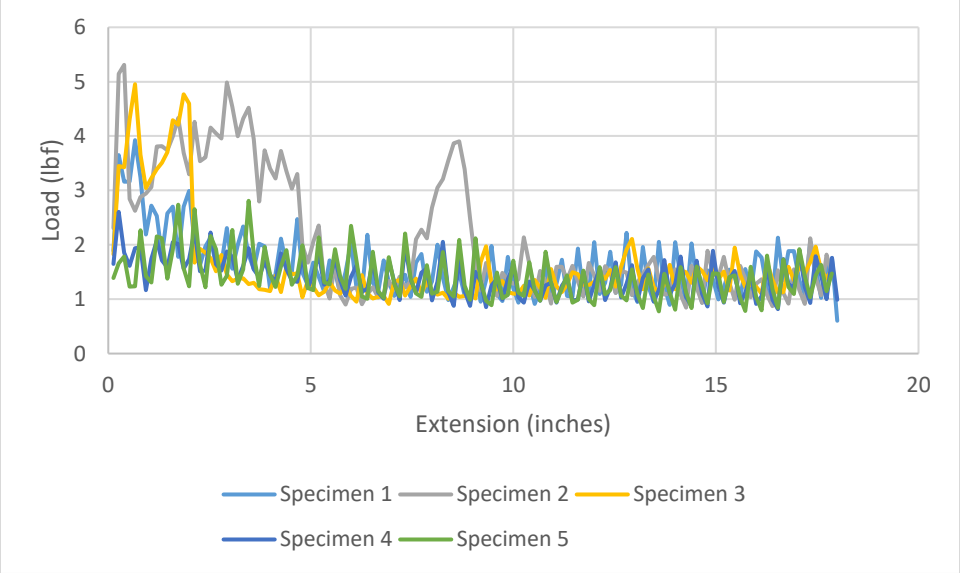

Figure C.8: T-peel test graph for seaming variables 185 °C, 400 kPa, 6 m/min

Appendix D

Statistical analysis of T-peel test

Table D.1: Summary of Fit for T-peel test

RSquare	0.962749
RSquare Adj	0.953757
Root Mean Square Error	0.170041
Mean of Response	2.911892
Observations (or Sum Wgts)	37

Table D.2: Analysis of Variance for T-peel test

Source	DF	Sum of Squares	Mean Square	F Ratio
Model	7	21.671061	3.09587	107.0714
Error	29	0.838507	0.02891	Prob > F
C. Total	36	22.509568		<.0001*

Table D.3: Parameter estimates for T-peel test

Term	Estimate	Std Error	t Ratio	Prob>|t|
Intercept	2.9839167	0.028384	105.13	<.0001*
Temperature (deg)[155]	-0.084917	0.028384	-2.99	0.0056*
Pressure (bar)[1]	-0.271417	0.028384	-9.56	<.0001*
Temperature (deg)[155]*Pressure (bar)[1]	-0.321583	0.028384	-11.33	<.0001*
Speed (m/ min)[3]	-0.102083	0.028384	-3.60	0.0012*
Temperature (deg)[155]*Speed (m/ min)[3]	-0.490917	0.028384	-17.30	<.0001*
Pressure (bar)[1]*Speed (m/ min)[3]	0.2895833	0.028384	10.20	<.0001*
Temperature (deg)[155]*Pressure (bar)[1]*Speed (m/ min)[3]	0.3354167	0.028384	11.82	<.0001*

Table D.4: Effects test for T-peel test

Source	Nparm	DF	Sum of Squares	F Ratio	Prob > F
Temperature (deg)	1	1	0.2587816	8.9500	0.0056*
Pressure (bar)	1	1	2.6437505	91.4349	<.0001*
Temperature (deg)*Pressure (bar)	1	1	3.7113722	128.3589	<.0001*
Speed (m/ min)	1	1	0.3739875	12.9345	0.0012*
Temperature (deg)*Speed (m/ min)	1	1	8.6489423	299.1262	<.0001*
Pressure (bar)*Speed (m/ min)	1	1	3.0095016	104.0845	<.0001*
Temperature (deg)*Pressure (bar)*Speed (m/ min)	1	1	4.0375389	139.6395	<.0001*

Appendix E

Strength values of Solar Cap Fabric, Harness A, and Harness B after 6 days of total exposure

Table E.1: Strength of solar cap fabric after UV exposure

#	Strength (N/cm)						
	Day 0	**Day 1**	**Day 2**	**Day 3**	**Day 4**	**Day 5**	**Day 6**
1	135.65	113.98	97.02	62.59	91.12	76.21	89.95
2	130.27	73.62	103.56	90.28	100.69	80.41	115.13
3	129.70	97.47	109.73	107.92	94.99	65.99	106.47
4	132.87	113.80	90.16	83.39	94.25	101.39	91.51
5	128.19	98.76	112.58	103.43	93.15	105.88	92.20
Mean	131.34	108.41	102.61	96.26	94.84	85.98	99.05
CV (%)	2.00	7.45	8.00	10.24	3.38	17.71	10.10

Table E.2: Strength of harness A after UV exposure

#	Strength (N/ cm)						
	Day 0	**Day 1**	**Day 2**	**Day 3**	**Day 4**	**Day 5**	**Day 6**
1	22.74	20	14.09	14.74	12.34	10.42	8.87
2	21.77	21.16	15.43	11.5	11.78	10.7	9.45
3	21.26	16.57	16.12	14.86	12.64	9.32	7.43
4	22.73	21.84	16.71	10.79	10.28	12.58	9.26
5	23.67	17.04	17.2	12.61	13.32	9.53	8.06
Mean	22.44	19.32	15.91	12.9	12.07	10.51	8.61
CV (%)	3.74	11.09	6.82	12.84	8.49	11.02	8.83

Table E.3: Strength of harness B after UV exposure

#	Strength (N/ cm)						
	Day 0	**Day 1**	**Day 2**	**Day 3**	**Day 4**	**Day 5**	**Day 6**
1	64.27	81.07	70.77	84.82	75.44	75.09	54.67
2	87.82	83.65	79.79	85.66	69.52	78.35	74.94
3	93.63	79.3	79.22	67.12	75.81	67.84	75.46
4	86.02	79.23	87.66	66.37	78.46	62.83	74.93
5	89.39	75.78	68.06	88.62	68.22	70.9	74.14
Mean	89.22	79.8	77.1	78.52	73.49	71	74.87
CV (%)	3.15	3.23	9.08	12.35	5.35	7.65	0.63

Appendix F

Statistical Analysis of Solar Cap Fabric with and without laminate, Harness A, Harness B, and Laminate after Exposure to 100 ppm ozone concentration for 1 day, and 10 ppm concentration for 10 days

Table F.1: Strength of individual specimen of laminate, solar cap fabric with and without laminate backing, harness A, and harness B after total ozone exposure

Ozone Treatment	Strength (N/ cm)				
	Laminate	Solar Cap Fabric (with laminate)	Solar Cap Fabric (without laminate)	Harness A	Harness B
Untreated	762.60	135.65	135.65	22.74	64.27
Untreated	786.79	130.27	130.27	21.77	87.82
Untreated	767.07	129.70	129.70	21.26	93.63
Untreated	762.81	132.87	132.87	22.73	86.02
Untreated	764.22	128.19	128.19	23.67	89.39
Mean (N/ cm)	**772.16**	**131.34**	**131.34**	**22.44**	**89.22**
CV (%)	**1.36**	**2.01**	**2.01**	**3.74**	**3.15**
100 ppm 1 Day	769.17	113.96	122.83	22.26	73.31
100 ppm 1 Day	725.12	139.84	154.30	23.48	72.37
100 ppm 1 Day	744.68	129.67	132.22	24.94	67.41
100 ppm 1 Day	760.12	121.10	130.07	21.08	87.57
100 ppm 1 Day	730.67	148.43	134.19	24.27	84.72
Mean (N/ cm)	**746.32**	**130.60**	**134.72**	**23.20**	**77.08**
CV (%)	**2.41**	**9.51**	**7.81**	**5.98**	**10.02**
10 ppm 10 days	727.33	130.28	119.93	24.42	93.30
10 ppm 10 days	756.68	145.40	123.73	20.72	96.58
10 ppm 10 days	757.41	134.33	121.03	23.76	90.21
10 ppm 10 days	730.78	146.85	130.27	23.42	84.72

Table F.1 (continued).

10 ppm 10 days	755.56	131.22	112.23	24.69	81.14
Mean (N/ cm)	**747.14**	**137.62**	**121.44**	**23.40**	**89.19**
CV (%)	**1.88**	**5.15**	**4.81**	**6.05**	**6.29**